6.2

ÁREA: B
MÓDULO: B5

SOLUCIONES ANALÍTICAS.
CURVAS CARACTERÍSTICAS 1 Y 2

Ponente: César Sagaseta Millán
Ingeniero de Caminos
Universidad de Cantabria
Día: 02/03/07
Hora: 16:00 a 18:00

Master en Túneles y Obras Subterráneas

Área B. Diseño y Proyecto de Túneles

Módulo B5: Dimensionado y Proyecto de Sostenimientos

Soluciones Analíticas-1
Tensiones y deformaciones alrededor del túnel

César Sagaseta
E.T.S. Ing. Caminos
Universidad de Cantabria
Santander

Contenido

- **Introducción**
- ***Caso básico***
  - Túnel circular, tensiones isótropas, profundidad infinita, terreno elástico
- **Terreno elastoplástico**
  - Tresca (ϕ=0). Mohr Coulomb (c, ϕ). Hoek-Brown
- **Tensiones anisótropas (k0≠1). Profundidad finita**
- **Interacción terreno-revestimiento**
  - Diagrama de interacción.
  - Influencia de la rigidez. Influencia del tiempo de instalación.
  - Sostenimiento primario y revestimiento secundario (NMA)

Caso básico (elástico)

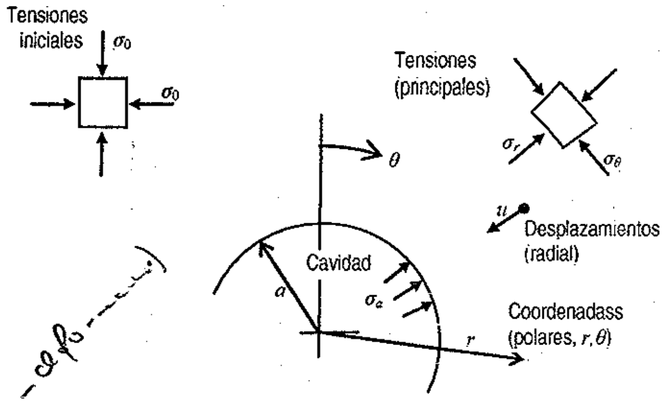

Equilibrio

$$\frac{d\sigma_r}{dr} - \frac{\sigma_\theta - \sigma_r}{r} = 0$$

equilibrio (radial)

Ley de Hooke (Tensión – deformación)

$$\left.\begin{aligned}
\varepsilon_r &= \frac{1}{E}\left[\Delta\sigma_r - \nu\left(\Delta\sigma_\theta + \Delta\sigma_z\right)\right] \\
\varepsilon_\theta &= \frac{1}{E}\left[\Delta\sigma_\theta - \nu\left(\Delta\sigma_r + \Delta\sigma_z\right)\right] \\
\varepsilon_z &= \frac{1}{E}\left[\Delta\sigma_z - \nu\left(\Delta\sigma_r + \Delta\sigma_\theta\right)\right] = 0
\end{aligned}\right\} \rightarrow \left\{\begin{aligned}
\sigma_r &= \frac{2G}{1-2\nu}\left[(1-\nu)\varepsilon_r + \nu\varepsilon_\theta\right] \\
\sigma_\theta &= \frac{2G}{1-2\nu}\left[(1-\nu)\varepsilon_\theta + \nu\varepsilon_r\right] \\
\sigma_z &= \nu\left(\sigma_r + \sigma_\theta\right)
\end{aligned}\right.$$

Ec. de Euler

$$\boxed{\begin{aligned} & r^2 \frac{d^2u}{dr^2} + r\frac{du}{dr} - u = 0 \\ & u = \frac{c_1}{r} + c_2 r \end{aligned}}$$

Ec. de Compatibilidad $\varepsilon_r = \dfrac{du}{dr}$; $\varepsilon_\theta = \dfrac{u}{r}$

Resolución

$C_2 = 0$ porque el desp. tendería a infinito

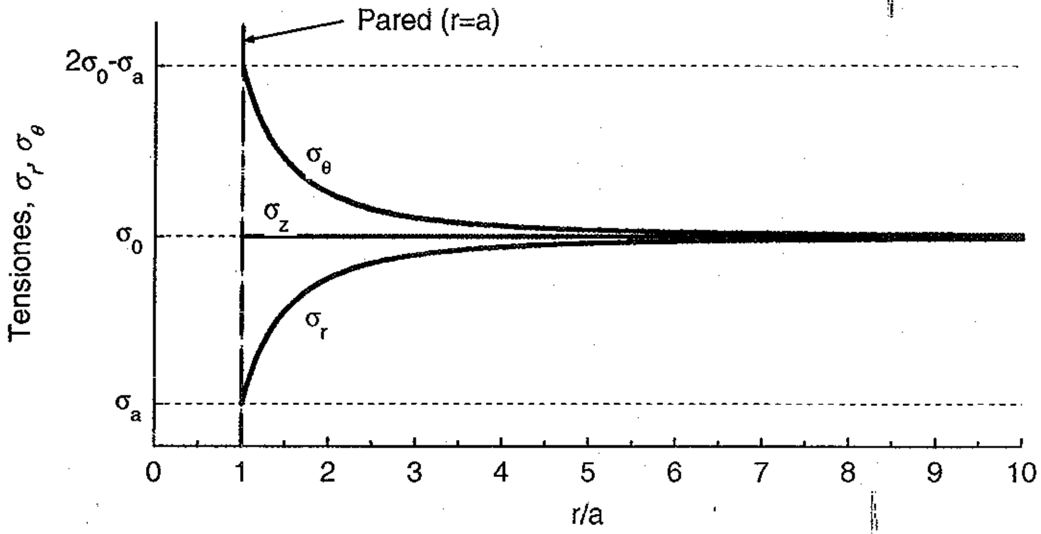

$$\sigma_r = \sigma_{r0} + \Delta\sigma_r = \sigma_0 - (\sigma_0 - \sigma_a)\frac{a^2}{r^2}$$

$$\sigma_\theta = \sigma_{\theta 0} + \Delta\sigma_\theta = \sigma_0 + (\sigma_0 - \sigma_a)\frac{a^2}{r^2}$$

$$\sigma_z = \sigma_{z0} + \Delta\sigma_z = \sigma_0 + \nu(\Delta\sigma_r + \Delta\sigma_\theta) = \sigma_0$$

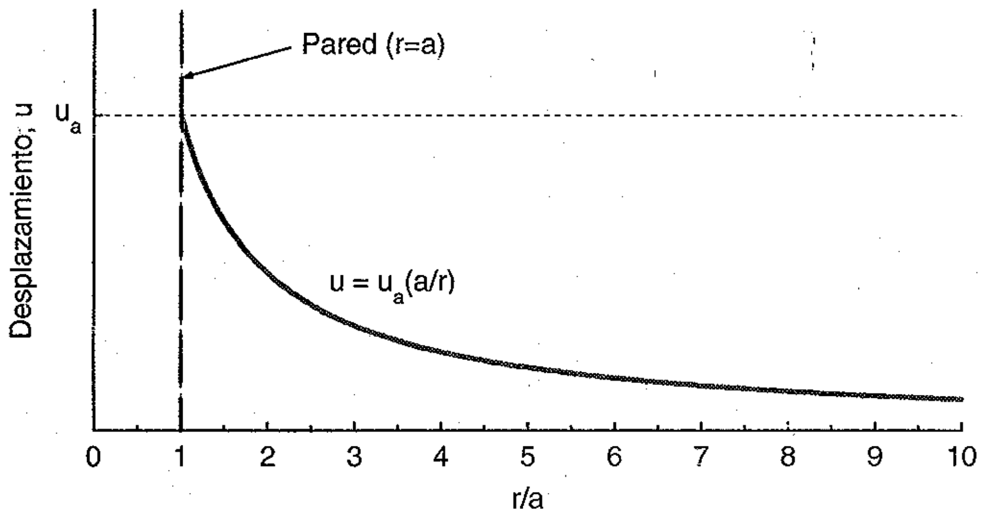

$$\frac{u}{a} = \frac{1}{2G}(\sigma_0 - \sigma_a)\frac{a}{r}$$

$u_a = \frac{1}{2G}(\sigma_0 - \sigma_a)$

Los tensiones $\overline{r^2}$ se atenúan mucho + rápido que los desplaz. $\overline{r}$

Al excavar el TN la tensión radial se relaja y la circunferencial aumenta la misma cuantía.

En la pared del túnel:
$\sigma_r = \sigma_a$
$\sigma_\theta = 2\sigma_0 - \sigma_a$

$\Delta\sigma_{media} = 0$

El desviador $\sigma_r - \sigma_\theta$ provoca que si lo aumenta el terreno se producirá una zona plástica

Cl Ieun

Caso elastoplástico (Tresca, ϕ=0)

Ecuaciones en zona elástica

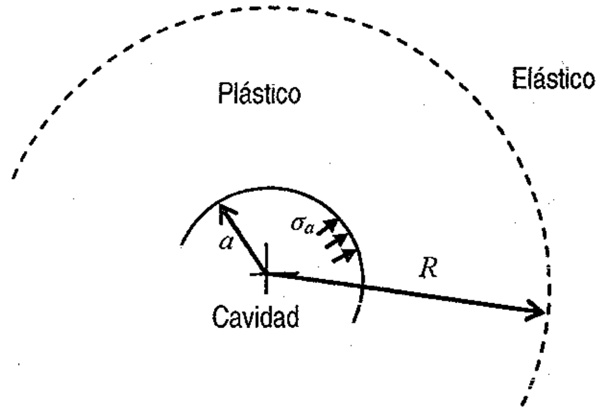

$$\frac{d\sigma_r}{dr} - \frac{\sigma_\theta - \sigma_r}{r} = 0 \qquad \text{equilibrio (radial)}$$

$$\left.\begin{aligned}
\varepsilon_r &= \frac{1}{E}\left[\Delta\sigma_r - \nu\left(\Delta\sigma_\theta + \Delta\sigma_z\right)\right] \\
\varepsilon_\theta &= \frac{1}{E}\left[\Delta\sigma_\theta - \nu\left(\Delta\sigma_r + \Delta\sigma_z\right)\right] \\
\varepsilon_z &= \frac{1}{E}\left[\Delta\sigma_z - \nu\left(\Delta\sigma_r + \Delta\sigma_\theta\right)\right] = 0
\end{aligned}\right\} \rightarrow \left\{\begin{aligned}
\sigma_r &= \frac{2G}{1-2\nu}\left[(1-\nu)\varepsilon_r + \nu\varepsilon_\theta\right] \\
\sigma_\theta &= \frac{2G}{1-2\nu}\left[(1-\nu)\varepsilon_\theta + \nu\varepsilon_r\right] \\
\sigma_z &= \nu\left(\sigma_r + \sigma_\theta\right)
\end{aligned}\right.$$

$$\varepsilon_r = \frac{du}{dr}$$

$$\varepsilon_\theta = \frac{u}{r}$$

Caso elastoplástico

Ecuaciones en zona plástica

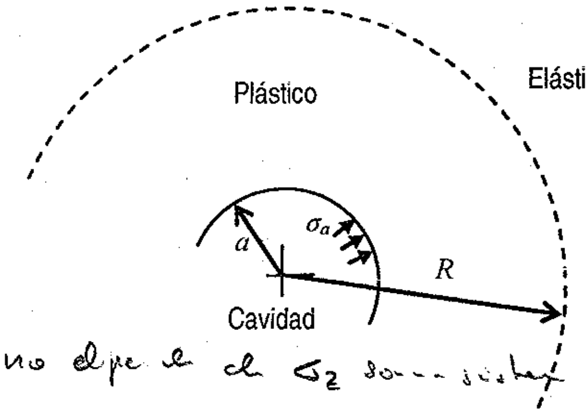

Equilibrio interno $\quad \dfrac{d\sigma_r}{dr} - \dfrac{\sigma_\theta - \sigma_r}{r} = 0$ (1) $\quad$ equilibrio (radial)

Si el criterio de rotura no depende de σ_z son suficientes las ec. con dos incógnitas (1) y (2)

Criterio de rotura $\rightarrow f(\sigma_r, \sigma_\theta, \sigma_z) = 0$ (2)

¡Ojo! siempre que σ_z sea la tensión intermedia

$$\text{Si } \sigma_r \le \sigma_z \le \sigma_\theta \rightarrow \begin{cases} \text{Tresca: } \sigma_\theta - \sigma_r = 2c_u \\ \text{Mohr - Coulomb: } (1 - \operatorname{sen}\phi)\sigma_\theta - (1 + \operatorname{sen}\phi)\sigma_r - 2c\cos\phi = 0 \\ \text{Hoek - Brown: } \sigma_\theta = \sigma_r + \sqrt{m\sigma_c\sigma_r + s\sigma_c^2} \end{cases}$$

c_u → Resist. al corte sin drenaje → $\phi = 0$ sin fricción

De $\quad \sigma_\theta = f(\sigma_r)$ (Del criterio de rotura se despeja σ_θ y se sustituye en (1) y ... (3)

$$\frac{d\sigma_r}{dr} - \frac{g(\sigma_r)}{r} = 0 \rightarrow \frac{d\sigma_r}{g(\sigma_r)} = \frac{dr}{r} \;(3) \quad \text{(variables separadas)}$$

$$\boxed{N = \frac{\sigma_0 - \sigma_a}{c_u}}$$

N → se utiliza en estabilidad en el frente (valor de rotura = N = 6)

Factor de carga (*overload factor*). *Peck (1969)*

c_u = resist. al corte sin drenaje

Cimentaciones

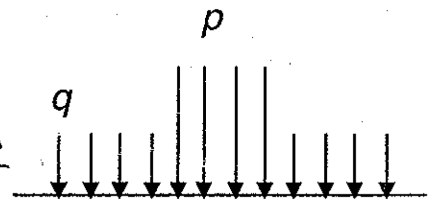

$$p = qN_q + cN_c$$

$$\text{si}\,\phi = 0 \rightarrow N_q = 1 \rightarrow N_c = \frac{p-q}{c}$$

p → presión en línea de la cim.

q → presión sin resistencia

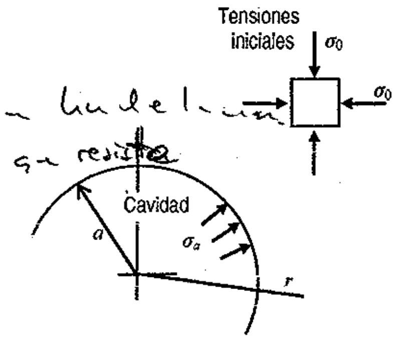

$$\boxed{N_0 = (\text{sin revestir}, \sigma_a = 0) = \frac{\sigma_0}{c_u}} \qquad N = N_0\left(1 - \frac{\sigma_a}{\sigma_0}\right)$$

N_0 → factor de carga sin revestimiento

Máximo valor de N_0 ?

$$N_0 = \frac{\sigma_0}{c_u} = \frac{\sigma_0 / \sigma'_0}{c_u / \sigma'_0} \le \frac{\overbrace{\gamma_{sat}/\gamma_{sum}}^{\approx 2}}{\underbrace{(0{,}2 - 0{,}4)}_{\text{valor para fangos}}} = (8-10)$$

$$\boxed{I_r = \frac{G}{c_u} = \text{Índice de rigidez} = (50 - 200)}$$

G → $\frac{\text{Deformabilidad}}{\text{resistencia al corte}}$

$\frac{\sigma_r+\sigma_\theta}{2} = \sigma_0$

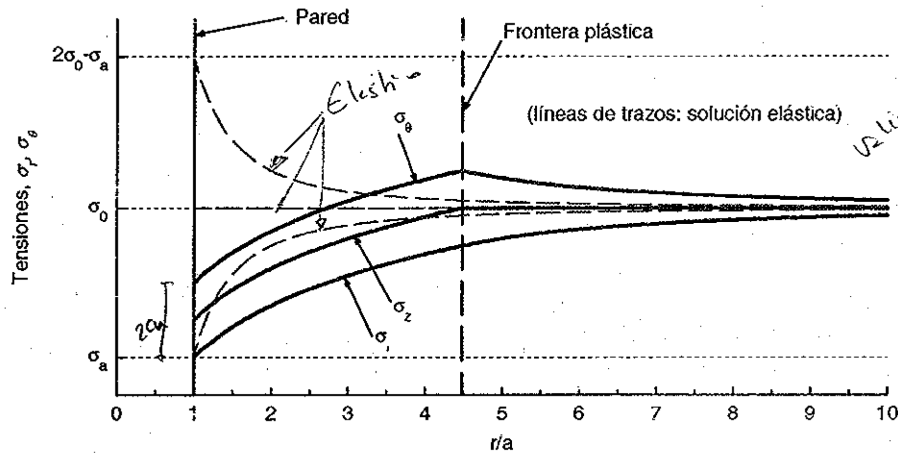

Válidas hasta R

$$\sigma_r = \sigma_a + 2c_u \ln\left(\frac{r}{a}\right) \quad \rightarrow \text{Tresca.}$$

$$\sigma_\theta = \sigma_r + 2c_u = \sigma_a + 2c_u + 2c_u \ln\left(\frac{r}{a}\right)$$

$$\sigma_z = \frac{1}{2}(\sigma_r + \sigma_\theta) = \sigma_a + c_u + 2c_u \ln\left(\frac{r}{a}\right)$$

$$2\sigma_a + 2c_u\left[1 + 2\ln\left(\frac{R}{a}\right)\right] = 2\sigma_0$$

R → radio de la zona plástica

$$\frac{R}{a} = e^{\frac{1}{2}\left(\frac{\sigma_0-\sigma_a}{c_u}-1\right)} = e^{\frac{N-1}{2}}$$ → Crece exponencialmente ~~entre~~ con valores de N

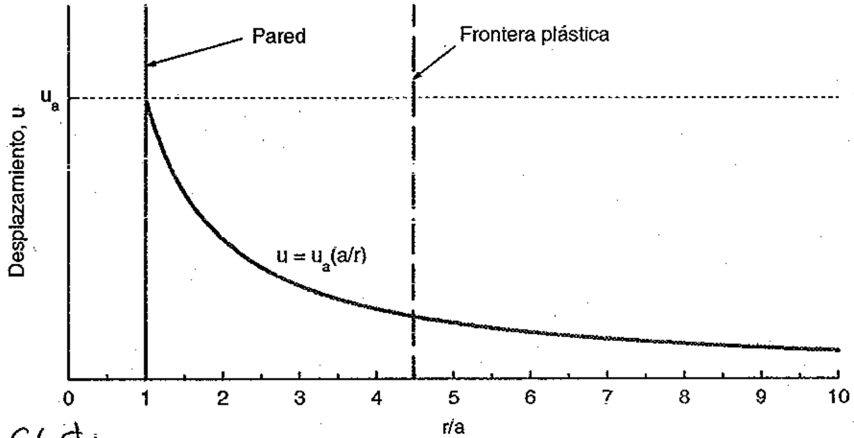

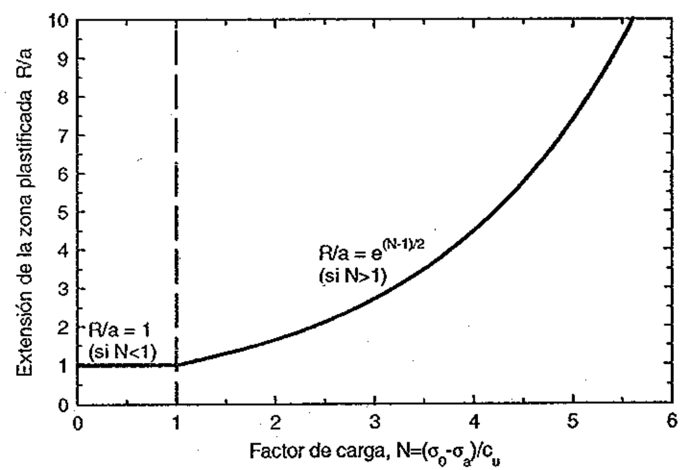

Con $N<1$ → Elástico

$1<N<3$ → Zona plástica deform. volum.

$$u = (\sigma_0 - \sigma_{rR})\frac{1}{2G}R\frac{R}{r} = \frac{1}{2I_r}e^{N-1}a\frac{a}{r}$$

$3<N<6$ → Rotura zona plástica muy grande

Con $N<1$ → Elástico

$1<N<3$ Algo de zona plástica def. volum.

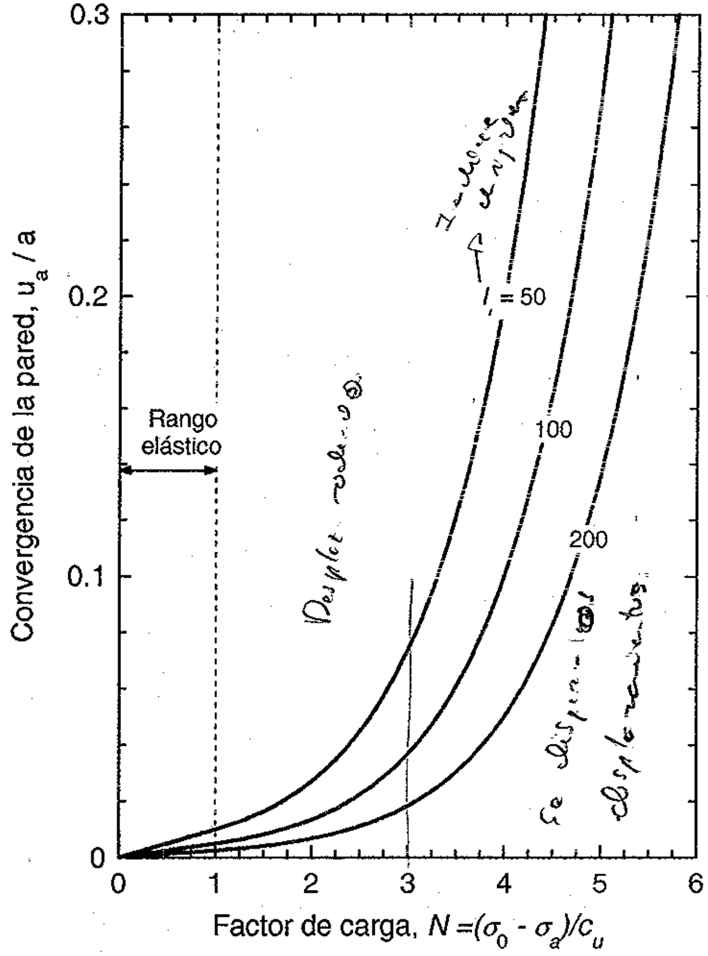

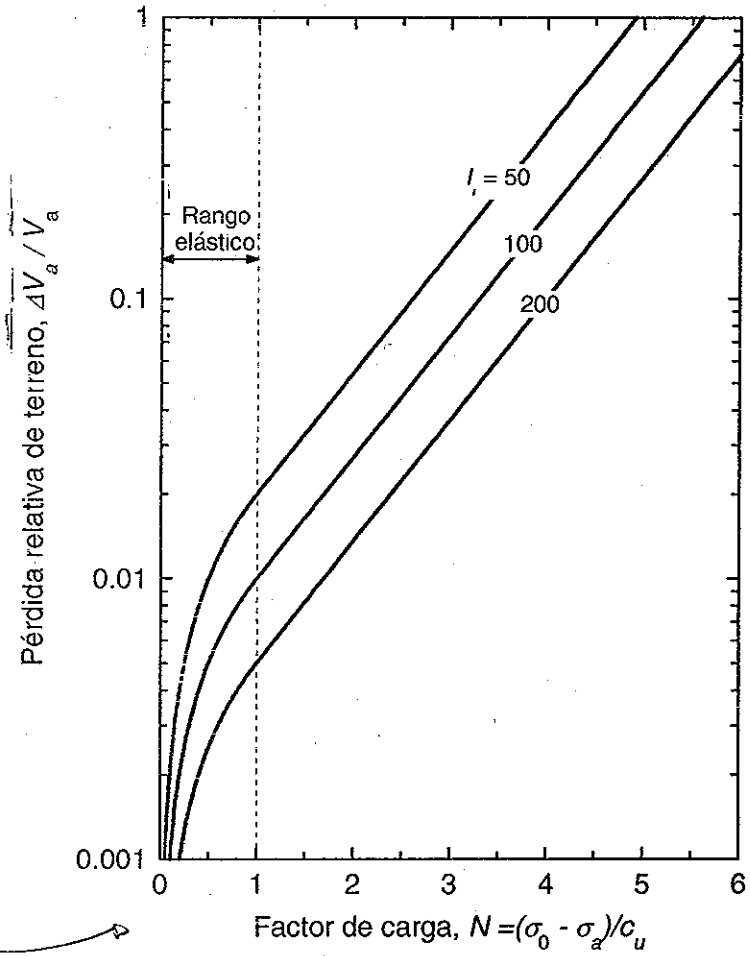

Diagramas
iguales el dcho en escala
logarítmica

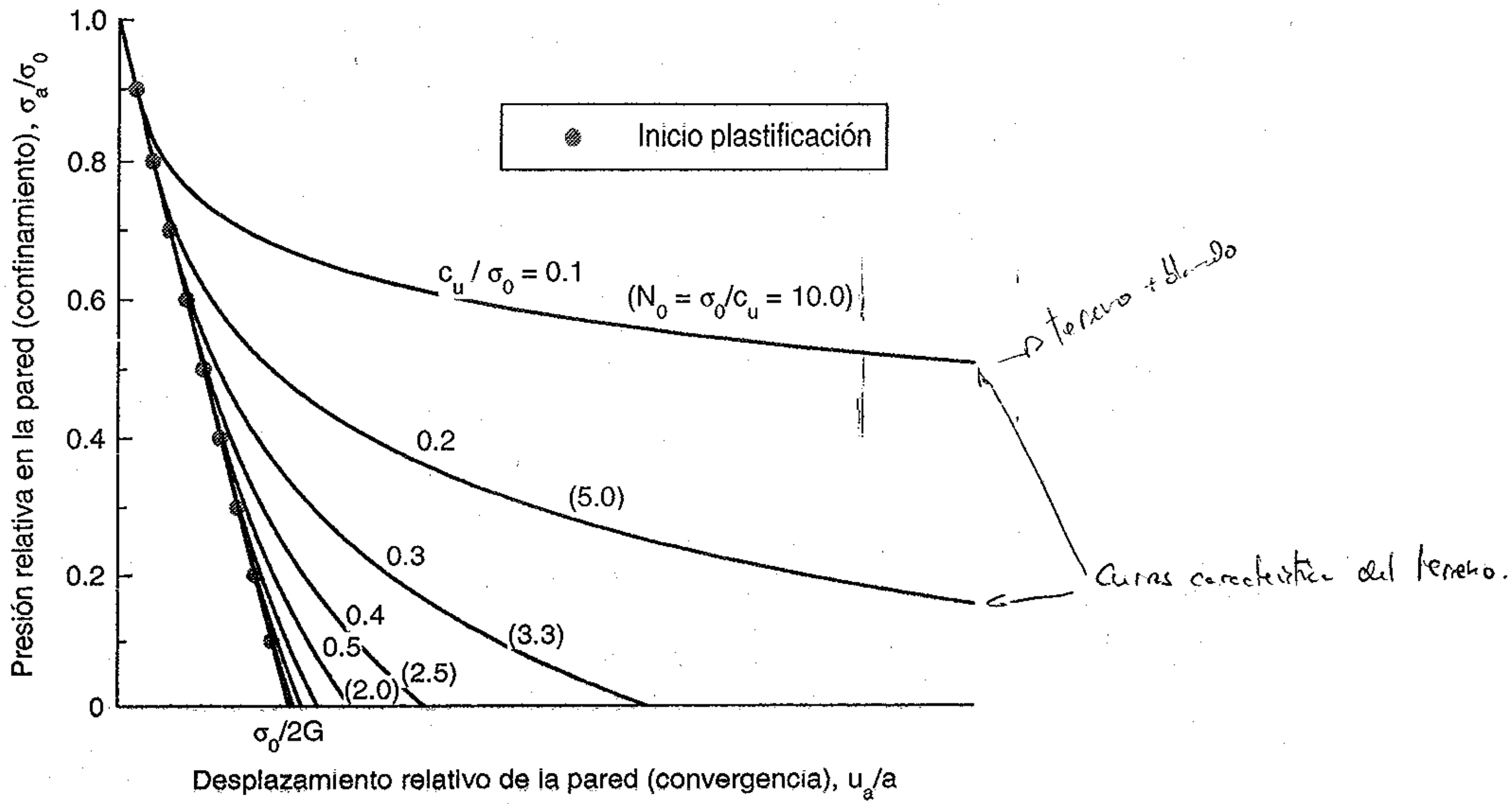

Diagrama convergencia–confinamiento.

$$\varepsilon_a = \frac{u_a}{a} = \begin{cases} = \dfrac{1}{2G}(\sigma_0 - \sigma_a) = \dfrac{1}{2I_r} N & \text{para} \quad N \le 1 \\[2ex] = \dfrac{1}{2I_r} e^{N-1} & \text{para} \quad N \ge 1 \end{cases}$$

Caso elastoplástico (Mohr-Coulomb, c,ϕ,ψ)

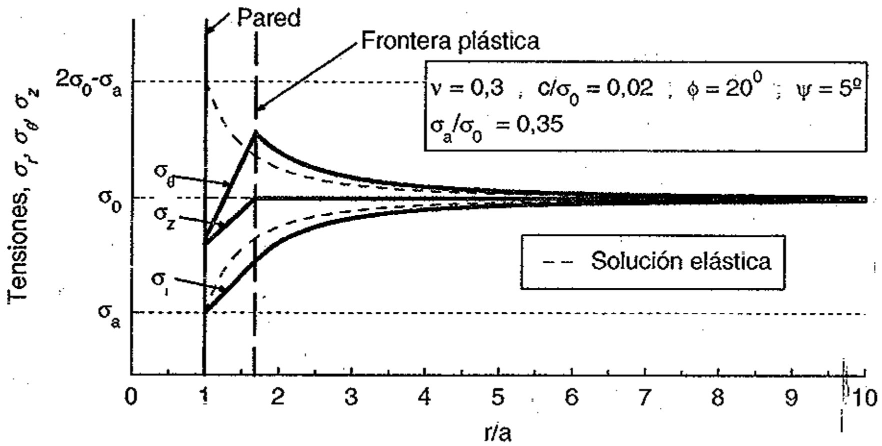

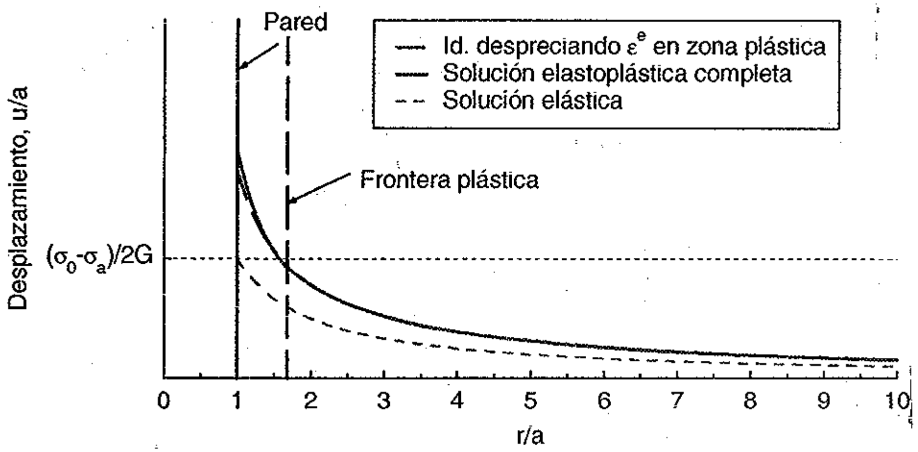

$$\sigma_r = -c\,\mathrm{cotg}\,\phi + (\sigma_a + c\,\mathrm{cotg}\,\phi)\left(\frac{r}{a}\right)^{\frac{2\,\mathrm{sen}\,\phi}{1-\mathrm{sen}\,\phi}}$$

$$\sigma_\theta = -c\,\mathrm{cotg}\,\phi + \frac{1+\mathrm{sen}\,\phi}{1-\mathrm{sen}\,\phi}(\sigma_a + c\,\mathrm{cotg}\,\phi)\left(\frac{r}{a}\right)^{\frac{2\,\mathrm{sen}\,\phi}{1-\mathrm{sen}\,\phi}}$$

No son de tipo logarítmico, sino exponencial

$$\sigma_z = (1-2\nu)\sigma_0 + \nu(\sigma_r + \sigma_\theta)$$

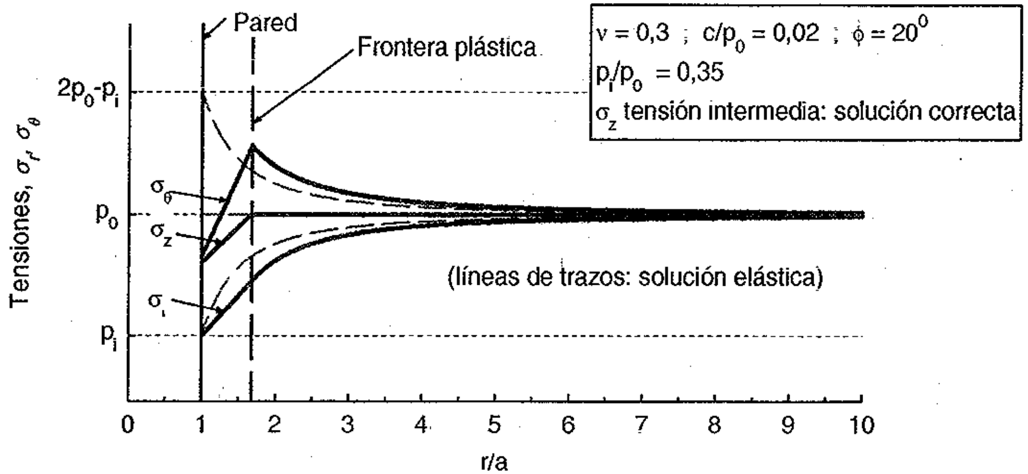

Llega un momento en el que σ_z no es la intermedia → y pasa a ser la mayor

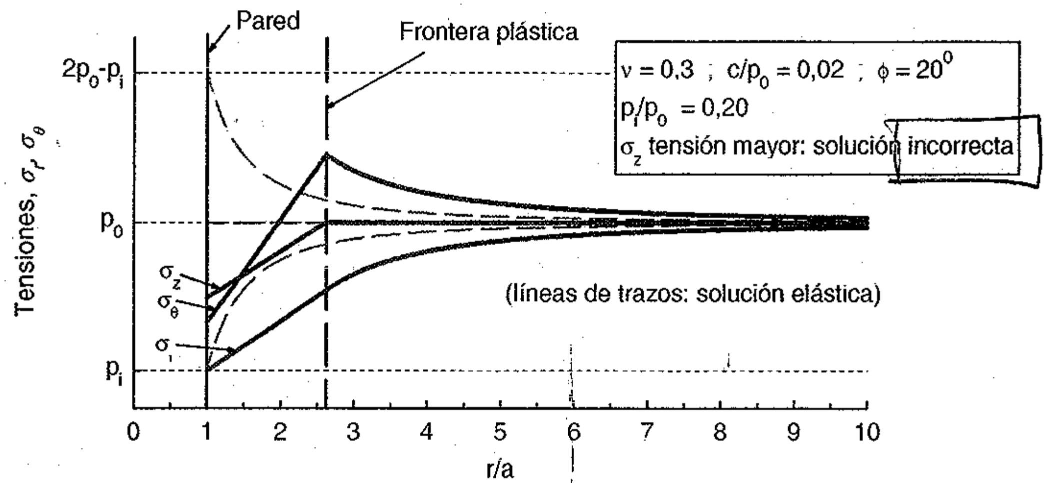

$\phi = 0$ Carga rápida sin drenaje.

$$\frac{R}{a} = \left[(1 - \operatorname{sen}\phi) \frac{\sigma_0 + c \operatorname{cotg}\phi}{\sigma_a + c \operatorname{cotg}\phi} \right]^{\frac{1-\operatorname{sen}\phi}{2\operatorname{sen}\phi}} = \left[(1 - \operatorname{sen}\phi)(1 + N \operatorname{tg}\phi) \right]^{\frac{1-\operatorname{sen}\phi}{2\operatorname{sen}\phi}}$$

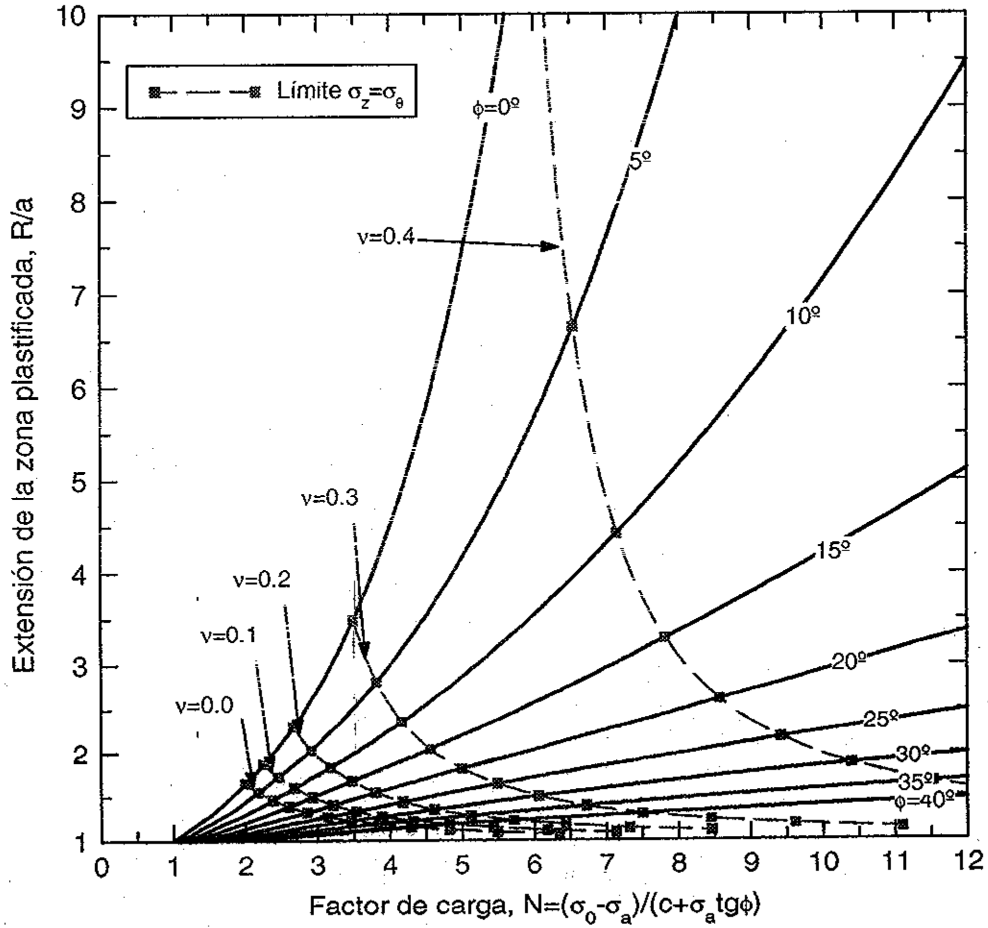

lo + normal

Solución en desplazamientos (rigurosa)

$$\frac{u}{a}=\frac{\sigma_0+c\cot g\phi}{2G}\left[A\frac{r}{a}+B\left(\frac{r}{a}\right)^k+C\left(\frac{r}{a}\right)^{-\alpha}\right]$$

siendo:

$$A=-(1-2\nu)$$

$$B=(1-\operatorname{sen}\phi)\frac{1-2\nu+\operatorname{sen}\phi\operatorname{sen}\psi}{1-\operatorname{sen}\phi\operatorname{sen}\psi}\left(\frac{R}{a}\right)^{1-k}$$

$$C=\left[1-2\nu+\operatorname{sen}\phi-(1-\operatorname{sen}\phi)\frac{1-2\nu+\operatorname{sen}\phi\operatorname{sen}\psi}{1-\operatorname{sen}\phi\operatorname{sen}\psi}\right]\left(\frac{R}{a}\right)^{\alpha+1}$$

$$\alpha=\frac{1+\operatorname{sen}\psi}{1-\operatorname{sen}\psi}\qquad k=\frac{1+\operatorname{sen}\phi}{1-\operatorname{sen}\phi}$$

En la pared de la cavidad $(r=a)$:

$$\varepsilon_a=\frac{u_a}{a}=\frac{\sigma_0+c\cot g\phi}{2G}(A+B+C)$$

Solución en desplazamientos (despreciando deformación elástica en la zona plástica)

$$\frac{u}{a}=\frac{\sigma_0+c\cot g\phi}{2G}\operatorname{sen}\phi\left(\frac{R}{a}\right)^{\alpha+1}\left(\frac{r}{a}\right)^{-\alpha}$$

y en la pared de la cavidad:

$$\varepsilon_a=\frac{u_a}{a}=\frac{\sigma_0+c\cot g\phi}{2G}\operatorname{sen}\phi\left(\frac{R}{a}\right)^{\alpha+1}$$

Caso elastoplástico (Hoek-Brown, m,s,σ_c)

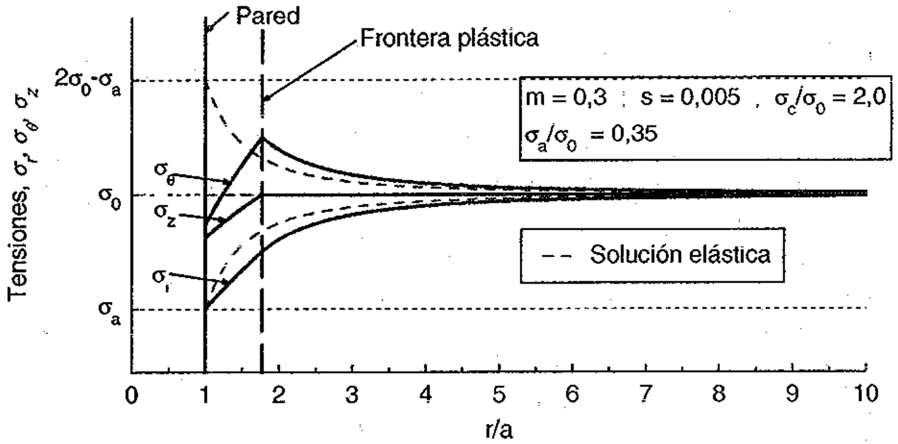

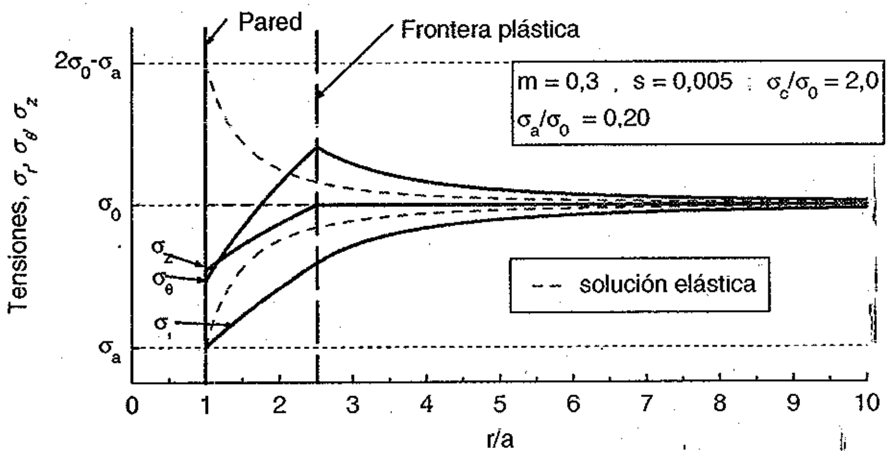

$$\sigma_r = \frac{1}{m\sigma_c}\left[\left(\sqrt{m\sigma_c\sigma_a + s\sigma_c^2} + \frac{m\sigma_c}{2}\ln\frac{r}{a}\right)^2 - s\sigma_c^2\right]$$

$$\sigma_\theta = \sigma_r + \sqrt{m\sigma_c\sigma_r + s\sigma_c^2}$$

→ Igual que Mohr-Coulomb llega momento que $\sigma_z > \sigma_\theta > \sigma_r$

Tensiones anisótropas (Kirsch, 1898)

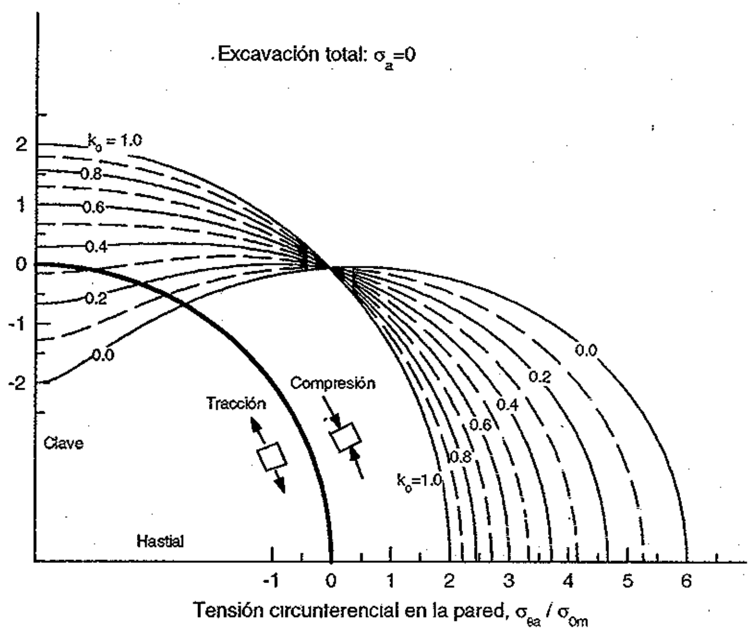

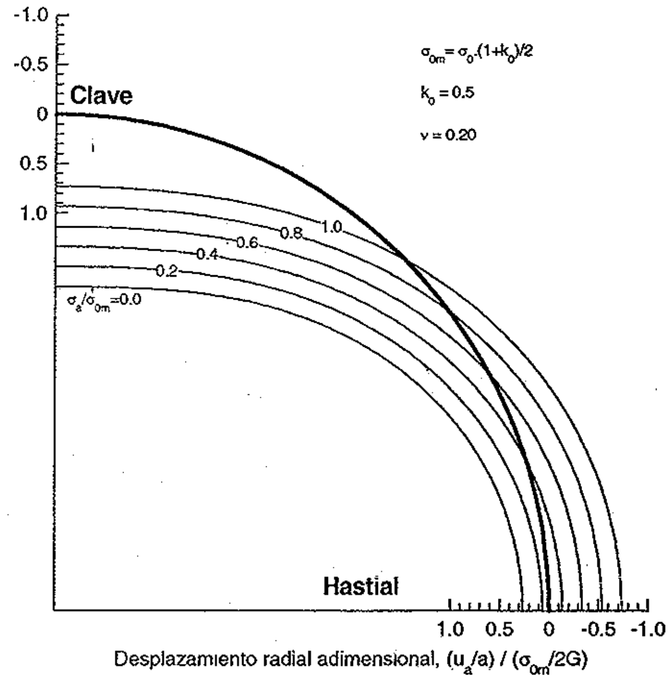

Interacción terreno-revestimiento

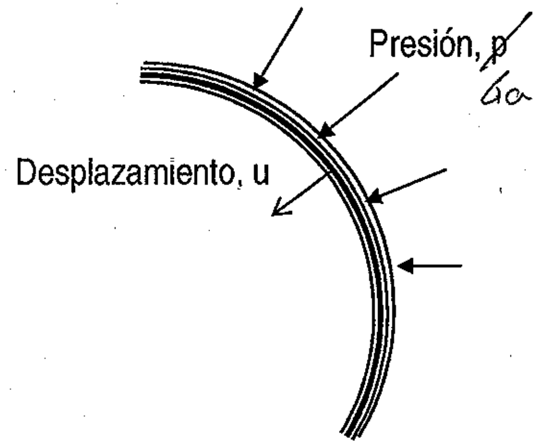

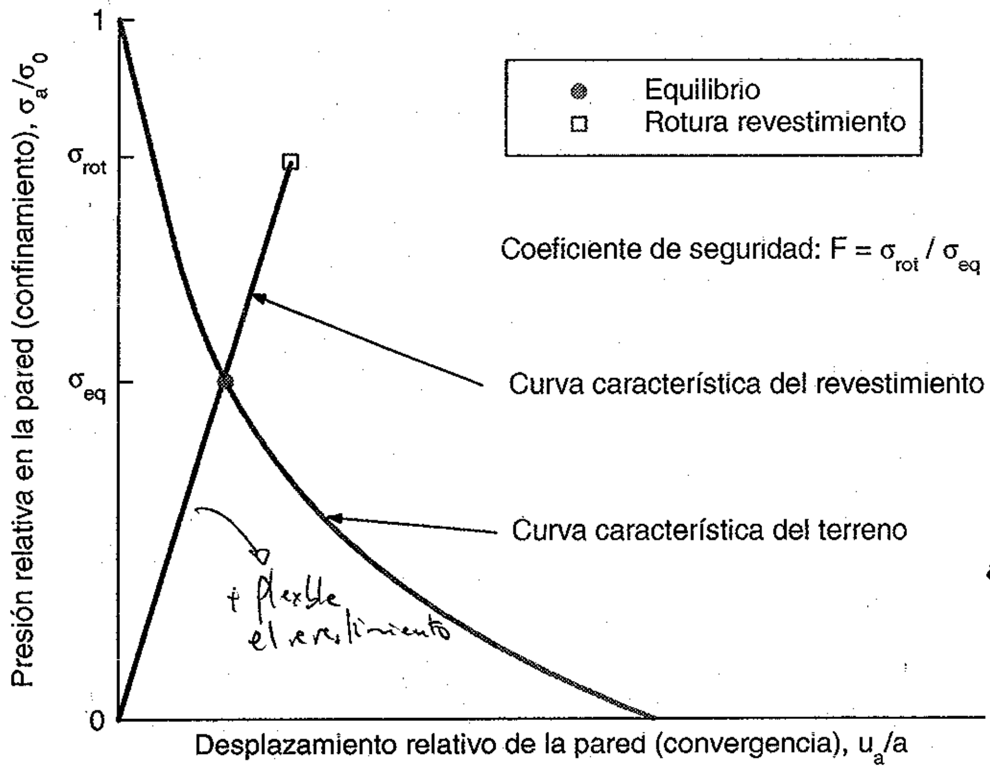

$$\frac{u_r}{a}=\frac{\sigma_a}{k_r}$$

$$\varepsilon_a=\frac{u_a}{a}=\begin{cases} =\dfrac{1}{2G}(\sigma_0-\sigma_a)=\dfrac{1}{2I_r}N & \text{para} \quad N\le 1\\ =\dfrac{1}{2I_r}e^{N-1} & \text{para} \quad N\ge 1\end{cases}$$

a > flexibilidad del revestimiento < σ soportará
(< kr)
a > flexibilidad < resistencia y por tanto llegará a rotura.

Interacción terreno-revestimiento

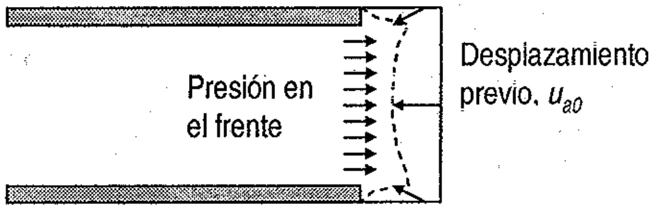

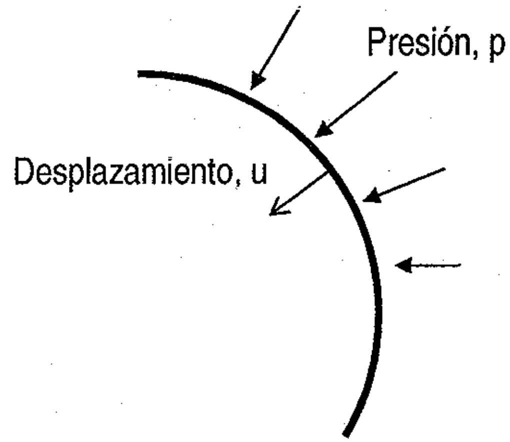

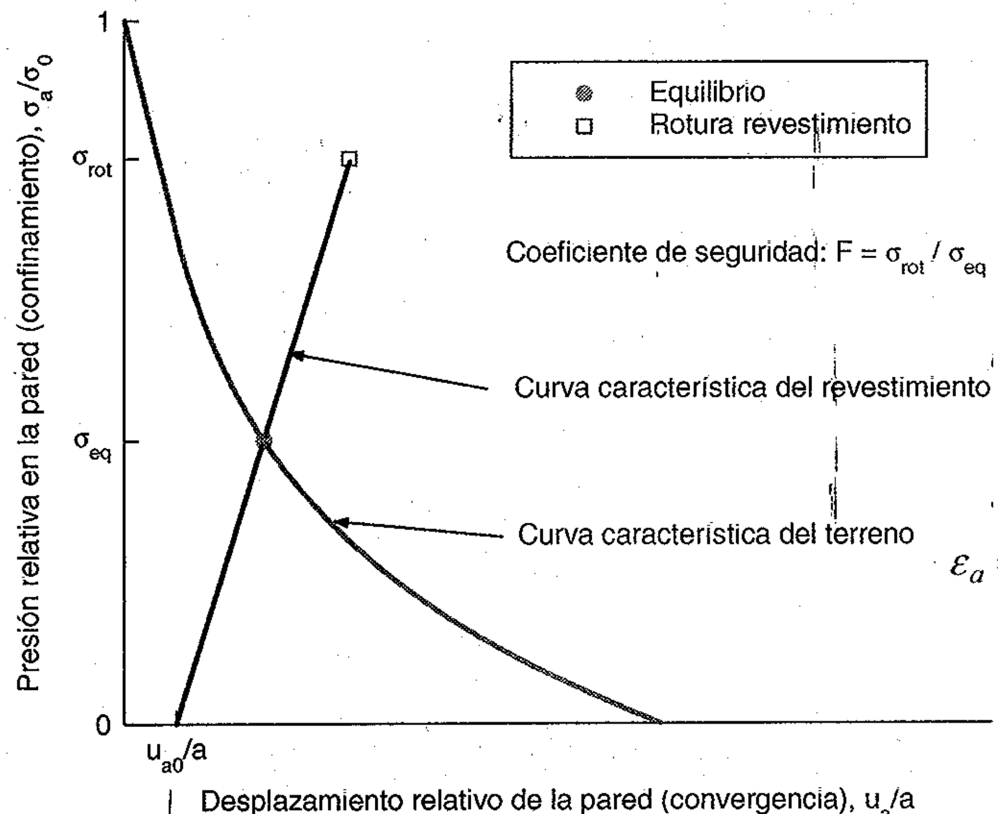

Deformación previa.

$$\frac{u_r}{a} = \frac{u_a - u_{a0}}{a} = \frac{\sigma_a}{k}$$

$$\varepsilon_a = \frac{u_a}{a} = \begin{cases} = \dfrac{1}{2G}(\sigma_0 - \sigma_a) = \dfrac{1}{2I_r} N & \text{para} \quad N \leq 1 \\ = \dfrac{1}{2I_r} e^{N-1} & \text{para} \quad N \geq 1 \end{cases}$$

Rigidez del revestimiento

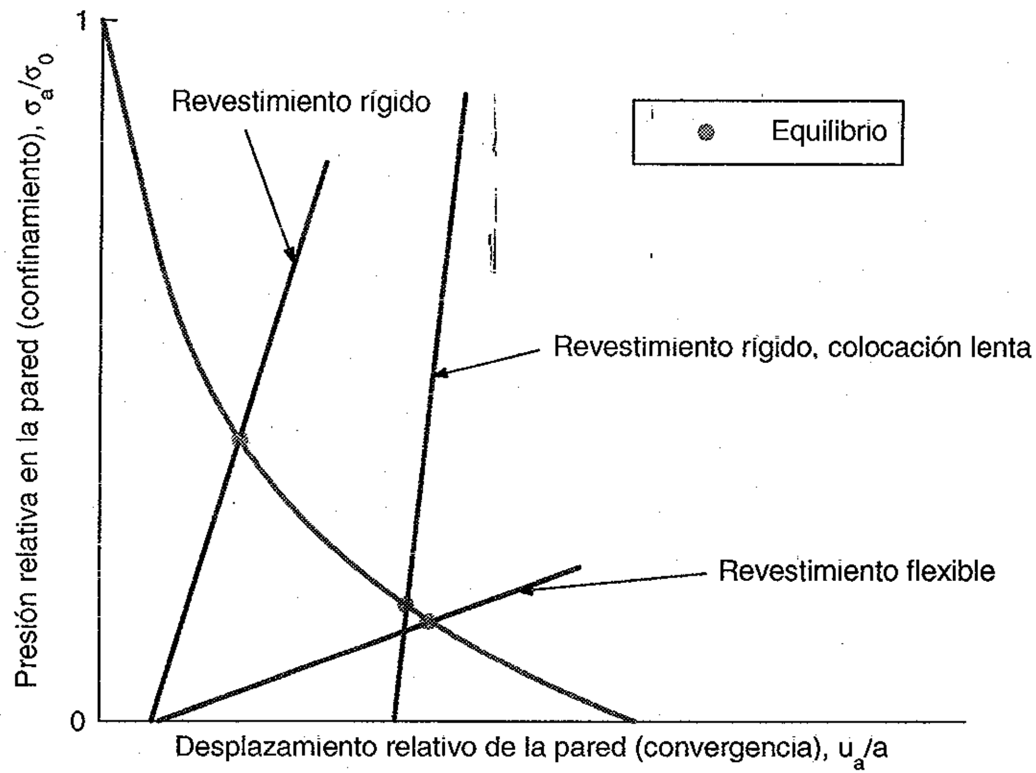

Degradación con el tiempo

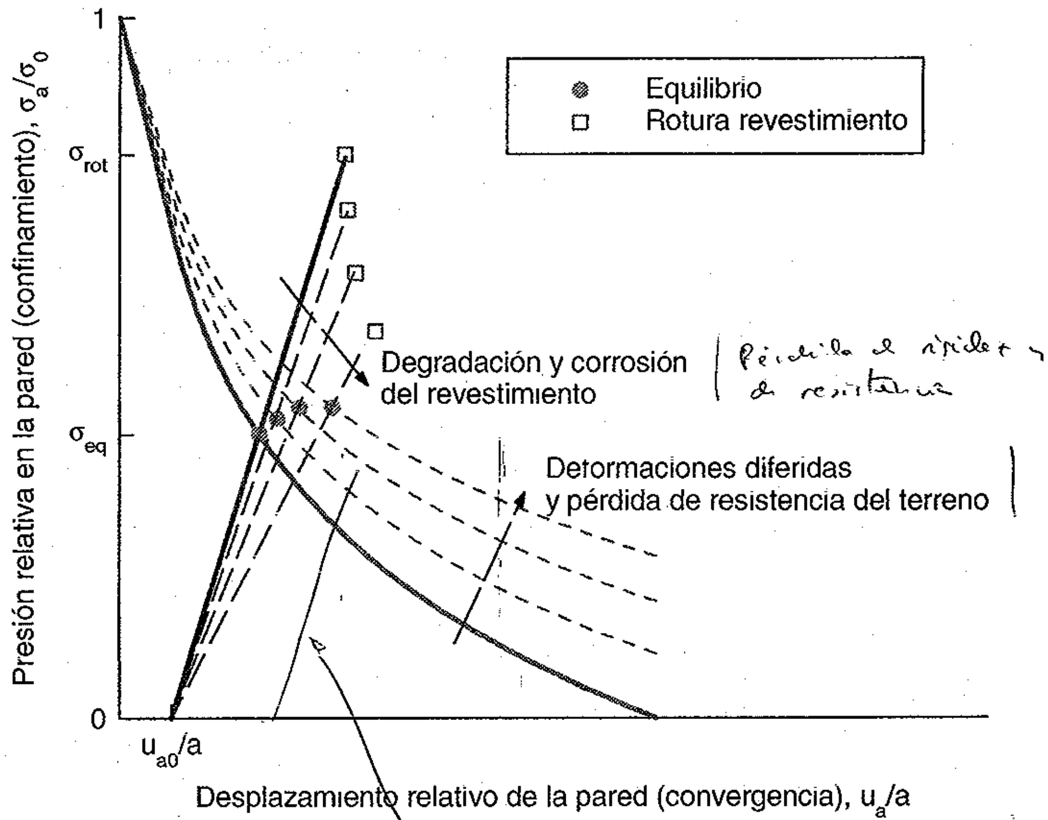

Sost.

revestimiento 2ndo, sólo actúa cuando el revest. 1ero deja de actuar

Método de Panet (AFTES, 2001)

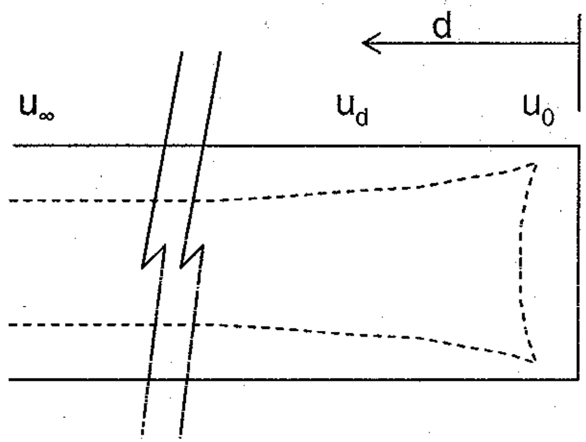

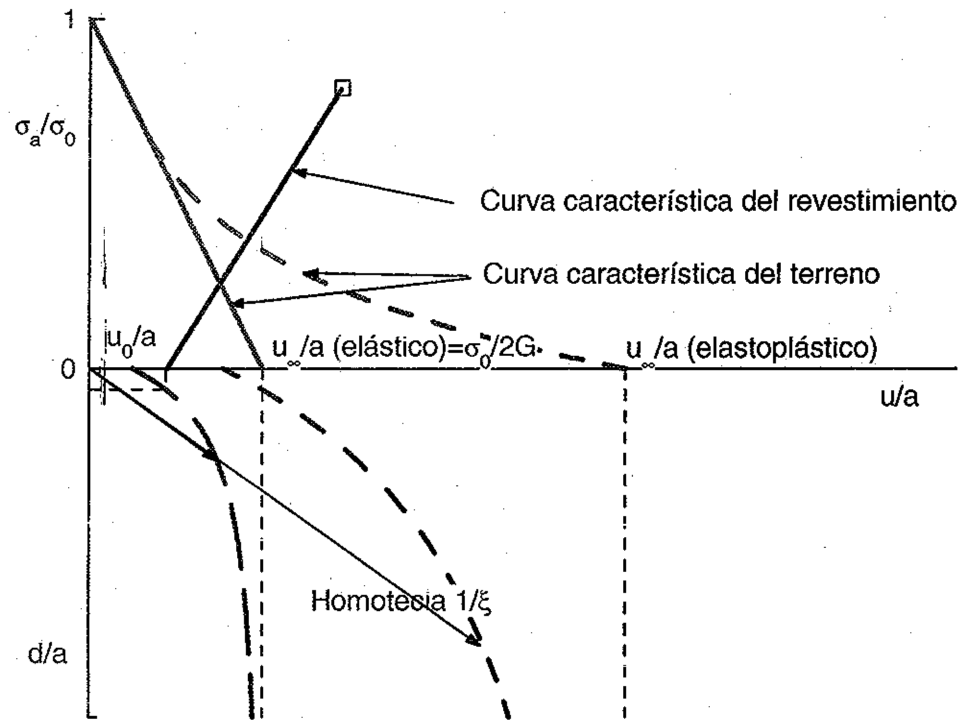

$$\left.\begin{aligned} u_d &= u_0 + a_d(u_\infty - u_0) \\ u_0 &= \alpha_0 u_\infty \\ \alpha_0 &= 0{,}25 \end{aligned}\right\}$$

$$a_d = 1 - \left(\frac{ma}{ma + \xi d}\right)^2$$

$$\text{Elástico}: m = 0{,}75 \ ; \ \xi = 1$$

Trata de evaluar de una forma racional el desplazamiento inicial en f de la distancia al frente de colocación del sost

Sostenimiento primario y revestimiento secundario. NMA.

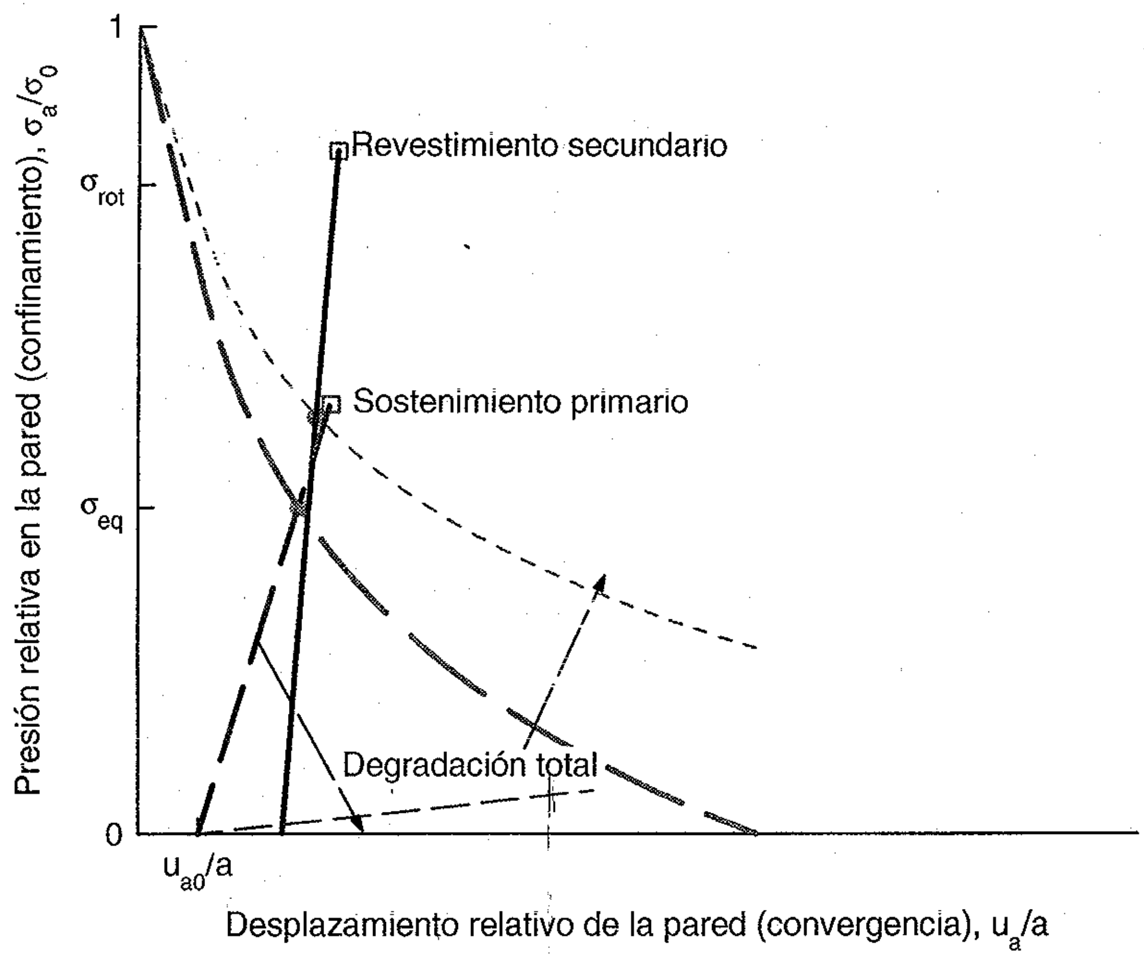

Ejemplo:

- Túnel en Madrid
  - $a = 5$ m
  - $H = 30$ m
  - $\Gamma = 20$ kN/m^3
  - $E_u = 100$ MPa
  - $c_u = 300$ kPa
  - $e = 0.1$ m HP
  - $E_r = 5000$ MPa
  - $\sigma_k = 20000$ kPa
- **Obtener presión sobre revestimiento, convergencia y coeficiente de seguridad, en función de la distancia al frente de la colocación del revestimiento**

Soluciones Analíticas-2
Deformaciones en zonas alejadas

César Sagaseta

E.T.S. Ing. Caminos

Universidad de Cantabria

Santander

Contenido

- **Introducción**
- **Fundamentos**
  - Componentes de la deformación del túnel (*contracción radial,ovalización, descenso uniforme)*
  - Deformaciones en zonas alejadas
    - Soluciones empíricas
    - Solución analítica
- **Aplicación a casos reales**
- **Extensión del Metro de Madrid 1995-99**
  - Terreno
  - Métodos constructivos
  - Instrumentación
  - Aplicación de la solución analítica. Parámetros

Componentes de la deformación del túnel

- **Contracción radial** : $\varepsilon = u_0/a$ (Ground loss : $\varepsilon_s = 2u_0/a$)
- **Ovalización:** $\delta = max(u')/a$ $(\rho = \delta/\varepsilon)$
- **Descenso uniforme:** $\eta = (u_z/a)/\varepsilon$

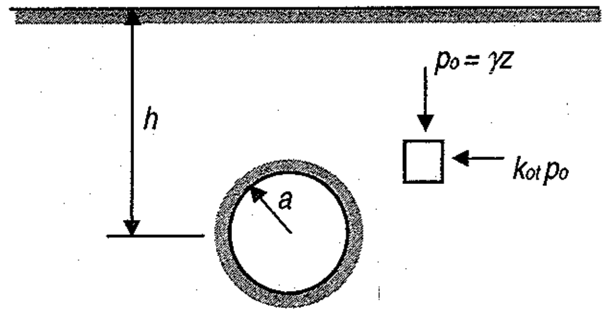

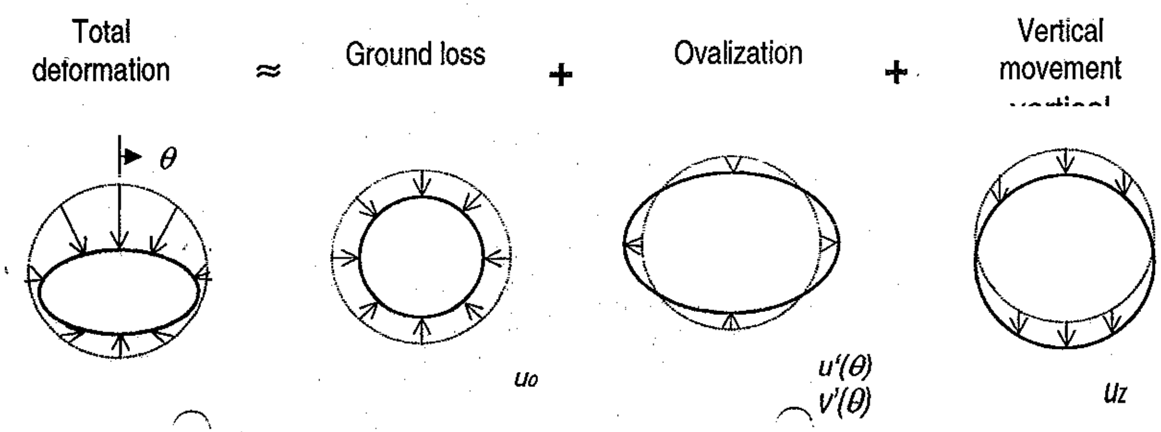

Contracción radial. Ground loss

$$\varepsilon = \frac{1}{2}\varepsilon_s = \begin{cases} \dfrac{p_0 - p_i}{2G} = \dfrac{1}{2I_r} N_i = \dfrac{1}{2I_r}\left(1 - \dfrac{p_i}{p_0}\right) N_0 & \text{if } N_i \le 1 \text{ (elastic)} \\ \dfrac{1}{2I_r} e^{N_i - 1} = \dfrac{1}{2I_r} e^{\left(1-\frac{p_i}{p_0}\right)N_0 - 1} & \text{if } N_i \ge 1 \text{ (elastic - plastic)} \end{cases}$$

$$\text{Overload factors: } \quad N_0 = \frac{p_0}{c_u} \quad ; \quad N_i = \frac{p_0 - p_i}{c_u} = N_0\left(1 - \frac{p_i}{p_0}\right)$$

$$\varepsilon = \frac{1}{2}\varepsilon_s = \begin{cases} \dfrac{1}{2I_r} N_c & \text{if } N_q \le \dfrac{1}{1 - sin\phi} \quad \text{(elastic)} \\ \dfrac{1}{2I_r} \dfrac{\cos\phi}{1 - sin\phi}\left[(1 - sin\phi)N_q\right]^{\frac{1-\sin\phi\sin\nu}{\sin\phi(1-\sin\nu)}} & \text{if } N_q \ge \dfrac{1}{1 - sin\phi} \quad \text{(elastic - plastic)} \end{cases}$$

$$\text{Overload factors: } \quad N_q = \frac{p_0 + c\cot\phi}{p_i + c\cot\phi} \quad ; \quad N_c = \left(N_q - 1\right)\cot\phi = \frac{p_0 - p_i}{c + p_i\tan\phi}$$

(limited range for $\sigma_\theta \ge \sigma_z \ge \sigma_r$)

Ground loss + Ovalización. Soluciones elásticas

- **Tensiones anisótropas ($k_0 \neq 1$)** (Kirsch, 1898)

$$\varepsilon = \frac{u_0}{a} = \frac{p_0}{2G}\left(\frac{1+k_{0t}}{2} - \frac{p_i}{p_0}\right) \qquad \delta = \frac{max(u')}{a} = \frac{p_0}{2G}\frac{1-k_{0t}}{2}(3-4\mu)$$

- **Superficie libre** (Verruijt, 1997)

$$\frac{u}{a} = \frac{p_0 - p_i}{2G}\left[1 + 2(1-\mu)\frac{\cos\theta}{h/a - \cos\theta}\right] \; ; \; \frac{v}{a} = \frac{p_0 - p_i}{2G} 2(1-\mu)\frac{\sin\theta}{h/a - \cos\theta}$$

$$\varepsilon = \frac{p_0 - p_i}{2G}\left[1 + 2(1-\mu)\frac{2\frac{h}{a}\left(\frac{h}{a} - \sqrt{\left(\frac{h}{a}\right)^2 - 1}\right) - 1}{1 - \frac{h}{a}\left(\frac{h}{a} - \sqrt{\left(\frac{h}{a}\right)^2 - 1}\right)}\right]$$

$$\delta = \frac{p_0 - p_i}{2G}(1-\mu)\frac{1}{\left(\frac{h}{a}\right)^2 - 1}$$

$$\frac{u_z}{a} = \frac{p_0 - p_i}{2G}(1-\mu)\frac{2\frac{h}{a}}{\left(\frac{h}{a}\right)^2 - 1}$$

• Superficie libre (Verruijt, 1997)

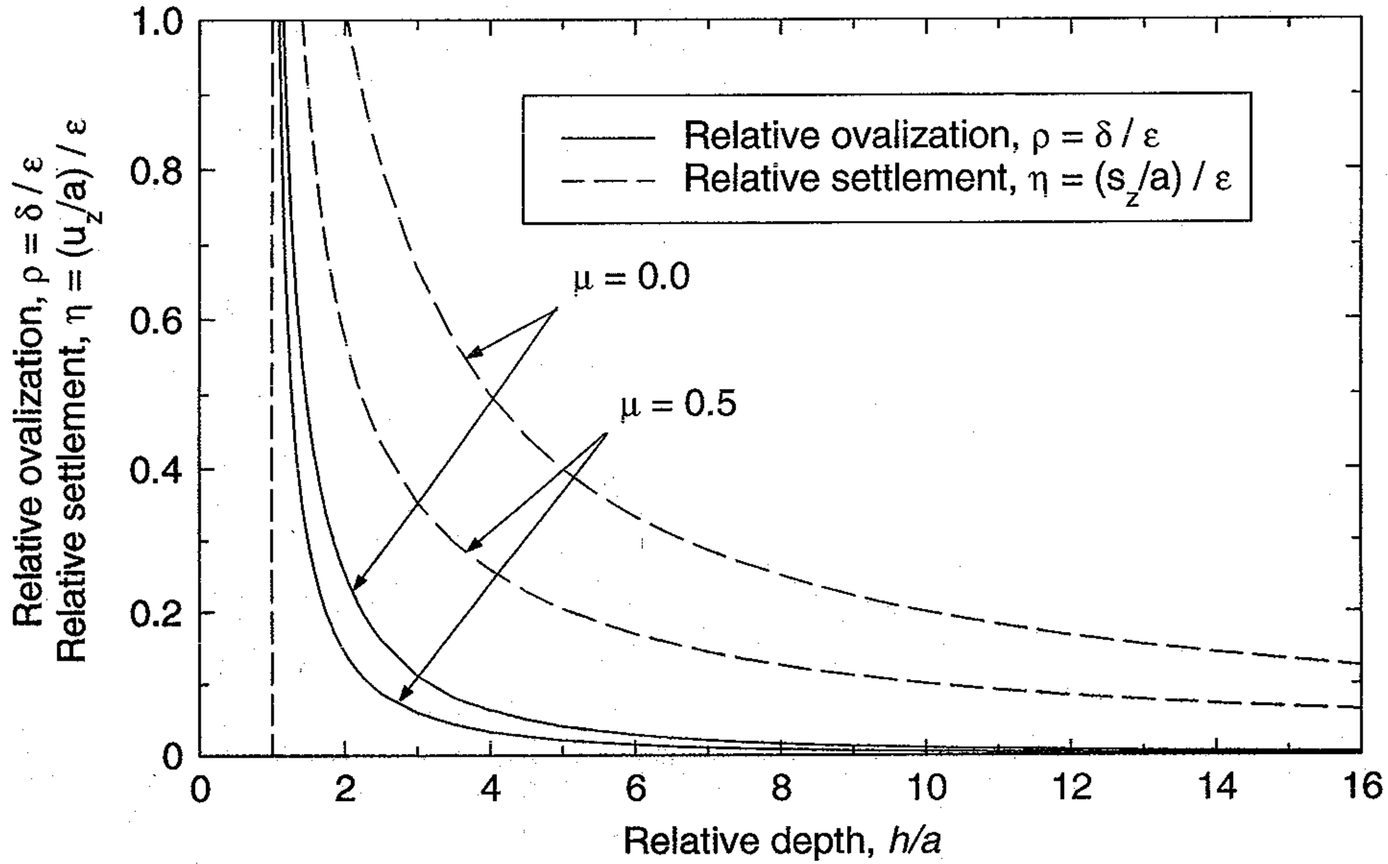

Comparación con casos reales. I)

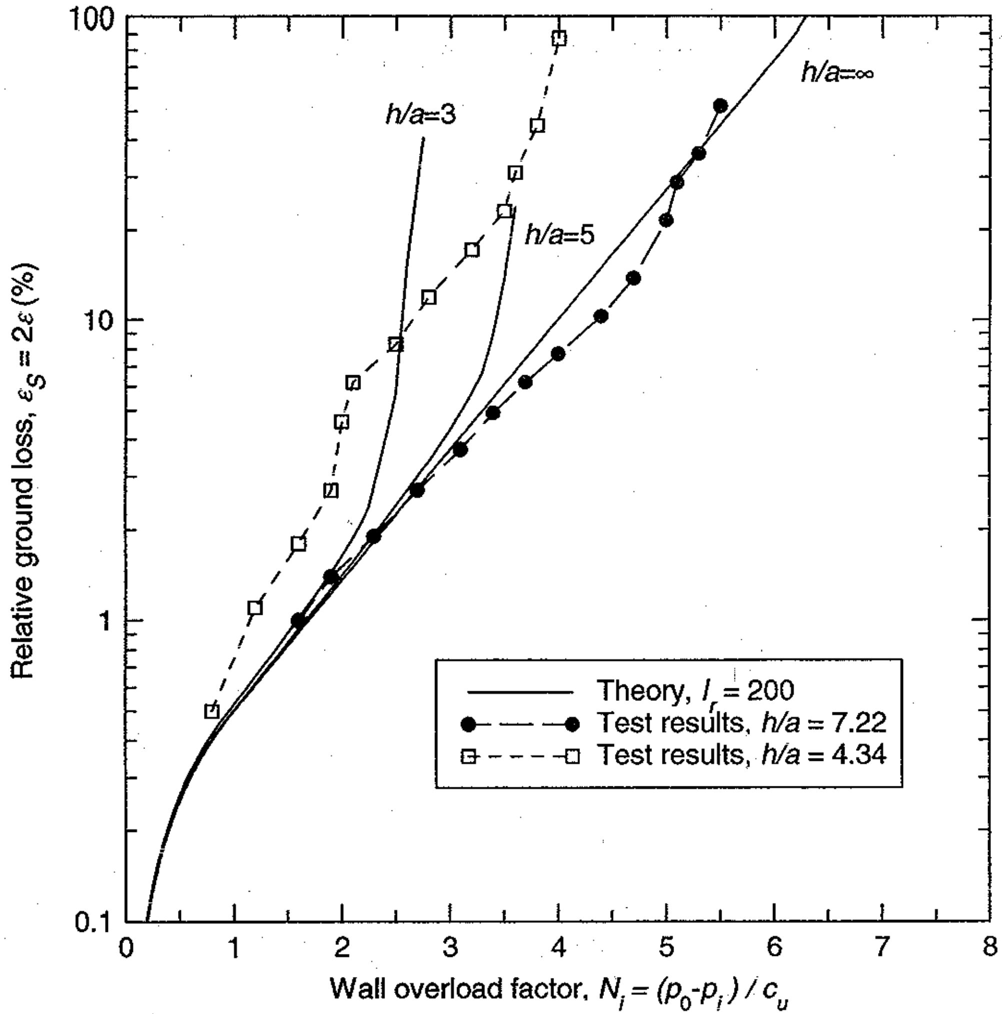

For $h/a = \infty : \varepsilon_s = \dfrac{1}{I_r} e^{N_i - 1}$

$\ln \varepsilon_s = N_i - 1 - \ln I_r$

Centrifuge tests

(Mair et al., 1981)

Comparación con casos reales. II)

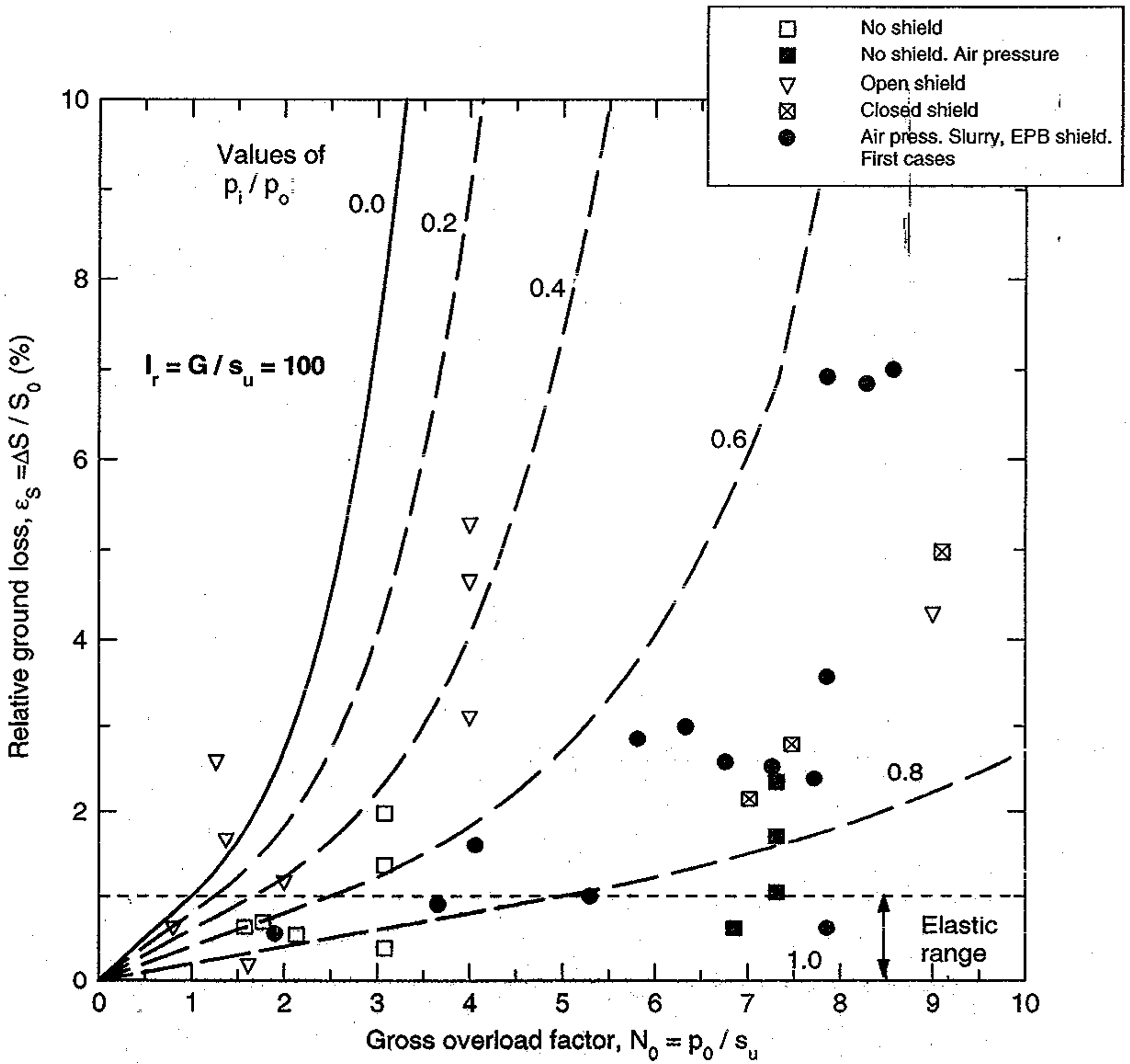

For $h/a = \infty$:

$$\varepsilon_s = \begin{cases} \dfrac{1}{I_r} N_t = \dfrac{1}{I_r} N_0 \left(1 - \dfrac{p_i}{p_0}\right) & (N_t \le 1) \\ \dfrac{1}{I_r} e^{N_t - 1} = \dfrac{1}{I_r} e^{N_0\left(1 - \frac{p_i}{p_0}\right) - 1} & (N_t \ge 1) \end{cases}$$

Tunnels in clay.

Ground loss

Comparación con casos reales. III)

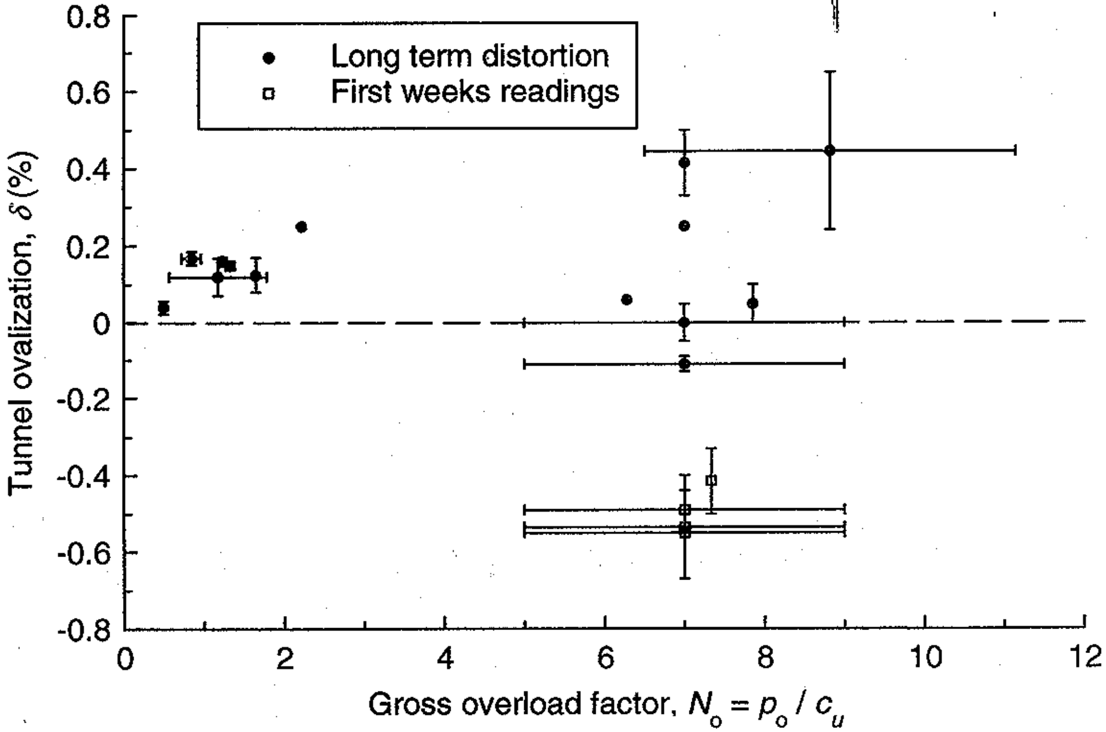

Tunnels in clay.

Ovalization

(Data from Peck, 1969)

Deformaciones en zonas alejadas. Solución analítica

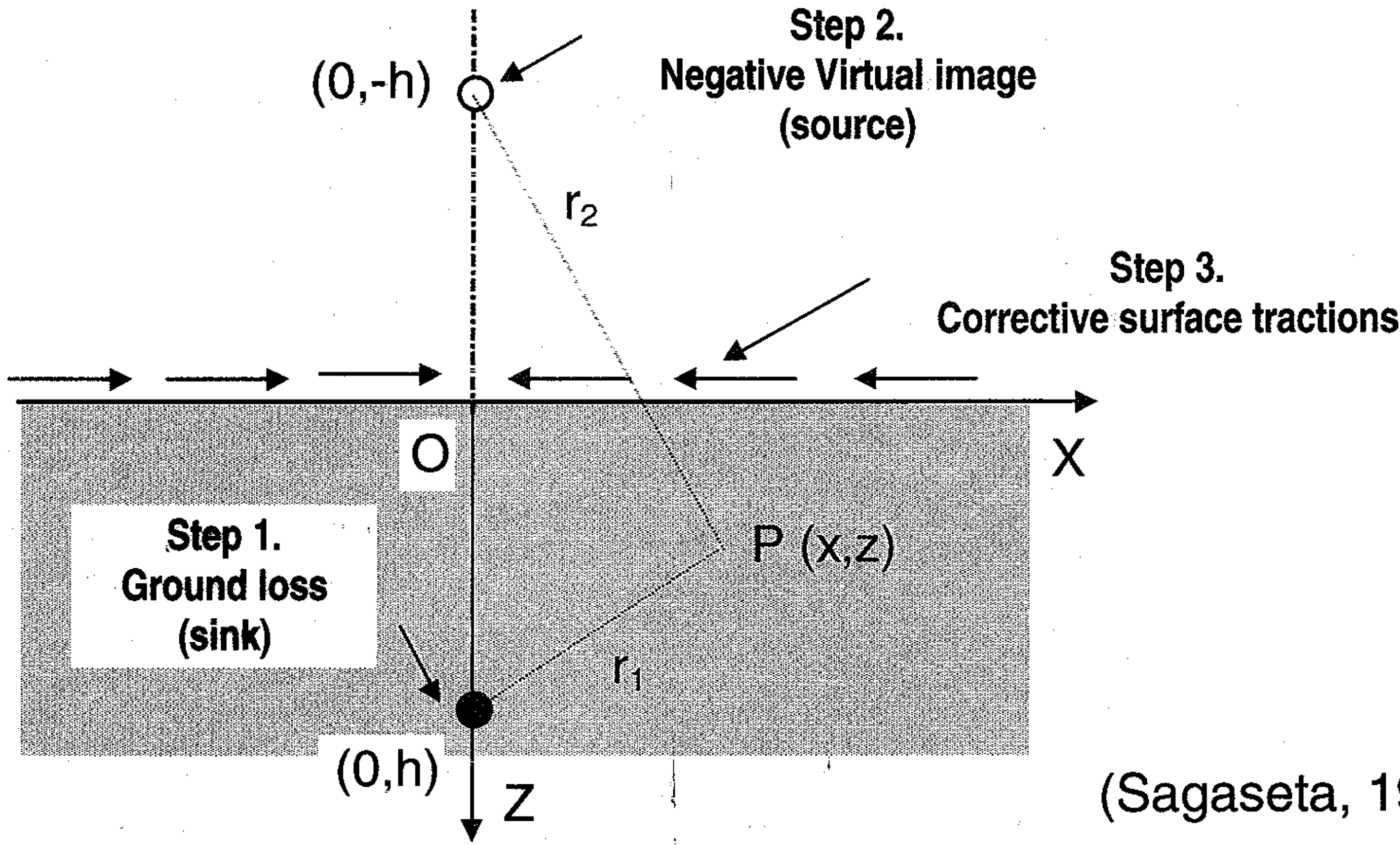

(Sagaseta, 1987)

Formulación (1)

- **Contracción radial** (Sagaseta, 1987)

$$s_x = -\varepsilon a \frac{a}{h}\left[x'\left(\frac{1}{r'^2_1}+\frac{1}{r'^2_2}\right)-4x'z'z'_2\frac{1}{r'^4_2}\right]$$

$$s_z = -\varepsilon a \frac{a}{h}\left[z'_1\left(\frac{1}{r'^2_1}+\frac{1}{r'^2_2}\right)-4x'^2z'\frac{1}{r'^4_2}\right]$$

$$s_{x(z=0)} = 2\varepsilon a \frac{a}{h}\frac{x'}{1+x'^2}$$

$$s_{z(z=0)} = 2\varepsilon a \frac{a}{h}\frac{1}{1+x'^2}$$

$$\left(x_i' = \frac{x_i}{h}\right)$$

- **Ovalización** (Verruijt and Booker, 1996)

$$\text{Additional}:\begin{cases} s_x = \delta a \dfrac{a}{h}\left[x'\left(\dfrac{x'^2-z'^2_1}{r'^4_1}+\dfrac{x'^2-z'^2_2}{r'^4_2}\right)-4x'z'\dfrac{x'^2-3z'^2_2}{r'^6_2}\right] \\ s_z = \delta a \dfrac{a}{h}\left[z'_1\left(\dfrac{x'^2-z'^2_1}{r'^4_1}+\dfrac{x'^2-z'^2_2}{r'^4_2}\right)-4z'z'_2\dfrac{3x'^2-z'^2_2}{r'^6_2}\right] \end{cases}$$

Formulación (2)

- **Deformaciones volumétricas**

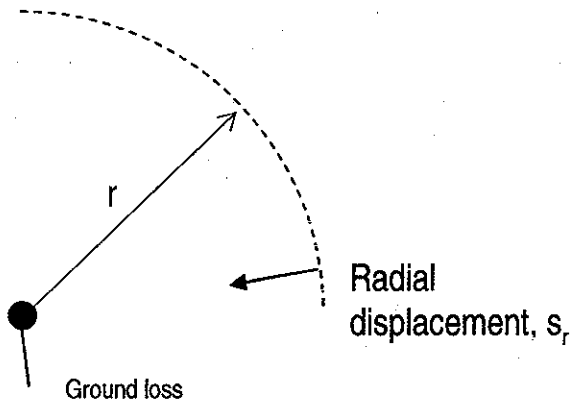

a) Basic case (incompressible):

$$\varepsilon_{vol} = \frac{\partial s_r}{\partial r} + \frac{s_r}{r} = 0 \quad \rightarrow \quad s_r = \frac{k}{r}$$

b) Compressibility (dilatancy):

$$\left.\begin{aligned} \varepsilon_{vol} &= -\sin\nu \cdot \gamma_{max} \\ \varepsilon_{vol} &= \frac{\partial s_r}{\partial r} + \frac{s_r}{r} \\ \gamma_{max} &= \frac{\partial s_r}{\partial r} - \frac{s_r}{r} \end{aligned}\right\} \rightarrow s_r = \frac{k}{r^m} \quad \left(m = \frac{1+\sin\nu}{1-\sin\nu} \right)$$

Formulación (3)

- **Efecto combinado** (González & Sagaseta, 2001)

$$\frac{s_x}{2\varepsilon a\left(\frac{a}{h}\right)^{2\alpha-1}} = -\frac{x'}{2r'^{2\alpha}_1}\left(1-\rho\frac{x'^2-z'^2_1}{r'^2_1}\right)-\frac{x'}{2r'^{2\alpha}_2}\left(1-\rho\frac{x'^2-z'^2_2}{r'^2_2}\right)+$$

$$+\frac{4x'z'}{2r'^{2\alpha}_2}\left(\frac{z'_2}{r'^2_2}-\rho\frac{x'^2-3z'^2_2}{r'^4_2}\right)$$

$$\frac{s_z}{2\varepsilon a\left(\frac{a}{h}\right)^{2\alpha-1}} = -\frac{z'_1}{2r'^{2\alpha}_1}\left(1-\rho\frac{x'^2-z'^2_1}{r'^2_1}\right)+\frac{z'_2}{2r'^{2\alpha}_2}\left(1+\rho\frac{x'^2-z'^2_2}{r'^2_2}\right)-$$

$$-\frac{1}{2r'^{2\alpha}_2}\left(2(z'+\rho)\frac{x'^2-z'^2_2}{r'^2_2}+4\rho z'z'_2\frac{3x'^2-z'^2_2}{r'^4_2}\right)$$

(.. cont.)

Formulation (4)

- **Efecto combinado (cont.)**

At the surface $(z = 0)$:

$$s_x = -2\varepsilon a\left(\frac{a}{h}\right)^{2\alpha-1} \cdot \frac{x'}{\left(1+x'^2\right)^{\alpha}}\left(1+\rho\frac{1-x'^2}{1+x'^2}\right)$$

$$s_z = 2\varepsilon a\left(\frac{a}{h}\right)^{2\alpha-1} \cdot \frac{1}{\left(1+x'^2\right)^{\alpha}}\left(1+\rho\frac{1-x'^2}{1+x'^2}\right)$$

Exponent α: Elastic: 1 Fully plastic: 2

Average: 1-2, depending on h/a

Applications to actual tunnels

Case	Ground	Tunnel data			Surface settlements		Parameters of the solution				Reference
		h (m)	a (m)	Method	V_s (%)	s_{max} (mm)	ε (%)	δ (%)	ρ	α	
Green Park. London	Stiff clay	29.4	2.07	Open shield	1.6	6.5	1.2	0.84	0.7	1.0	Attewell & Farmer, 1974
Thunder Bay	Soft clay	10.7	1.24	Open shield	8.3	50	7.5	7.5	1.0	1.0	Palmer & Belshaw, 1978
Heathrow express	Stiff clay	19	4.25	Open face	1.5	40	1.0	0.8	0.8	1.0	Deane & Bassett, 1995
Sewer. Bangkok	Clay	18.5	1.33	Open face	3.8	12	3.4	3.4	1.0	1.0	Phienwej, 1997
Baixa Station. Lisbon	Sand	25	5.6	Open face	0.8	30	2.4	2.4	1.0	1.5	Sagaseta et al., 1999
Sewer. Cairo	Clay	14	2.6	Air pr. shield	1.2	15	0.75	0.6	0.8	1.0	El Nahas et al., 1997
N-2. San Francisco	Soft clay	10	1.8	EPB shield	3.1	30	0.95	3.34	3.5	1.0	Clough et al., 1983
Sewer. Mexico City	Soft clay	12.75	2.0	EPB shield	3.6	30	0.4	1.8	4.5	1.0	Romo, 1997
Lyon Metro. P1-S1	Silt, sand	16	3.13	Slurry shield			0.162	0.355	2.2	1.7	Kastner et al., 1996
				(†)			- 0.121	0.000	0.0		
							0.041	0.355	8.7		
Lyon Metro. P2-S	Silt, sand	13	3.13	Slurry shield			0.015	0.076	5.1	1.7	Kastner et al., 1996
				(†)			- 0.191	0.020	- 0.1		
							- 0.176	0.096	- 0.6		

(†): The first row of values is for the passage of the tunnel face, the second one for the incremental movements due to the tail grout and third one the final (accumulated) displacements

Lyon Metro (Kastner et al., 1996)

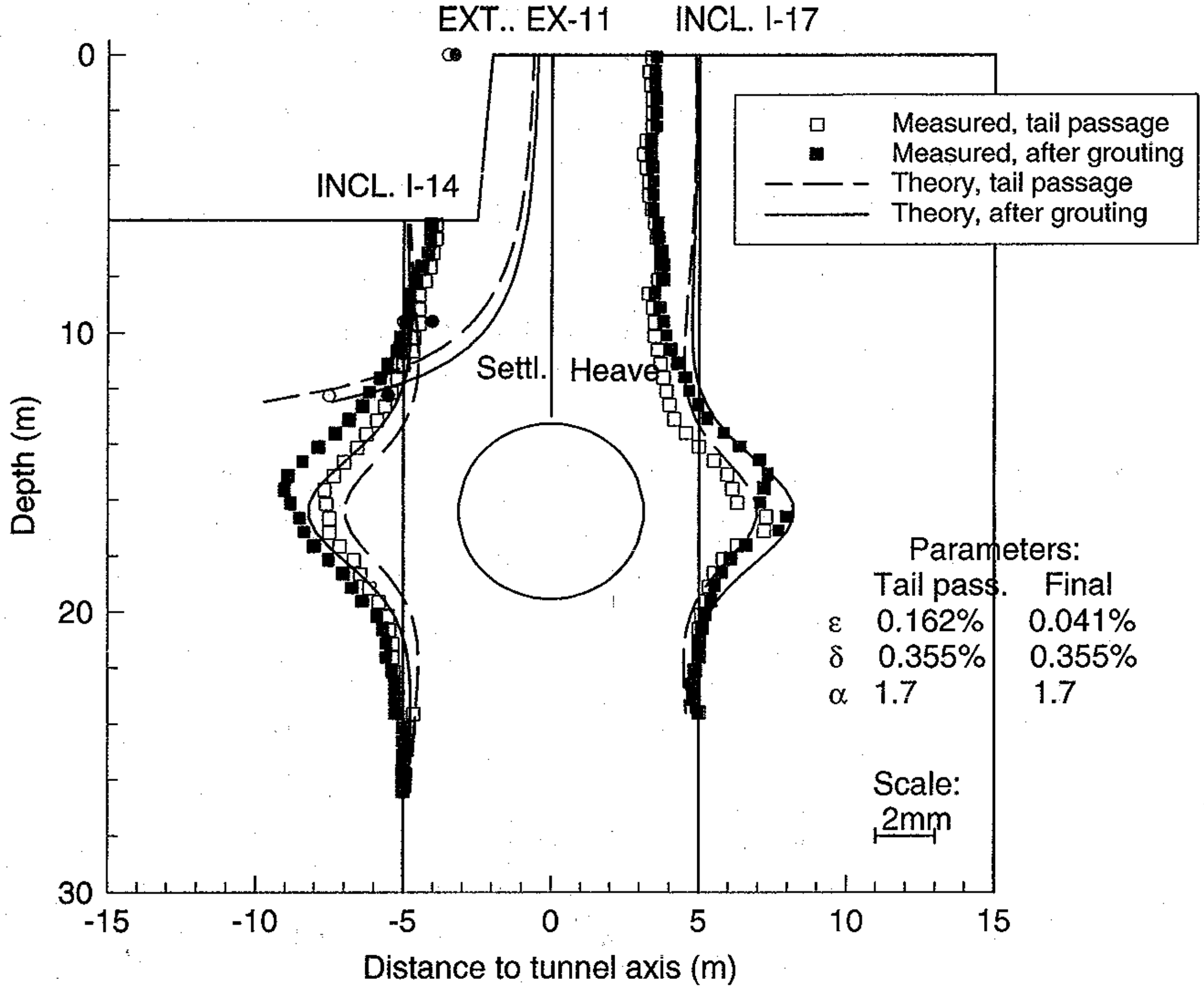

Madrid Metro. 1995-99 Extension Plan

(total: ≈ 40 km of new tunnels)

Some data:

Total length: 37.9 km

• E.P.B. 9.5 m diameter:	18.34 km
• E.P.B. 6.7 m diameter:	10.87 km
• Hand excavation (belgian method):	8.08 km

Stations: 35

• Cut and cover:	34
• Manual excavation (multistage):	1

Main design and construction criteria:

Maximum open face excavation area: 7 m^2

All full open face methods (N.A.T.M., premill, ...) discarded

Ground conditions

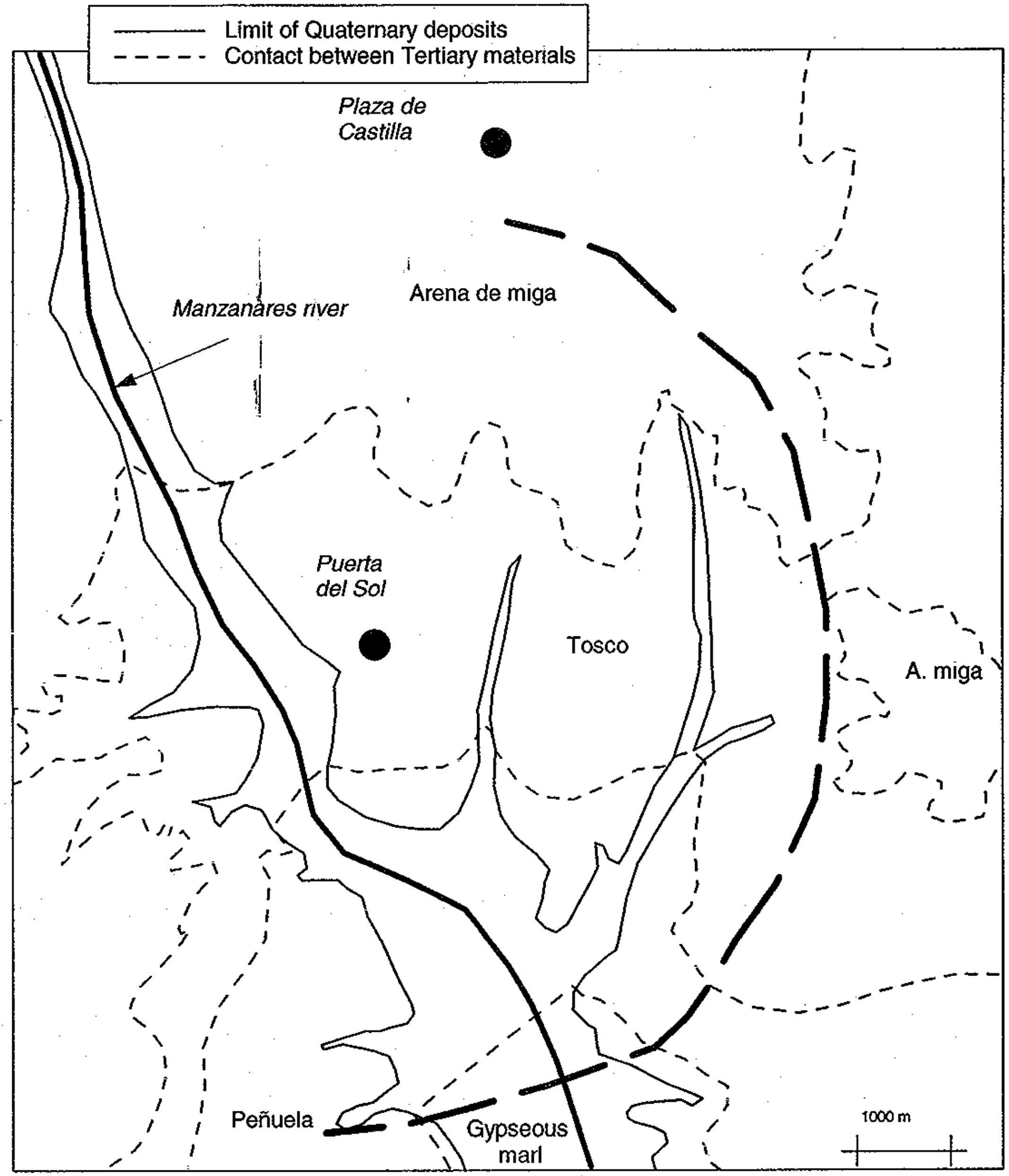

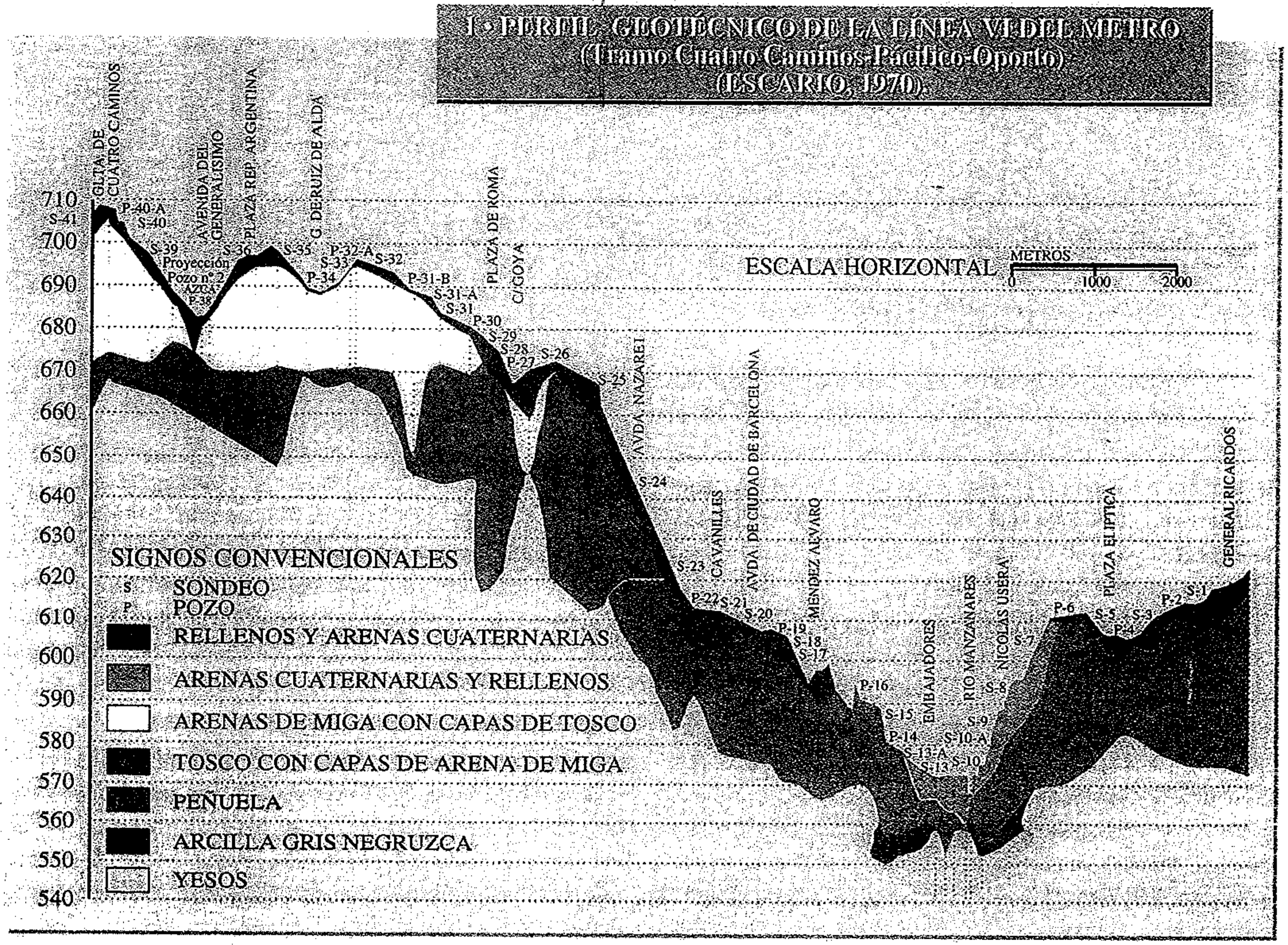
1 · PERFIL GEOTÉCNICO DE LA LÍNEA VI DEL METRO
(Tramo Cuatro Caminos-Pacífico-Oporto)
(ESCARIO, 1970).
ESCALA HORIZONTAL
METROS
0
1000
2000
SIGNOS CONVENCIONALES
S SONDEO
P POZO
RELLENOS Y ARENAS CUATERNARIAS
ARENAS CUATERNARIAS Y RELLENOS
ARENAS DE MIGA CON CAPAS DE TOSCO
TOSCO CON CAPAS DE ARENA DE MIGA
PEÑUELA
ARCILLA GRIS NEGRUZCA
YESOS
GLTA. DE CUATRO CAMINOS
AVENIDA DEL GENERALISIMO
PLAZA REP. ARGENTINA
G. DE RUIZ DE ALDA
PLAZA DE ROMA
C/GOYA
AVDA. NAZARET
CAVANILLES
AVDA. DE CIUDAD DE BARCELONA
MENDEZ ALVARO
EMBAJADORES
RIO MANZANARES
NICOLAS USERA
PLAZA ELIPTICA
GENERAL RICARDOS

Geotechnical properties of "tosco"

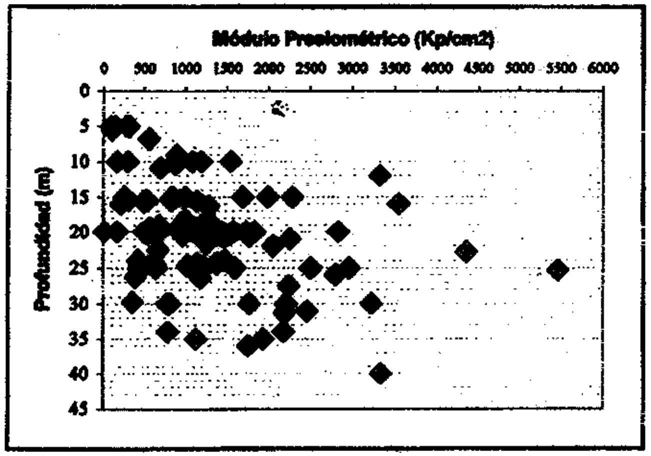

Figura 4.23. Distribución del módulo presiométrico con la profundidad en el tosco.

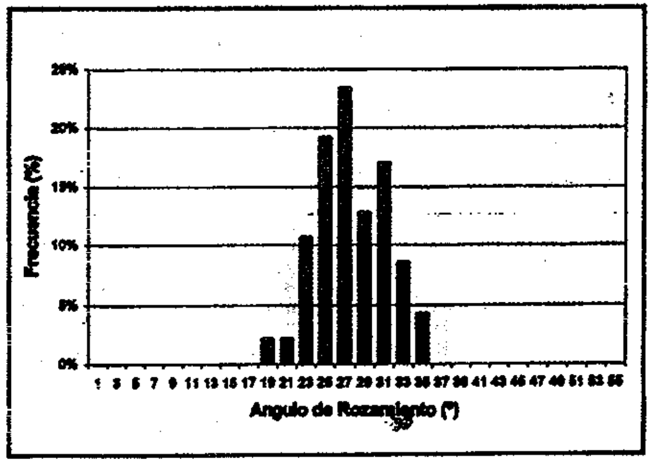

Figura 4.19. Ángulo de rozamiento en el tosco.

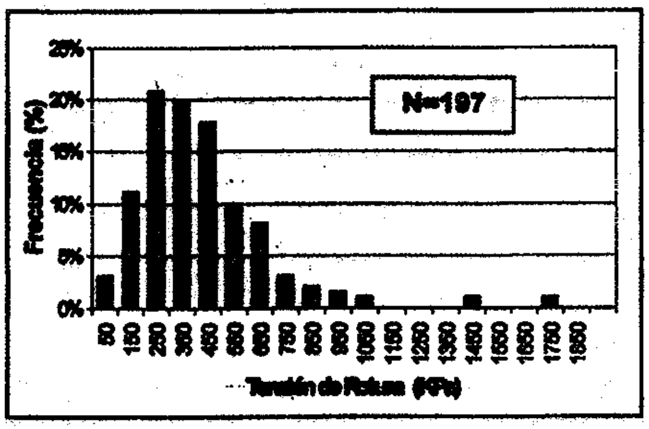

Figura 4.18. Compresión simple del tosco.

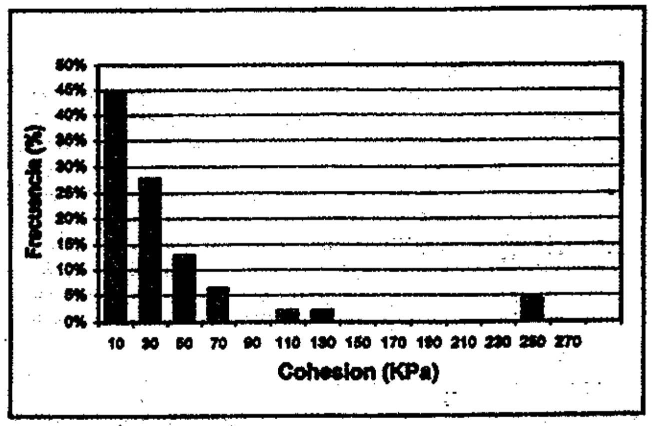

Figura 4.20. Cohesión efectiva en el tosco.

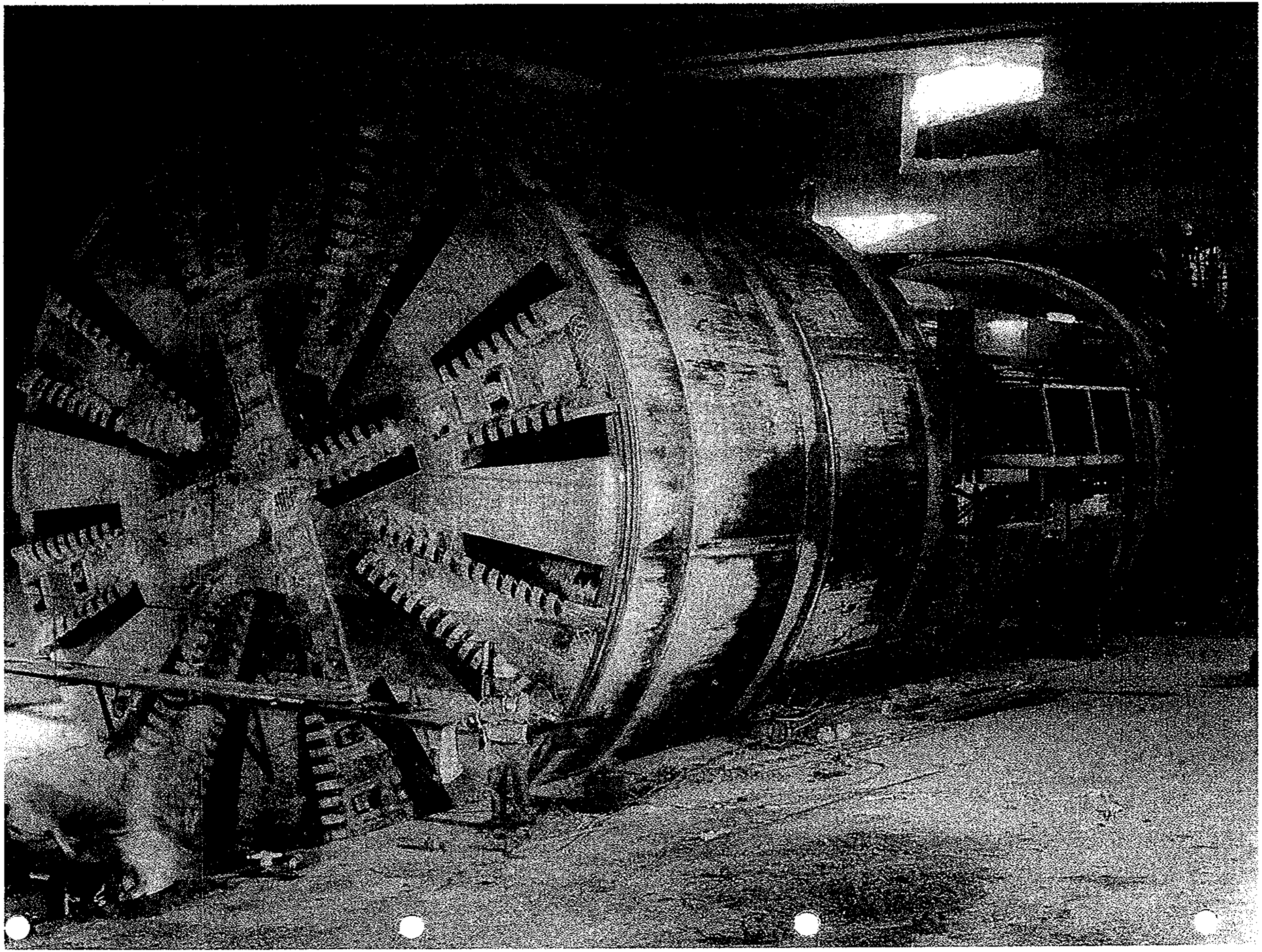

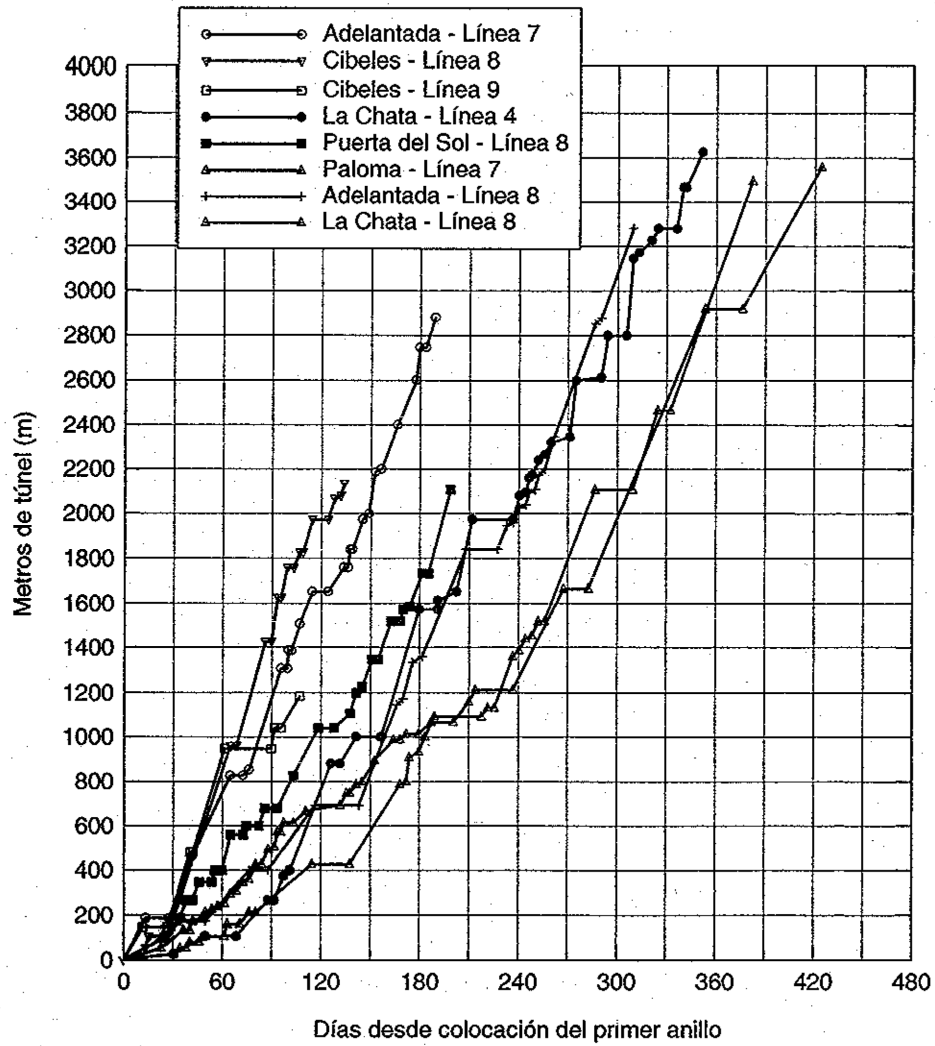

Adelantada - Línea 7
Cibeles - Línea 8
Cibeles - Línea 9
La Chata - Línea 4
Puerta del Sol - Línea 8
Paloma - Línea 7
Adelantada - Línea 8
La Chata - Línea 8
Metros de túnel (m)
0
200
400
600
800
1000
1200
1400
1600
1800
2000
2200
2400
2600
2800
3000
3200
3400
3600
3800
4000
0
60
120
180
240
300
360
420
480
Días desde colocación del primer anillo

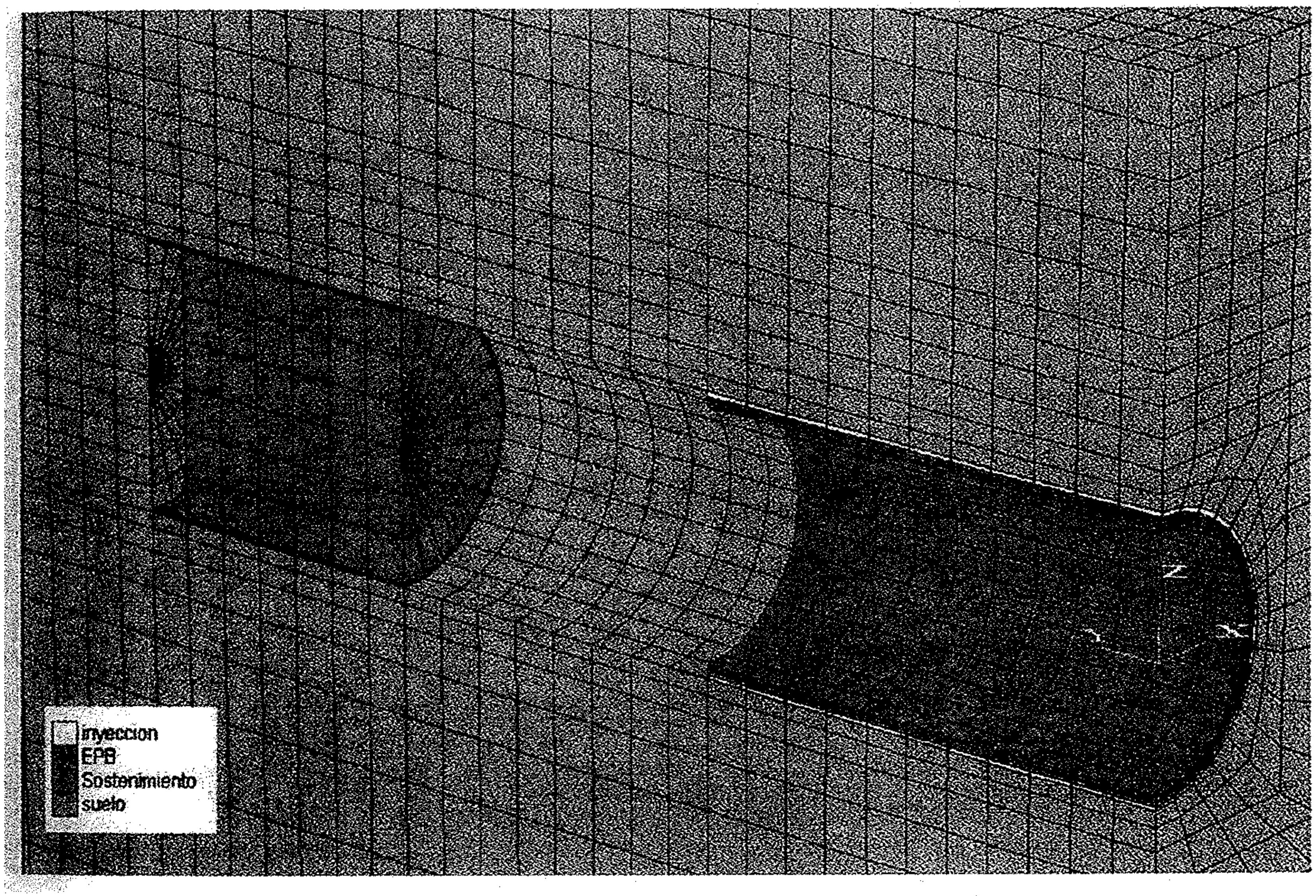

3-D numerical analysis (Medina, 1999)

Extension of Madrid Metro 1995-99

Summary of measured movements

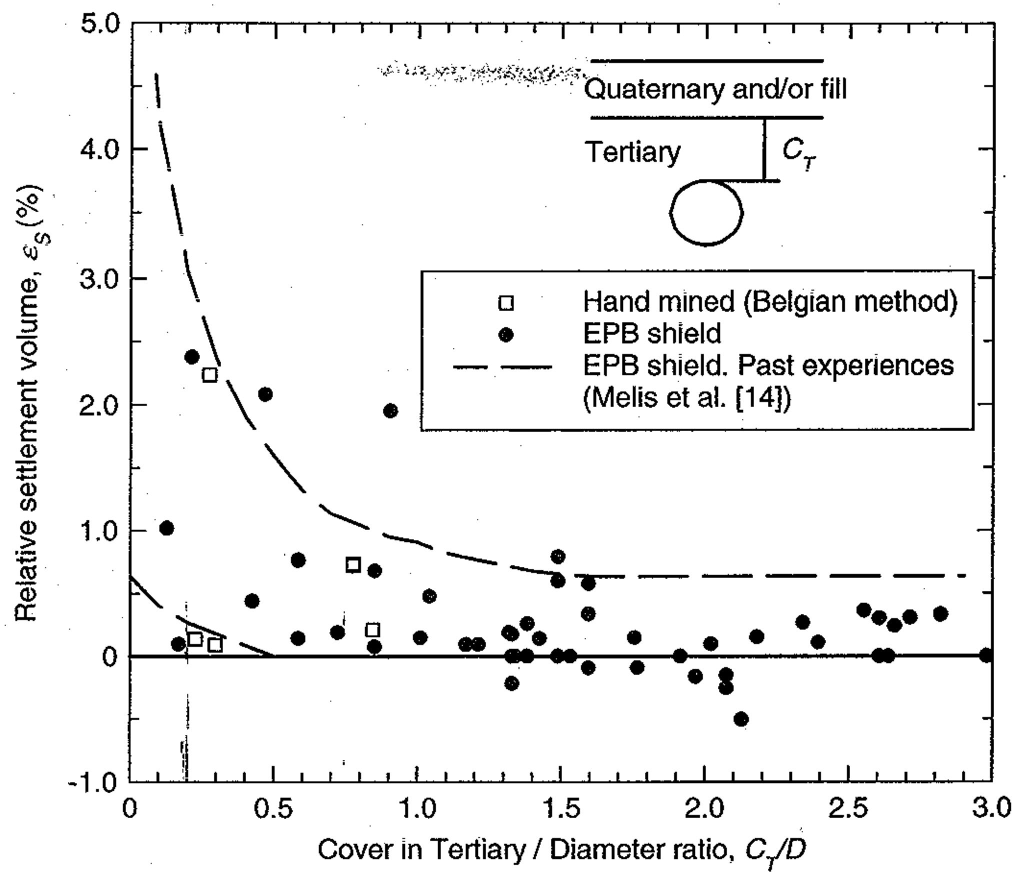

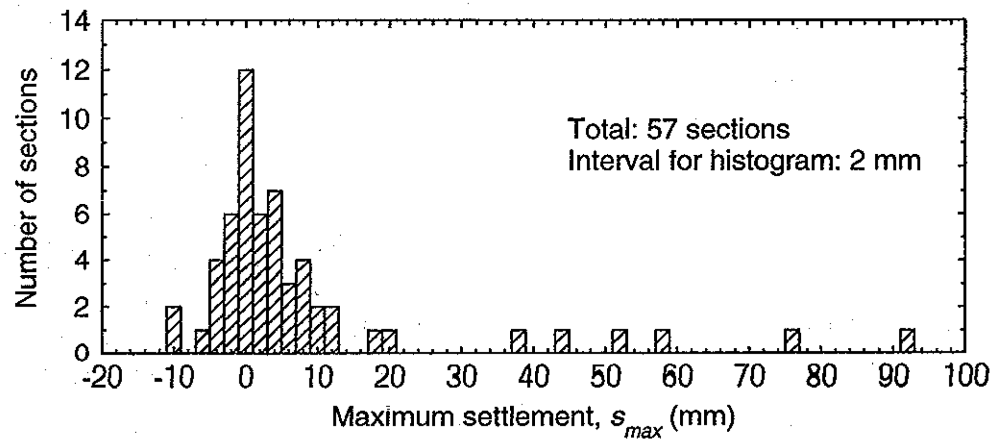

Fitted parameters of the solution

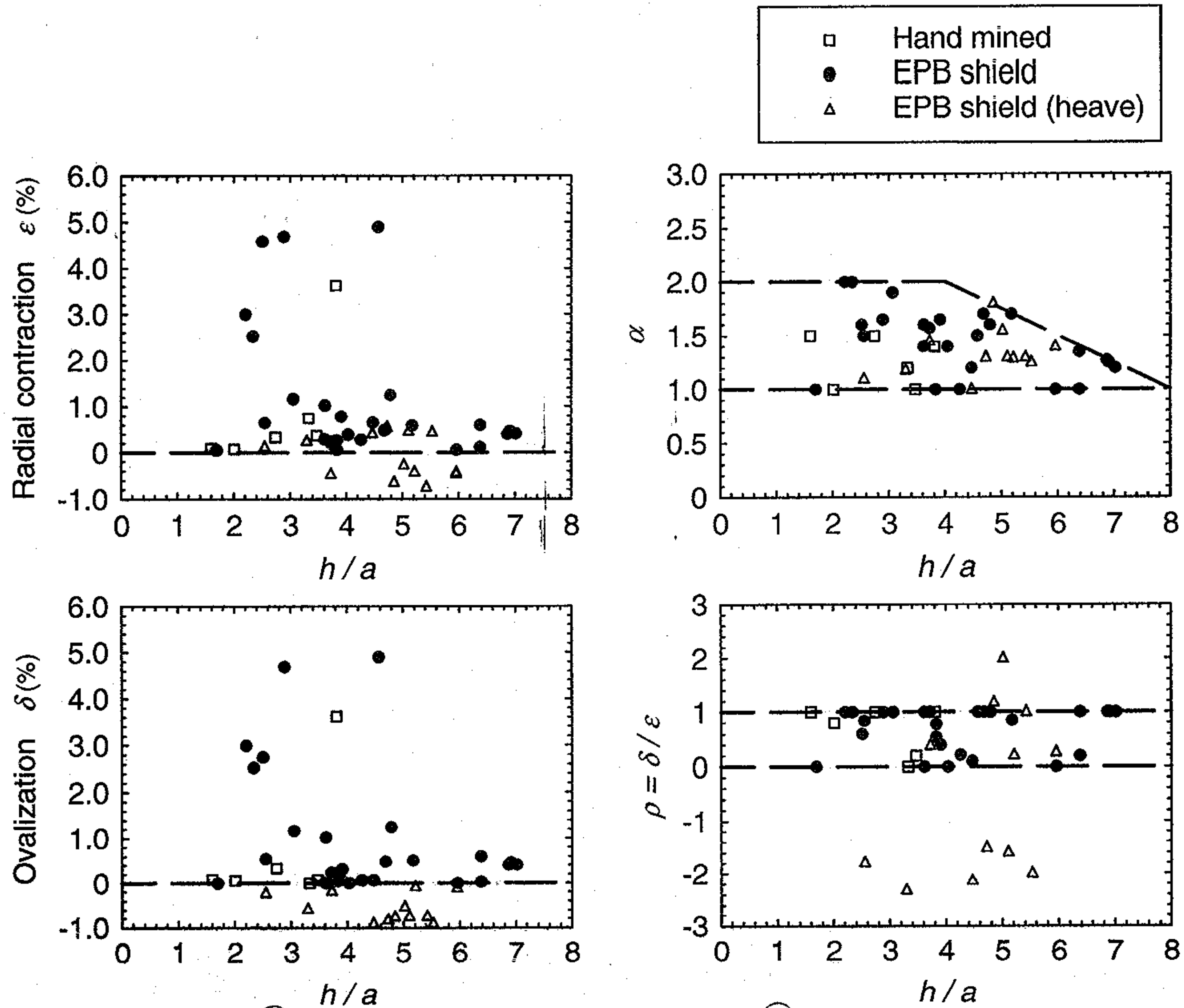

Fitted parameters of the solution (detail)

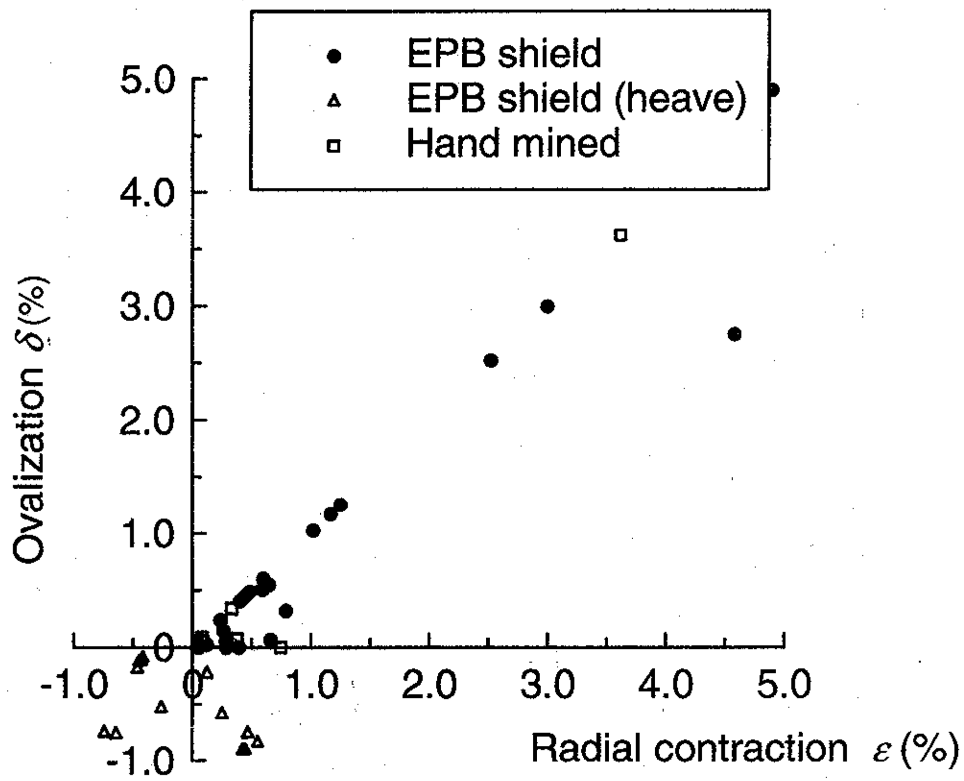

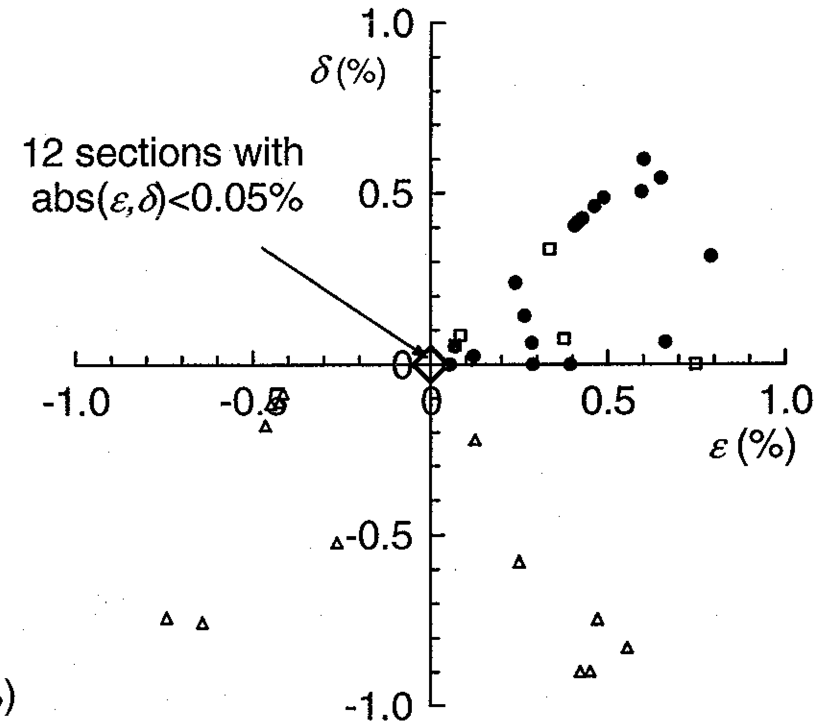

Volumetric compressibility exponent, α

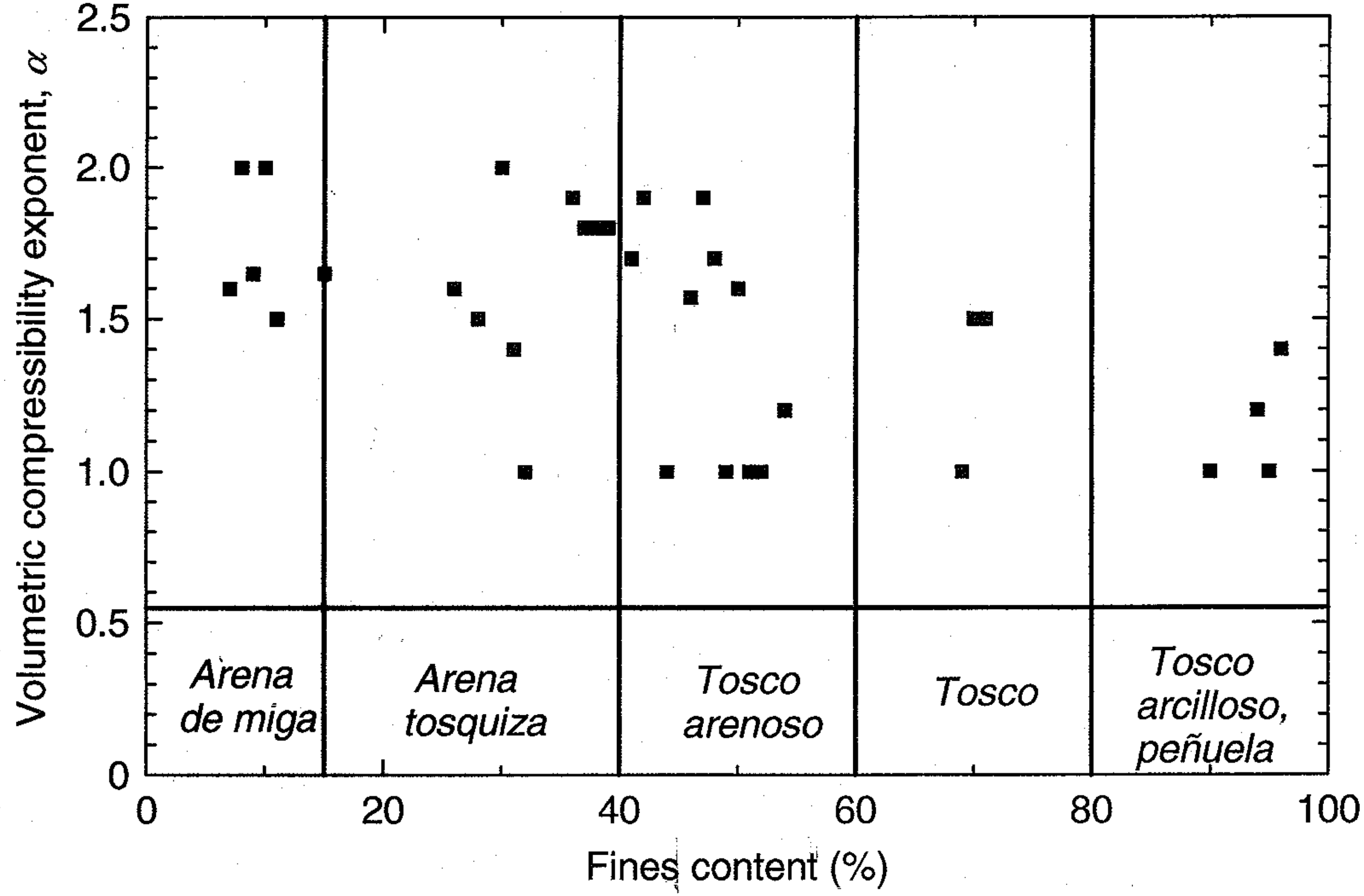

Case with settlements

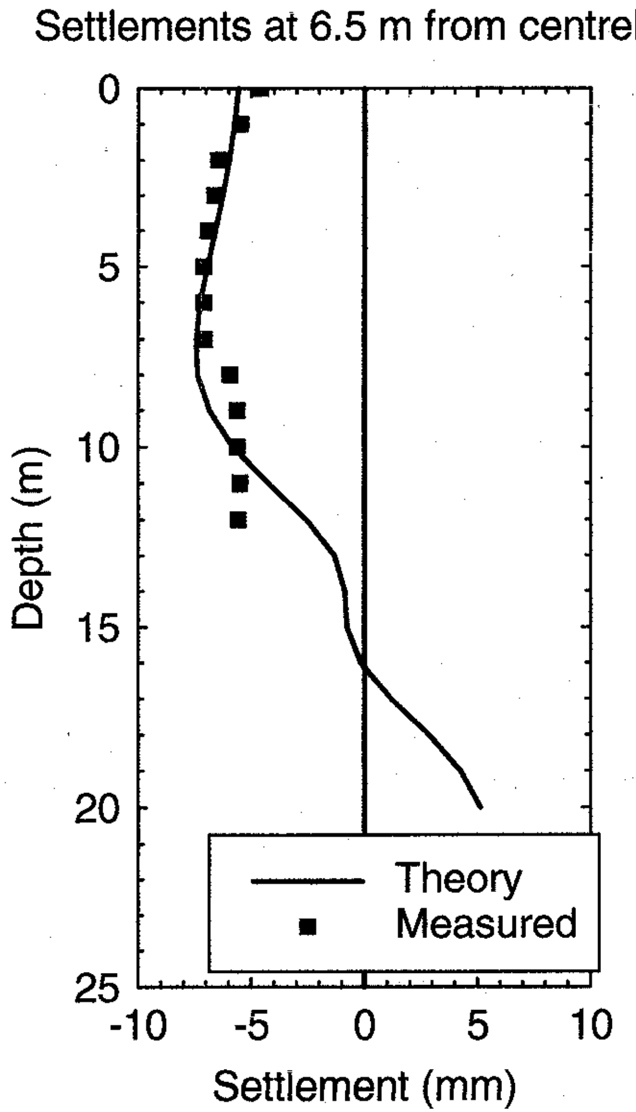

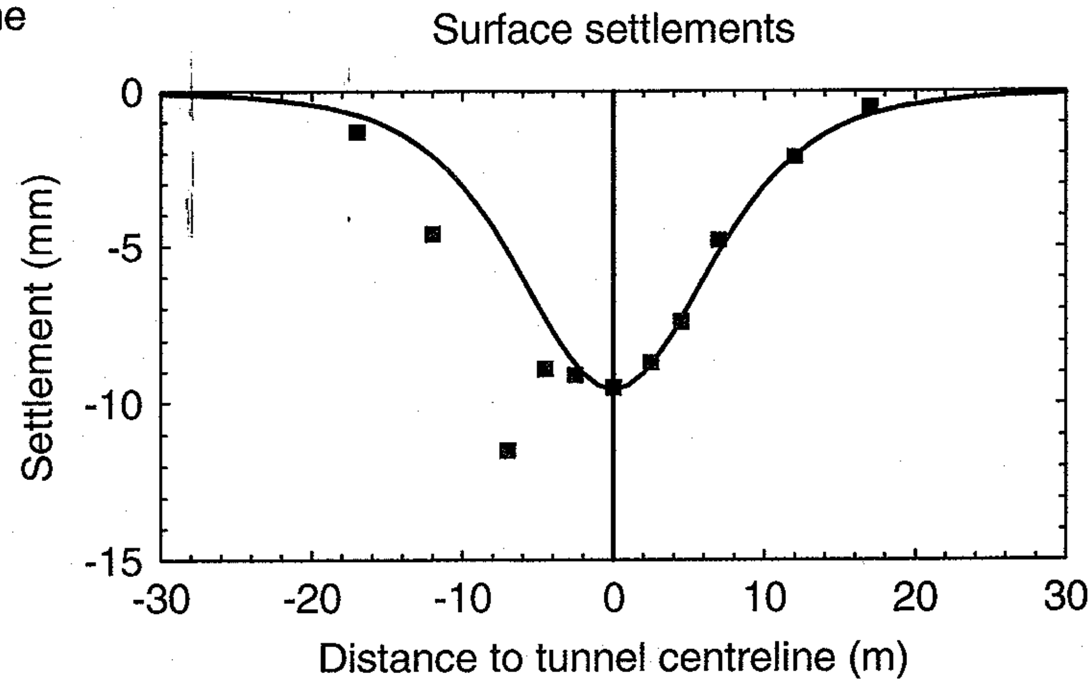

Solution parameters:

$s_{max} = 9.55$ mm

$\alpha = 1,9$

$\varepsilon = 1,16\%$

$\delta = 1,16\%$

$\rho = 1,0$

Depth, $h = 14,4$ m

Case with general heave

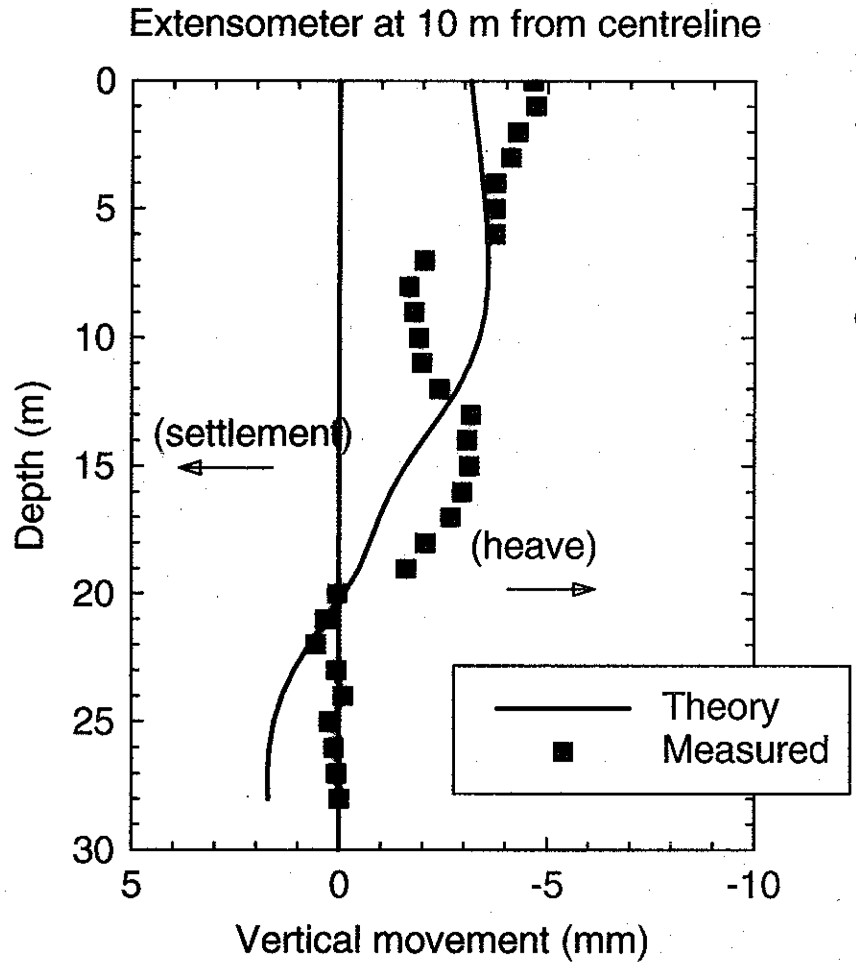

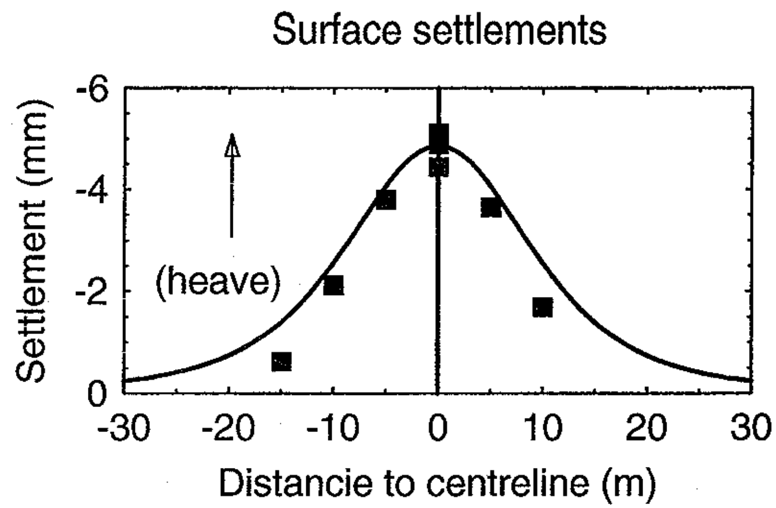

Solution parameters:
s_{max} = - 4,8 mm (heave)
$\Delta V_s / V_0$ = -0,187 % (heave)
$\alpha = 1.45$
$\varepsilon = -0.36\%$
$\delta = -0.27\%$
$\rho = 0{,}75$

Depth: h = 17.5 m

Case with heave and settlements

Inclinometer at 6 m from centreline

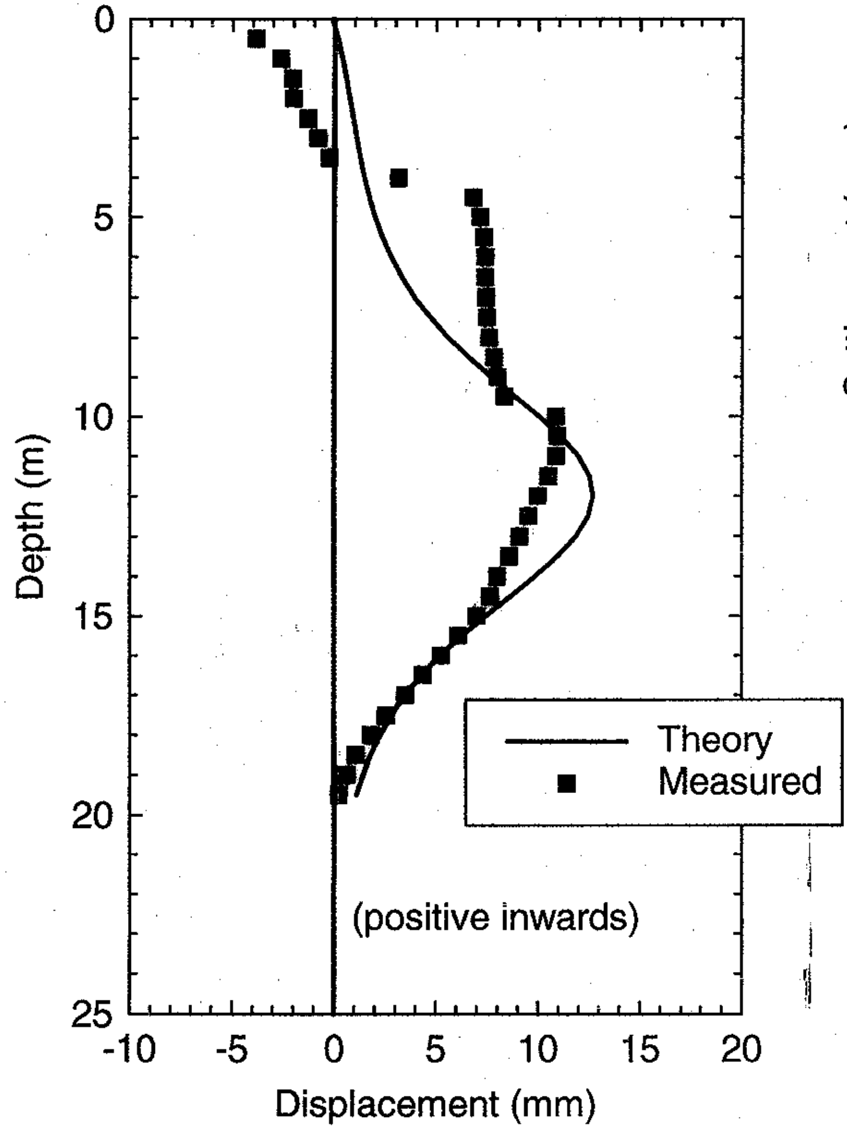

Surface and deep settlements

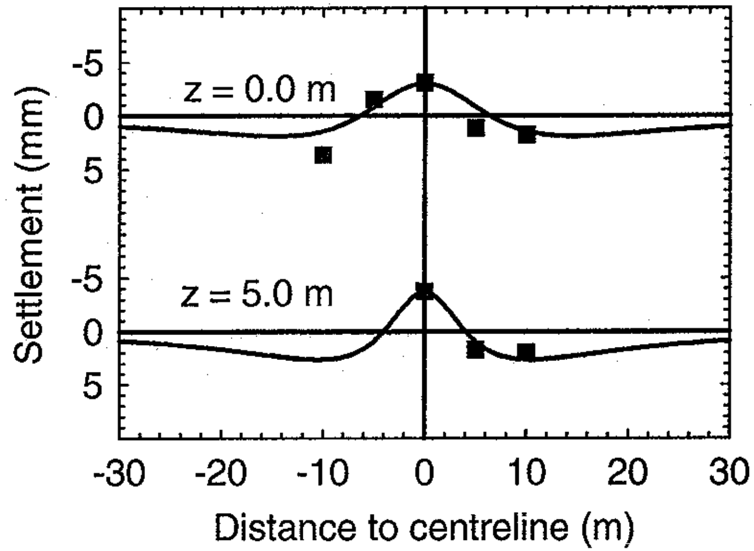

Solution parameters:
$s_{m,ax}$ = - 3,0 mm (heave)
$\Delta V_s / V_0$ = 0,145 % (settlement)
α = 1.1
ε = 0.1257%
δ = -0.2245%
ρ = - 1,79

Depth: h = 12 m

A section in Metrosur (extension plan 1999-2003)

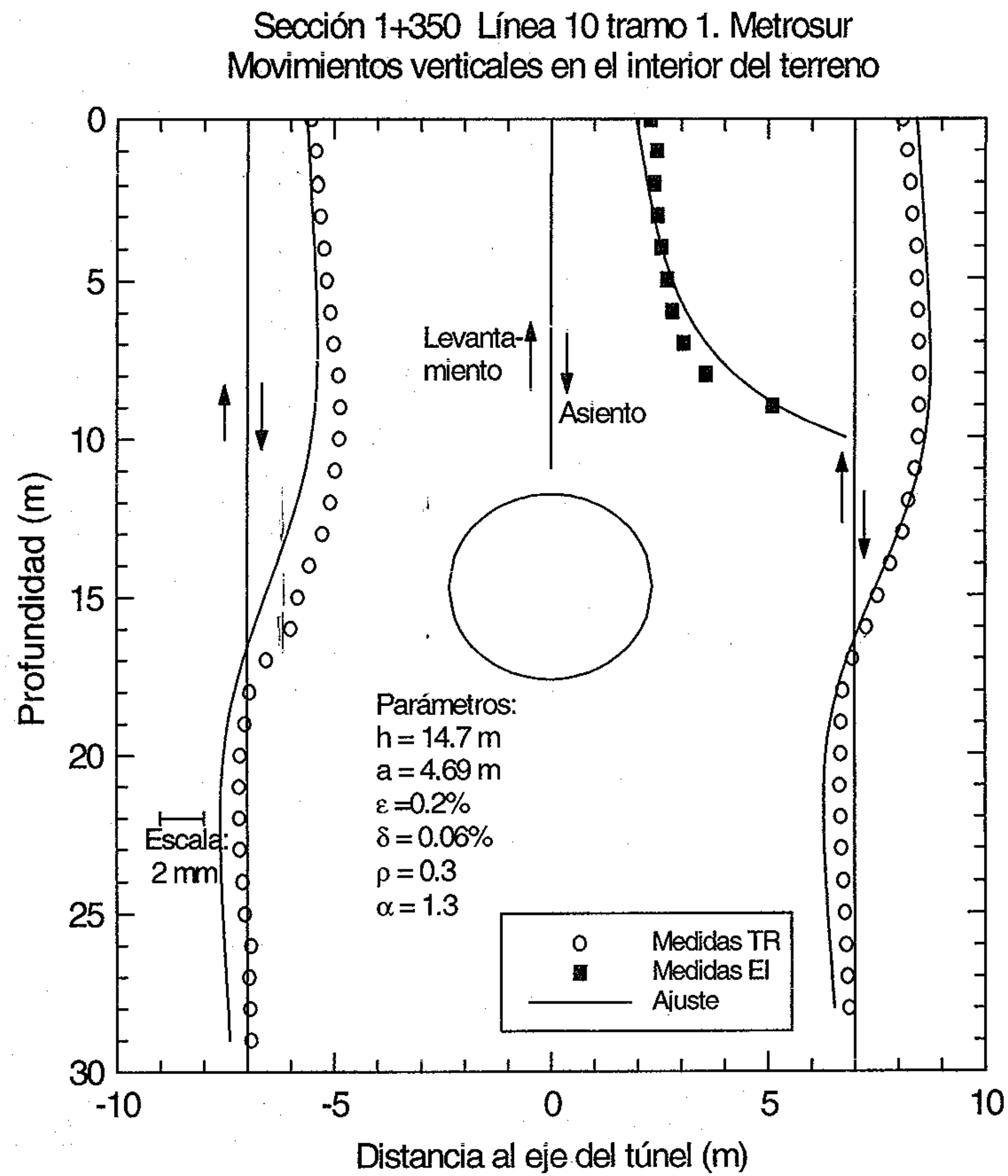

Application to pile driving

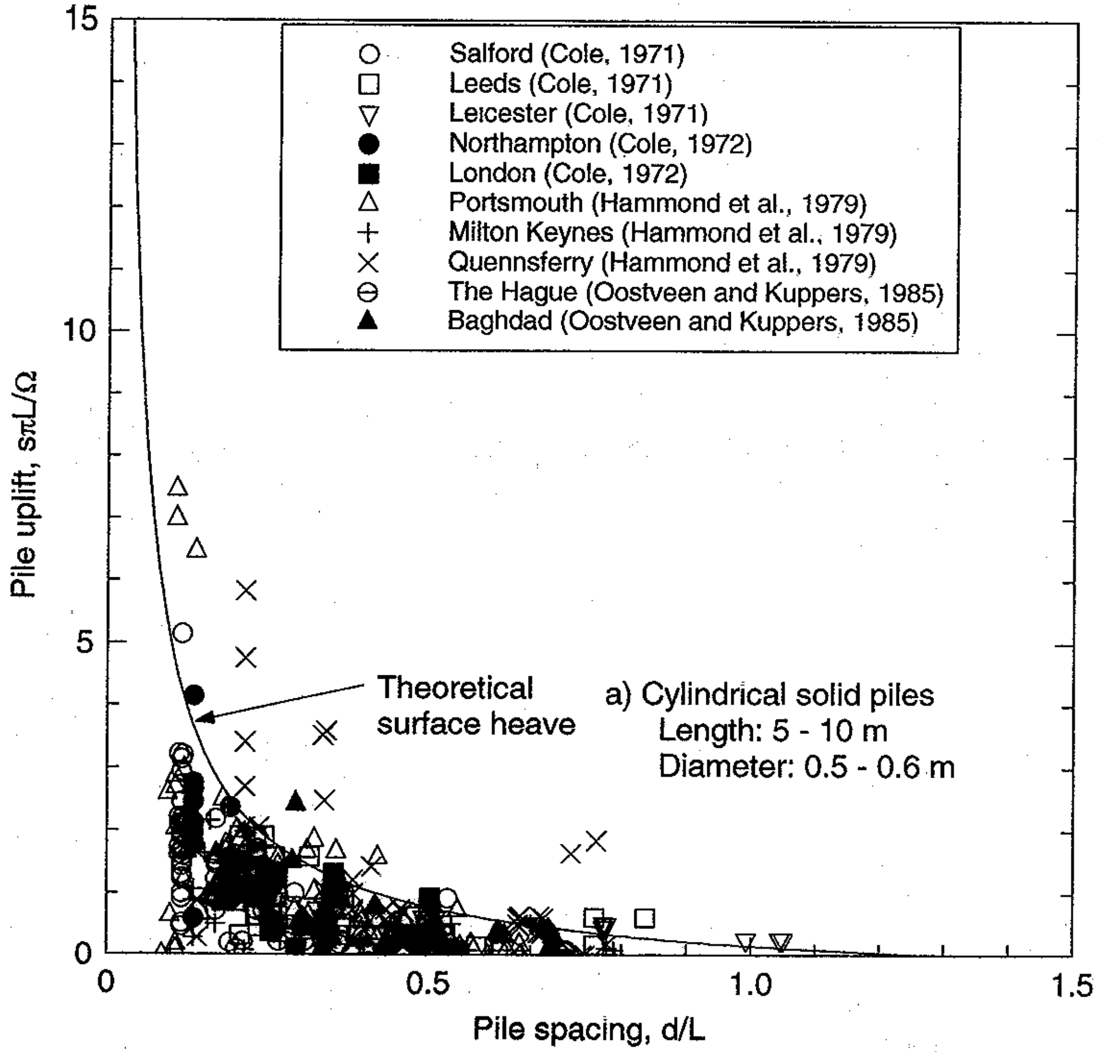

(Integration of point source along the pile axis)

(Sagaseta & Whittle, 2001)

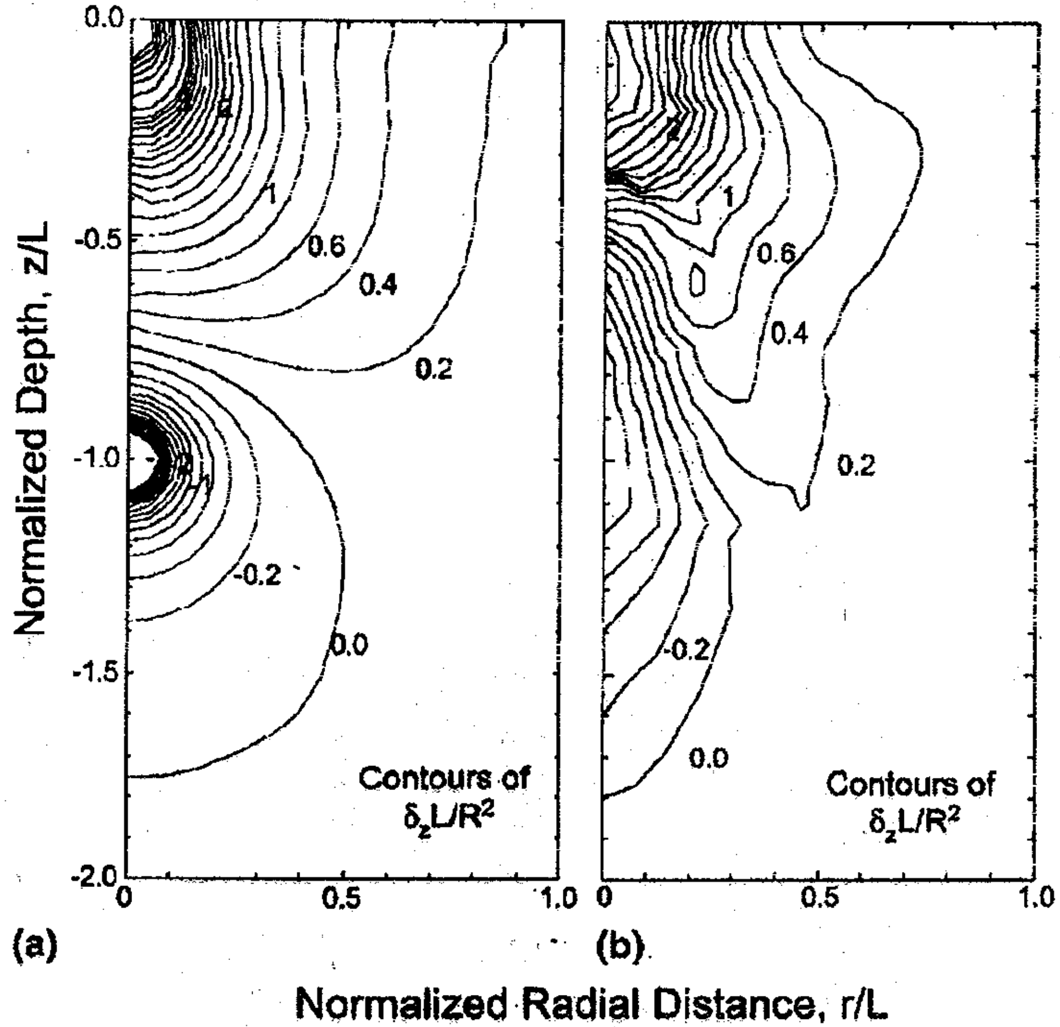

Pile driving tests at Hendon
(Cooke and Price, 1977)

(Sagaseta & Whittle, 2001)

Application to compensation grouting

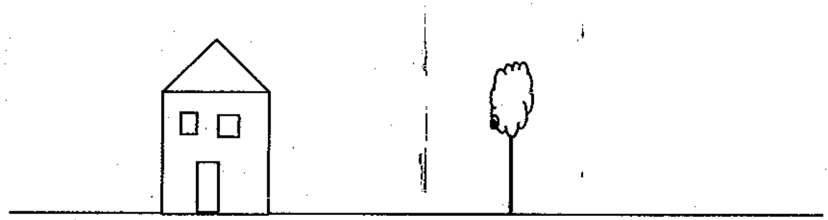

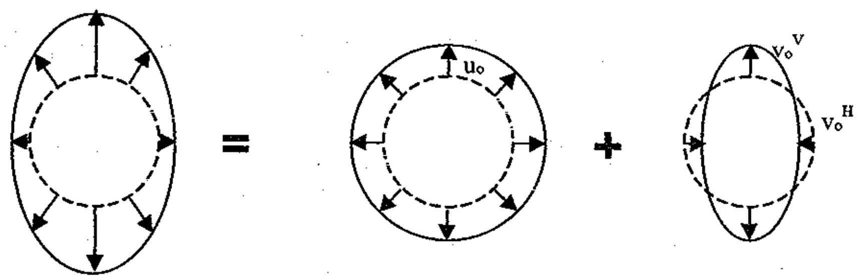

Deformación total   Deformación radial   Distorsión

Compensation grouting. Actual cases

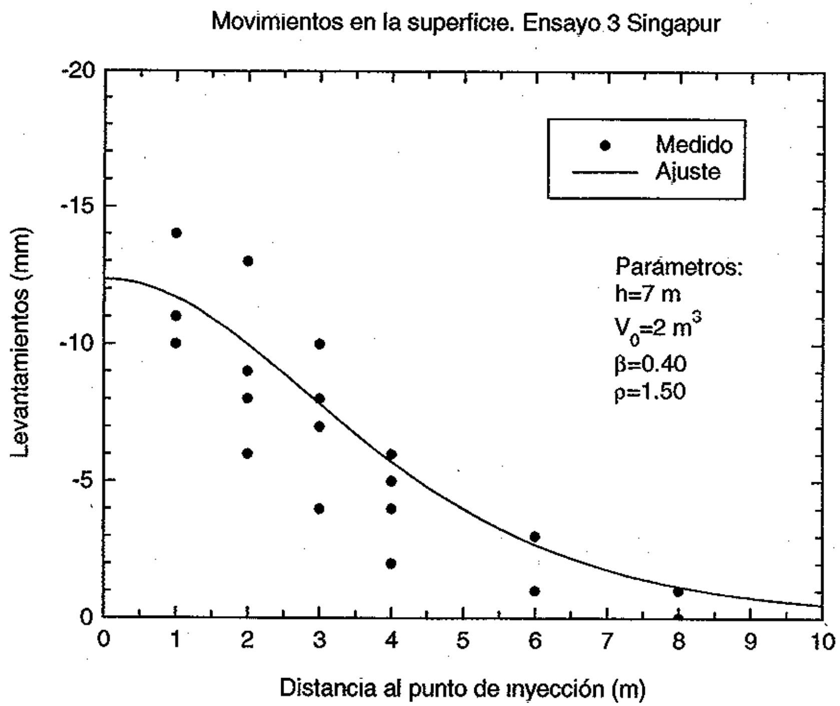

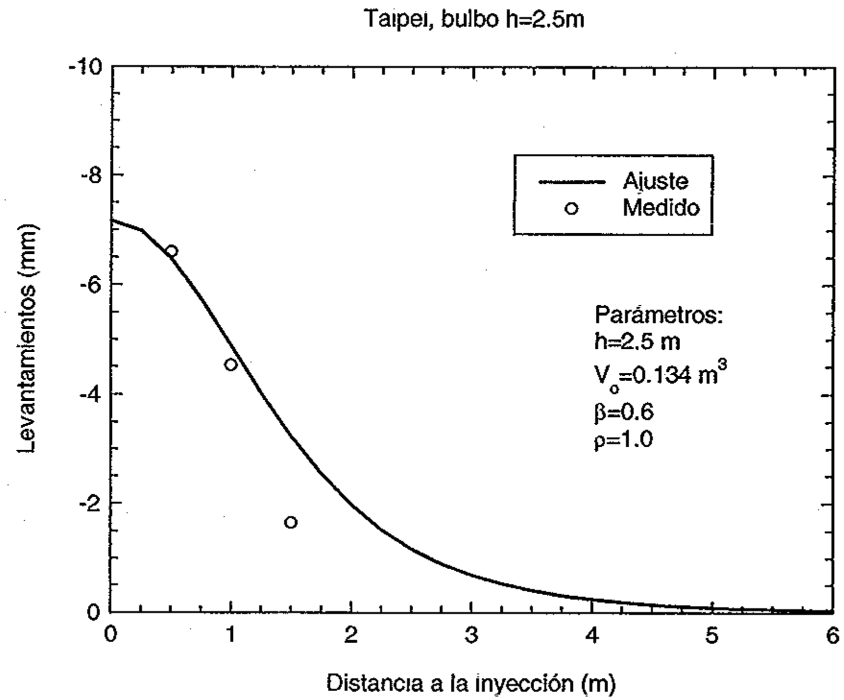

To conclude...

- In cases of 'simple' geometry, simple deformation patterns.
- Then, analytical solutions can provide useful results.
- In cases of careful tunnelling (EPB, ...), the control and continuous knowledge of construction variables provide a unique opportunity for a refined analysis of the results.
- In cases of careful tunnelling (EPB, ...), a *Class-A* prediction of the actual deformation pattern is not possible. The only reliable prediction is that if everything works well, the movements will be |*small*| (+ or -). However, once the actual results are known, *Class-C* predictions can be brilliant and rewarding.

Ground loss + Ovalization. Plastic strains

- In the elastic range, $\delta/\varepsilon \cong 0.10$
- δ/ε must increase with plastic strains
- Numerical analysis is needed

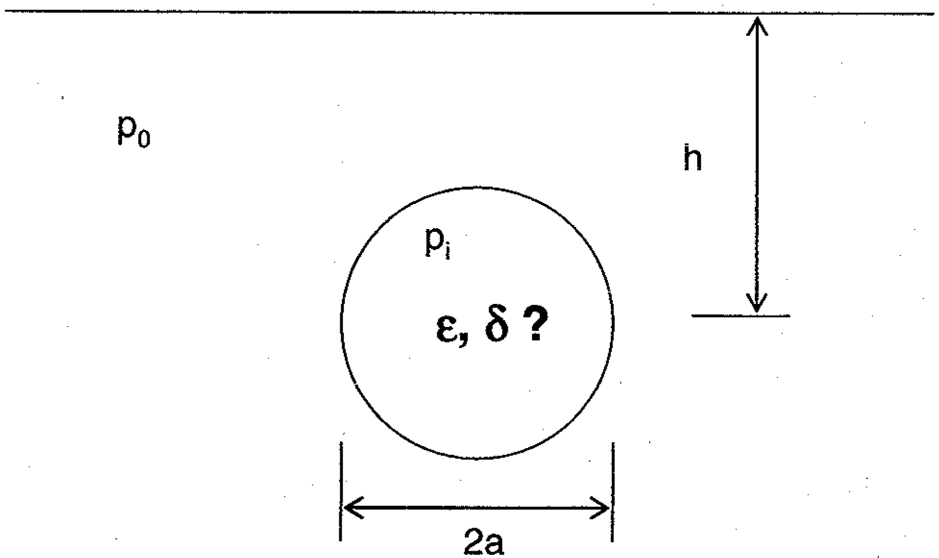

- Elastic- perfect plastic
- Tresca
- Uniform p_0, G, c_u
- k_0=1
- I_r=G/c_u=200
- N_0=p_0/c_u=1 to 6
- h/a= 3 , 5

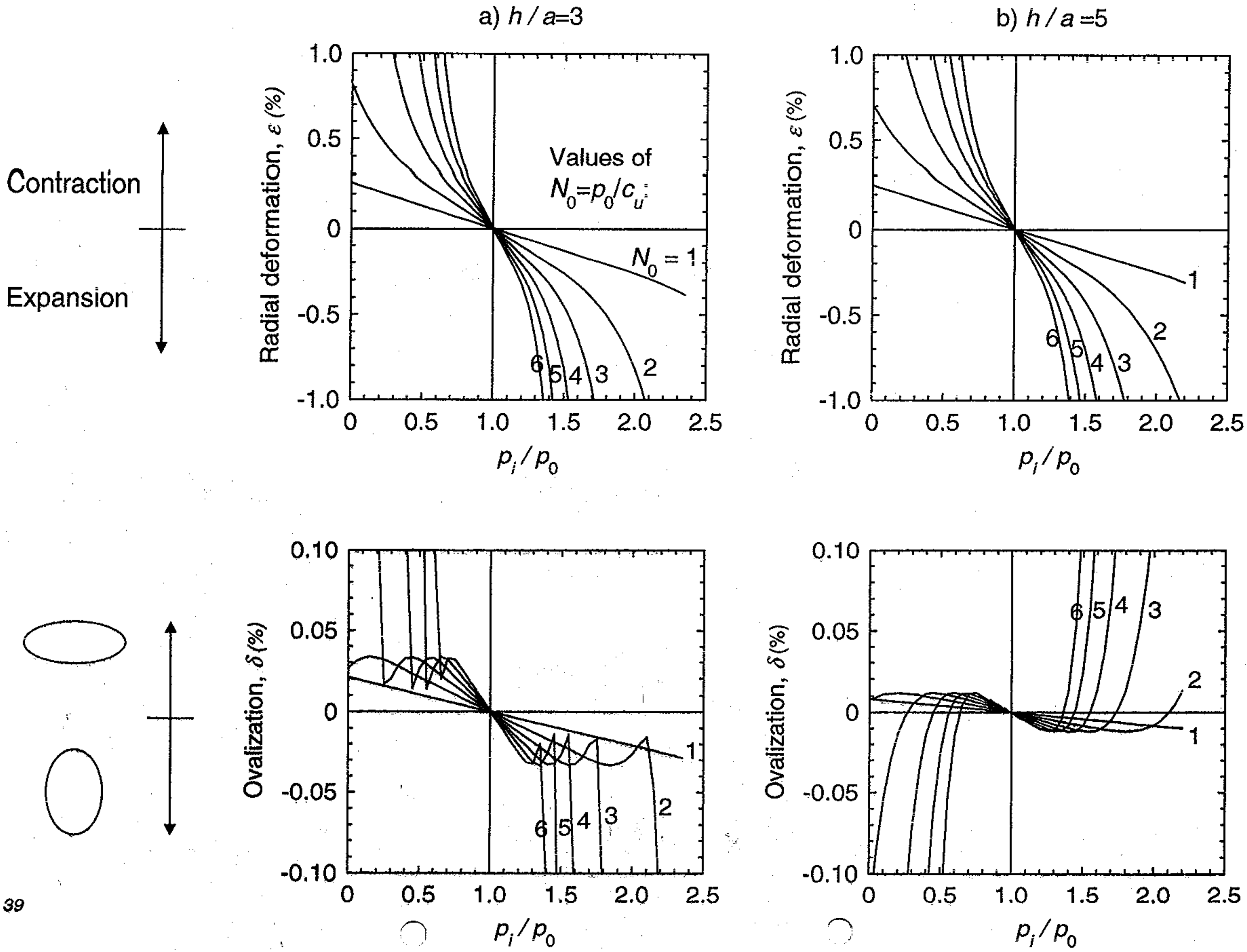
a) h / a=3
b) h / a =5
Contraction
Expansion
Radial deformation, ε (%)
Values of
N0=p0/cu:
N0 = 1
6 5 4 3 2
1
2
6 5 4 3
1.0
0.5
0
-0.5
-1.0
0 0.5 1.0 1.5 2.0 2.5
pi / p0
Ovalization, δ (%)
0.10
0.05
0
-0.05
-0.10
6 5 4 3
2
1

Asignatura: **TÚNELES Y EXCAVACIONES PROFUNDAS**

Tema 5: **TENSIONES Y DEFORMACIONES ALREDEDOR DE UNA CAVIDAD. APLICACION A TUNELES**

C. Sagaseta

Indice

1 INTRODUCCIÓN

En esta Nota se presentan las soluciones existentes para la distribución de tensiones y deformaciones alrededor de una cavidad cilíndrica o esférica en un medio elástico o elastoplástico. El objetivo es su aplicación a la excavación de túneles, si bien las soluciones son generales, y en algunos aspectos se extienden a otros casos, como la aplicación de una presión interior.

Las soluciones suelen aparecer en los textos de forma parcial, con notaciones diferentes, y no siempre libres de erratas o, más a menudo, sin exponer las hipótesis simplificativas hechas. Por ello se ha considerado conveniente reunirlas aquí.

La presentación se va a hacer partiendo de un caso básico sencillo (Figura 1):

- Espacio infinito homogéneo e isótropo, sometido inicialmente a una presión isótropa y uniforme, σ_0.
- Terreno elástico lineal o elastoplástico, según diversos criterios (Tresca, Mohr-Coulomb, Hoek-Brown, etc.).
- Excavación de una cavidad cilíndrica de longitud infinita (deformación plana) y radio a. En la pared de la cavidad se mantiene en principio una presión igual a la inicial, σ_0.
- Posteriormente se disminuye la presión en la pared hasta un cierto valor final, σ_a. Al cociente (σ_a/σ_0) se le denomina a veces confinamiento o confinamiento relativo (ver Figura 8). En el caso límite, la presión final puede ser nula $(\sigma_a = 0)$, lo que corresponde a una cavidad sin revestir.

A este caso se irán introduciendo progresivamente diversas variables adicionales:

- Estado inicial de tensiones no isótropo ($k_0 \neq 1$)
- Profundidad no infinita

La notación y convenio de signos se muestran en la Figura 1. Se utilizan coordenadas cilíndricas (r, θ, z), con el eje OZ a lo largo del eje del túnel. Se consideran positivos las compresiones y acortamientos, así como los desplazamientos radiales hacia el centro de la cavidad. El ángulo polar se mide hacia la derecha a partir de la clave.

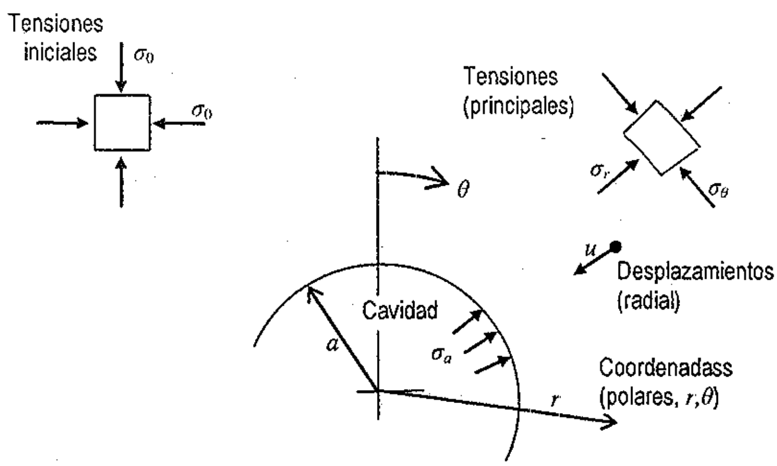

Figura 1. Notación y convenio de signos (todas las magnitudes dibujadas son positivas)

2 CAVIDAD CILINDRICA. COMPRESION INICIAL ISOTROPA

El estado inicial de tensiones es isótropo, con una presión σ_0 igual en todas direcciones (k_0=1). La presión interior, σ_a, es también isótropa.

2.1 Material elástico lineal

El material está definido por un módulo de elasticidad E y un coeficiente de Poisson ν, o un módulo transversal G $(G = E/2(1+\nu))$

Es un caso de deformación plana $(\varepsilon_z = 0)$. Además, existe simetría axial alrededor del eje del túnel. Por ello, son nulas las derivadas respecto a la coordenada z y respecto al ángulo polar, θ. Las derivadas parciales respecto al radio se transforman entonces en derivadas totales, dando lugar a un sistema de ecuaciones diferenciales ordinarias, resoluble por integración directa. El resultado es el siguiente:

- Tensiones:

$$\sigma_r = \sigma_{r0} + \Delta\sigma_r = \sigma_0 - (\sigma_0 - \sigma_a)\frac{a^2}{r^2}$$

$$\sigma_\theta = \sigma_{\theta 0} + \Delta\sigma_\theta = \sigma_0 + (\sigma_0 - \sigma_a)\frac{a^2}{r^2} \tag{1}$$

$$\sigma_z = \sigma_{z0} + \Delta\sigma_z = \sigma_0 + \nu(\Delta\sigma_r + \Delta\sigma_\theta) = \sigma_0$$

- Desplazamientos y deformaciones:

$$\frac{u}{a} = \frac{1}{2G}(\sigma_0 - \sigma_a)\frac{a}{r} \tag{2}$$

$$\varepsilon_r = \frac{\partial u}{\partial r} = -\frac{1}{2G}(\sigma_0 - \sigma_a)\frac{a^2}{r^2}$$

$$\varepsilon_\theta = \frac{u}{r} = \frac{1}{2G}(\sigma_0 - \sigma_a)\frac{a^2}{r^2} \tag{3}$$

$$\varepsilon_z = 0$$

$$\varepsilon_{vol} = \varepsilon_r + \varepsilon_\theta + \varepsilon_z = 0$$

- En la pared (r=a):

$$\sigma_{ra} = \sigma_a$$
$$\sigma_{\theta a} = \sigma_0 + (\sigma_0 - \sigma_a) = 2\sigma_0 - \sigma_a \tag{4}$$
$$\sigma_{za} = \sigma_0$$

$$\frac{u_a}{a} = \frac{1}{2G}(\sigma_0 - \sigma_a) \tag{5}$$

Es usual en túneles denominar <u>convergencia</u> a esta deformación relativa de la pared:

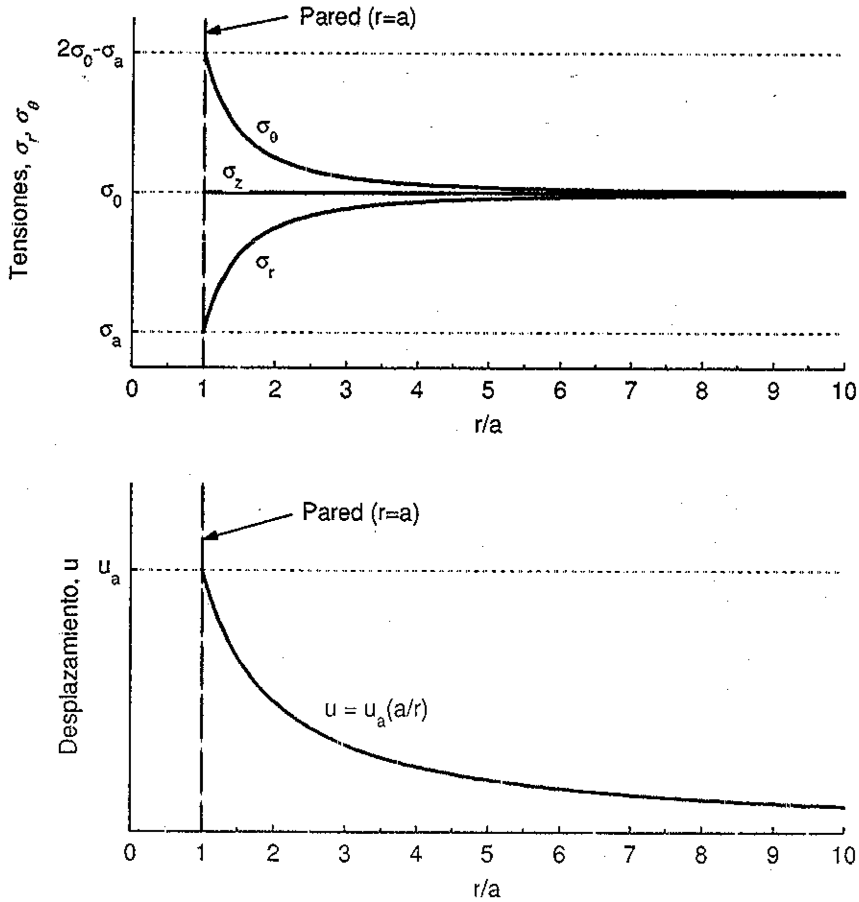

Figura 2. Material elástico. Tensiones y desplazamientos en el terreno

$$\varepsilon_a = \frac{u_a}{a} \tag{6}$$

Asimismo, se suele utilizar también la llamada pérdida de terreno (*'ground loss'*), que es la disminución de sección de la cavidad por la deformación. Suele expresarse como fracción de la sección de la cavidad. En el caso presente resulta:

$$\frac{\Delta V_a}{V_a} = \frac{2\ \pi\ a\ u_a}{\pi\ a^2} = 2\frac{u_a}{a} = 2\varepsilon_a = \frac{\sigma_0 - \sigma_a}{G} \tag{7}$$

En la Figura 2 se representa la distribución de tensiones y desplazamientos en el terreno. Sobre esta solución caben los siguientes comentarios:

a) Las tensiones son todas de compresión.
b) La tensión principal mayor es la circunferencial, la menor la radial y la intermedia la longitudinal $(\sigma_\theta \geq \sigma_z \geq \sigma_r)$.
c) La tensión media no varía respecto a la inicial $(\sigma_r + \sigma_\theta = 2\sigma_0)$.
d) Los máximos incrementos de tensión se producen en la pared, y son independientes del radio de la cavidad.
e) El máximo desviador $(\sigma_\theta - \sigma_r)$, en la pared de la cavidad, vale $(2\sigma_0)$.
f) Las tensiones no dependen de los parámetros elásticos.

g) Las deformaciones de cualquier punto consisten en una extensión radial $(\varepsilon_r < 0)$ y un acortamiento circunferencial $(\varepsilon_\theta > 0)$.
h) La deformación volumétrica unitaria (ε_{vol}) es nula en todos los puntos, en concordancia con la no variación de la tensión media.
i) Los desplazamientos son inversamente proporcionales al módulo transversal, G, y no dependen del coeficiente de Poisson, ν.
j) Los desplazamientos son radiales y decrecen con $(1/r)$.
k) La magnitud de los desplazamientos es proporcional al radio de la cavidad, a.

2.2 Material elastoplástico puramente cohesivo

2.2.1 Parámetros. Factor de carga, N. Índice de rigidez, I_r

Se utiliza el criterio de Tresca (cohesión c_u y ángulo de rozamiento ϕ=0):

$$f = \sigma_1 - \sigma_3 - 2c_u = 0 \tag{8}$$

Esto representa la situación sin drenaje en terreno arcilloso. Por tanto, para la deformación elástica deben usarse parámetros en totales en correspondencia con esta situación, es decir, que impliquen deformación sin cambio de volumen: coeficiente de Poisson ν=1/2, módulo E_u, módulo transversal G=E_u/3.

Suele utilizarse el parámetro denominado <u>índice de rigidez</u>, I_r, definido como cociente entre deformabilidad y resistencia al corte:

$$I_r = \frac{G}{c_u} \tag{9}$$

Este índice toma valores en el rango 50-300 en suelos reales (ver, p.ej la Figura 3).

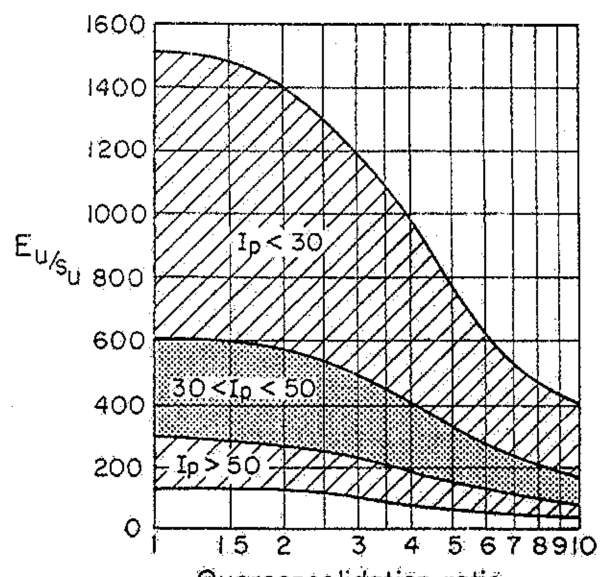

Figura 3. Relación modular en arcillas (E_u/c_u=$3I_r$), (Duncan y Buchigani, 1976).

También es usual utilizar un parámetro adimensional, N, denominado factor de carga (*overload factor*), definido por:

$$N = \frac{\sigma_0 - \sigma_a}{c_u} \qquad (10)$$

Este factor fue introducido por Peck (1969) y adoptado de forma universal en túneles en arcilla como medida de los esfuerzos cortantes movilizados. Su sentido físico viene de la consideración del valor límite de una presión activa, p, frente a una presión resistente, q. La expresión general de dicha carga límite, en ausencia de peso, es:

$$p = qN_q + cN_c \qquad (11)$$

En el caso presente (Figura 1), la presión "activa" es la presión exterior, σ_0, y la "resistente" la de la pared del túnel, σ_a. Al ser ϕ=0, el coeficiente N_q vale la unidad, con lo que la ecuación (11) conduce a:

$$\sigma_0 = \sigma_a + c_u N_c \qquad (12)$$

Comparando con (10), se puede identificar el factor de carga N con N_c

Existe cierta confusión sobre la presión interior, σ_a. El factor de carga se propuso originalmente para el análisis de la estabilidad del frente de los túneles. La presión σ_a debe entonces tomarse como la presión interior actuante en dicho frente, la cual es nula, salvo en túneles de frente presurizado (aire comprimido, ~~escudos de lodos~~ o de presión de tierras, etc.). Sin embargo, cuando se emplea para el estudio de la sección transversal, σ_a debe ser la presión interior en la pared del túnel, es decir, la presión soportada por el revestimiento. Esta segunda definición se adopta aquí.

Es interesante explorar el rango de valores posibles de este factor. El mínimo sería obviamente N=0, antes de hacer la excavación $(\sigma_a = \sigma_0)$. En cuanto al máximo, sería para excavación total $(\sigma_a = 0)$. En lo que sigue, denominamos a este valor factor de carga bruto, N_0:

$$N_0 = \frac{\sigma_0}{c_u} \qquad (13)$$

que puede expresarse como:

$$N_0 = \frac{\sigma_0}{c_u} = \frac{\sigma_0/\sigma'_0}{c_u/\sigma'_0} \qquad (14)$$

El denominador es la razón de resistencia al corte, cuyo valor mínimo se da en suelos normalmente consolidados, con $c_u/\sigma'_0 \cong (0{,}20-0{,}25)$. A su vez, el máximo valor del numerador se da cuando el nivel freático está en la superficie $(\sigma_0/\sigma'_0 = \gamma_{sat}/\gamma_{sum})$, y es del orden de 2. Todo ello lleva a que el factor de carga bruto, N_0 (excavación total) en suelos extremadamente blandos, podría alcanzar como máximo valores de 8 a 10. Como veremos más adelante, en estos casos no sería posible la excavación sin revestimiento, pues la rotura del terreno alrededor del túnel se produce para valores menores de N.

2.2.2 Límite del rango elástico

De acuerdo con las expresiones (4), la solución elástica indica que el máximo desviador se produce en la pared de la cavidad y vale $2(\sigma_0 - \sigma_a)$. Por tanto, la solución elástica es válida hasta un límite de σ_a, tal que la condición del criterio de plastificación (8) se alcance justamente en la pared.

Suponemos, por extensión de lo que ocurría en elasticidad, que la tensión radial es la menor, la circunferencial la mayor y la longitudinal la intermedia:

$$\sigma_\theta \geq \sigma_z \geq \sigma_r \tag{15}$$

Entonces se tiene:

$$f = \sigma_1 - \sigma_3 - 2c_u = \sigma_\theta - \sigma_r - 2c_u = 2(\sigma_0 - \sigma_a) - 2c_u = 0 \tag{16}$$

$$\sigma_a = \sigma_0 - c_u \tag{17}$$

Que equivale a un factor de carga N=1

2.2.3 Solución en tensiones. Extensión de la zona plástica

Dada la simetría axial y que en elasticidad los máximos desviadores se producen en la pared y decrecen hacia el interior del terreno (puntos d) y e) de la lista anterior), es obvio que la zona plástica debe ser una corona concéntrica con la cavidad y comenzando en la pared de la misma, hasta una frontera de radio R (Figura 4)

Al ser un caso en deformación plana, es posible una solución escalonada, resolviendo el problema primero en tensiones y analizando después las deformaciones

Consideremos por separado la corona plástica ($r \leq R$) y la zona elástica ($r \geq R$). En la zona plástica, las tensiones vienen definidas por la ecuación de equilibrio interno en dirección radial y la condición de plasticidad (8), teniendo en cuenta que σ_r es la tensión principal menor y σ_θ la mayor :

$$\begin{aligned} &\frac{d\sigma_r}{dr} - \frac{\sigma_\theta - \sigma_r}{r} = 0 \\ &\sigma_\theta - \sigma_r - 2c_u = 0 \end{aligned} \tag{18}$$

Eliminando σ_θ resulta:

$$\frac{d\sigma_r}{2c_u} = \frac{dr}{r} \tag{19}$$

que es una ecuación diferencial de variables separadas. Su integración, con la condición de contorno en la pared de la cavidad $(\sigma_r = \sigma_a \text{ para } r = a)$ lleva a:

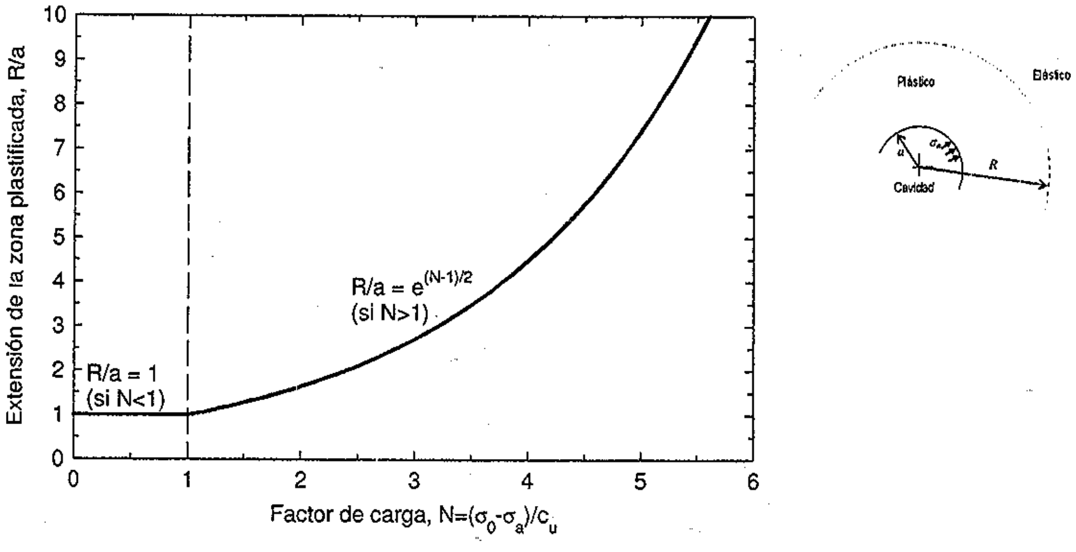

Figura 4. Material elastoplástico (Tresca). Extensión de la zona plastificada

$$
\begin{aligned}
\sigma_r &= \sigma_a + 2c_u \ln\left(\frac{r}{a}\right) \\
\sigma_\theta &= \sigma_r + 2c_u = \sigma_a + 2c_u + 2c_u \ln\left(\frac{r}{a}\right) \qquad (20) \\
\sigma_z &= \frac{1}{2}(\sigma_r + \sigma_\theta) = \sigma_a + c_u + 2c_u \ln\left(\frac{r}{a}\right)
\end{aligned}
$$

La expresión para la tensión longitudinal σ_z requiere un comentario. Para obtenerla se tiene que usar la condición de deformación plana $(\varepsilon_z = 0)$. En la zona plástica, la deformación tiene un sumando elástico y otro plástico:

$$\varepsilon_z = \varepsilon_z^e + \varepsilon_z^p = 0 \qquad (21)$$

La componente plástica es nula si σ_z es la tensión principal intermedia, pues en un material de Tresca el potencial plástico, como el criterio de rotura, no depende de σ_2. Entonces, la componente elástica debe ser también nula:

$$\varepsilon_z^e = \frac{1}{E}\left[\Delta\sigma_z - \nu(\Delta\sigma_\theta + \Delta\sigma_r)\right] = 0 \qquad (22)$$

Ello lleva a:

$$\Delta\sigma_z = \nu(\Delta\sigma_r + \Delta\sigma_\theta) \qquad (23)$$

$$\sigma_z - \sigma_0 = \nu\left[(\sigma_r - \sigma_0) + (\sigma_\theta - \sigma_0)\right] = \frac{1}{2}\left[(\sigma_r - \sigma_0) + (\sigma_\theta - \sigma_0)\right] \qquad (24)$$

$$\sigma_z = \frac{1}{2}(\sigma_r + \sigma_\theta) \qquad (25)$$

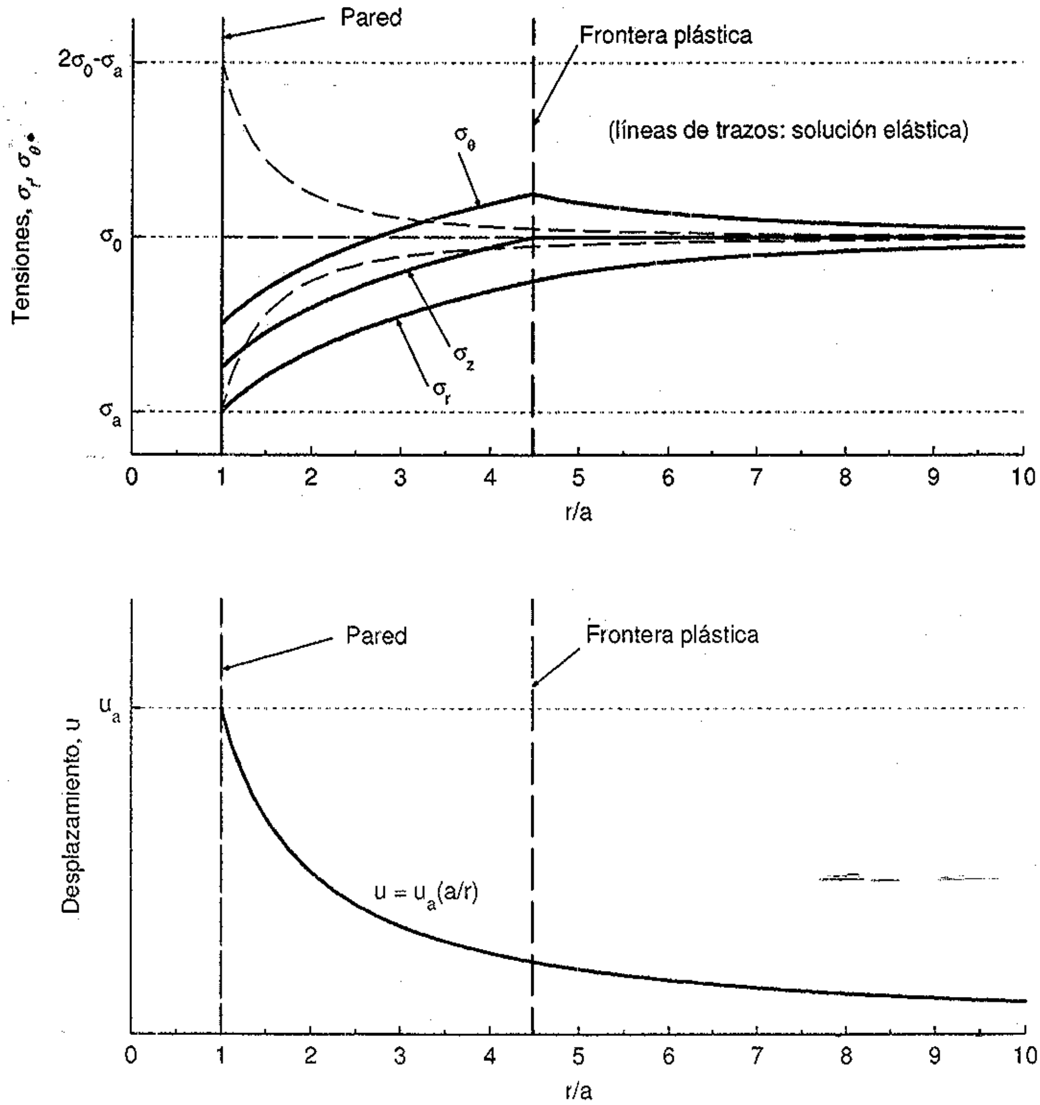

Figura 5. Material elastoplástico (Tresca). Tensiones y desplazamientos en el terreno

Esto confirma que σ_z es la tensión principal intermedia, como se había supuesto en (15), y por tanto la solución obtenida para la zona plástica (20) es correcta.

En la zona elástica ($r \geq R$), el campo de tensiones debe seguir cumpliendo las condiciones establecidas en el apartado 2.1, y por tanto se debe cumplir que:

$$\sigma_r + \sigma_\theta = 2\sigma_0 \quad \text{para} \quad r \geq R \tag{26}$$

Por lo tanto, en la frontera elástica (r=R), las tensiones definidas por (20) deben cumplir también la condición (26):

$$2\sigma_a + 2c_u\left[1 + 2\ln\left(\frac{R}{a}\right)\right] = 2\sigma_0 \tag{27}$$

ecuación que define el radio de la corona plástica, R, que puede ponerse en la forma:

$$\frac{R}{a}=e^{\frac{1}{2}\left(\frac{\sigma_0-\sigma_a}{c_u}-1\right)}=e^{\frac{N-1}{2}} \tag{28}$$

La Figura 4 muestra el valor del radio R de la zona plástica. Como puede verse, no existe zona plástica para $N<1$, cosa que ya se sabía (régimen elástico). Para $N>1$, el radio de la zona plástica aumenta con N; para N entre 2 y 3 es del orden del doble del radio del túnel; para N de 5 a 6, R se hace muy grande, del orden de 10 veces el radio del túnel, lo que desde el punto de vista práctico equivale a plastificación general.

Las tensiones en la zona elástica son las correspondientes a una cavidad ficticia de radio R, sometida a una presión interior radial σ_{rR} dada por la primera ecuación (20) particularizada para $r=R$. Esta presión resulta:

$$\sigma_{rR}=\sigma_0-c_u \tag{29}$$

Por lo tanto, en la zona elástica ($r<R$) las tensiones son:

$$\begin{aligned}
\sigma_r &= \sigma_0-c_u e^{N-1}\frac{a^2}{r^2}\\
\sigma_\theta &= \sigma_0+c_u e^{N-1}\frac{a^2}{r^2}\\
\sigma_z &= \sigma_0
\end{aligned} \tag{30}$$

La distribución de tensiones viene por tanto dada por las ecuaciones (20) en la zona plástica y (30) en la elástica. En la Figura 5 se puede ver el resultado. En la pared, la tensión radial vale σ_a y la circunferencial (σ_a+2c_u). Ambas crecen con la distancia r en la zona plástica, manteniéndose constante su diferencia ($2c_u$). En la zona elástica, la distribución es similar a la de la Figura 2.

La distribución de tensiones viene por tanto dada por las ecuaciones (20) en la zona plástica y (30) en la elástica. En la Figura 5 se puede ver el resultado. En la pared, la tensión radial vale σ_a y la circunferencial (σ_a+2c_u). Ambas crecen con la distancia r en la zona plástica, manteniéndose constante su diferencia ($2c_u$). En la zona elástica, la distribución es similar a la de la Figura 2, es decir, simétrica respecto a σ_0. Como referencia, se dibujan las tensiones elásticas para el mismo valor de σ_a.

2.2.4 *Solución en desplazamientos*

Los desplazamientos en la zona elástica tendrán una distribución del tipo de la ec. (2), para una cavidad de radio R (ec. 28), con presión interior σ_{rR} (ec. 29), es decir:

$$u=(\sigma_0-\sigma_{rR})\frac{1}{2G}R\frac{R}{r}=\frac{1}{2I_r}e^{N-1}a\frac{a}{r} \tag{31}$$

En la frontera elástica ($r=R$), el desplazamiento es:

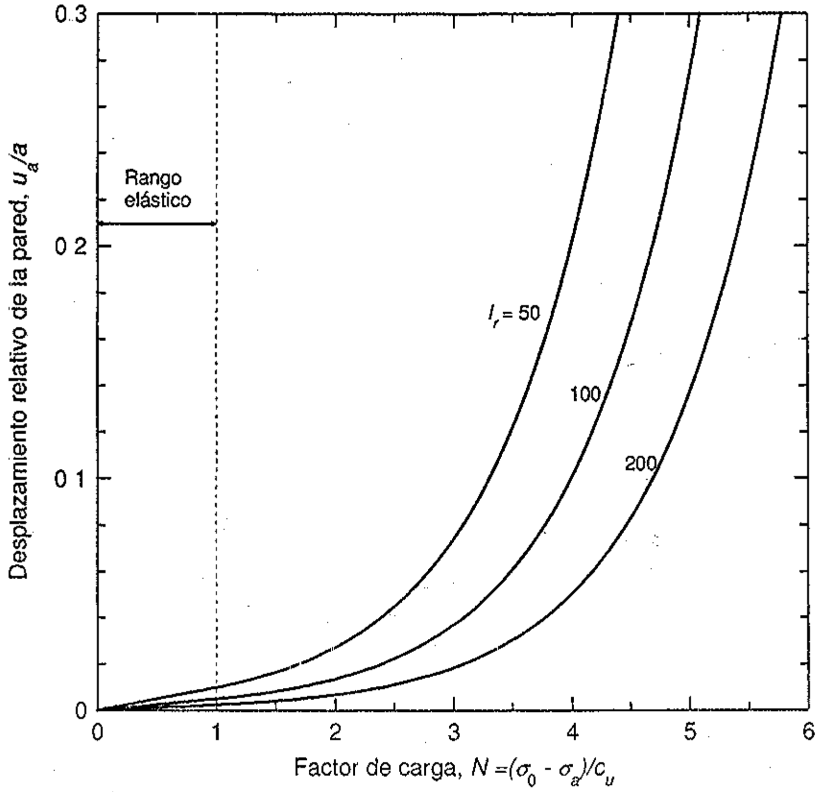

Figura 6. Material elastoplástico (Tresca) Desplazamiento relativo de la pared, u_a/a

$$\frac{u_R}{a} = \frac{1}{2I_r} e^{N-1} \frac{a}{R} = \frac{1}{2I_r} e^{\frac{N-1}{2}} \tag{32}$$

Para obtener los desplazamientos en la zona plástica sería preciso en principio utilizar las ecuaciones tensión-deformación plástica. Sin embargo, en este caso de suelo puramente cohesivo, con deformación sin cambio de volumen, la solución es trivial y el campo de desplazamientos, tanto en la zona elástica como en la plástica está definido por la condición de deformación a volumen constante, que puede expresarse como:

$$\varepsilon_{vol} = \varepsilon_r + \varepsilon_\theta + \varepsilon_z = \frac{du}{dr} + \frac{u}{r} = 0 \tag{33}$$

Esta es una ecuación diferencial ordinaria, y su solución general es:

$$u = \frac{C}{r} \tag{34}$$

A este mismo resultado se habría llegado expresando que el volumen de desplazamientos de un anillo de radio r es constante e independiente de r:

$$\Delta V = 2\pi r u = 2\pi a u_a = 2\pi R u_R = cte \tag{35}$$

que conduce a la misma solución (34).

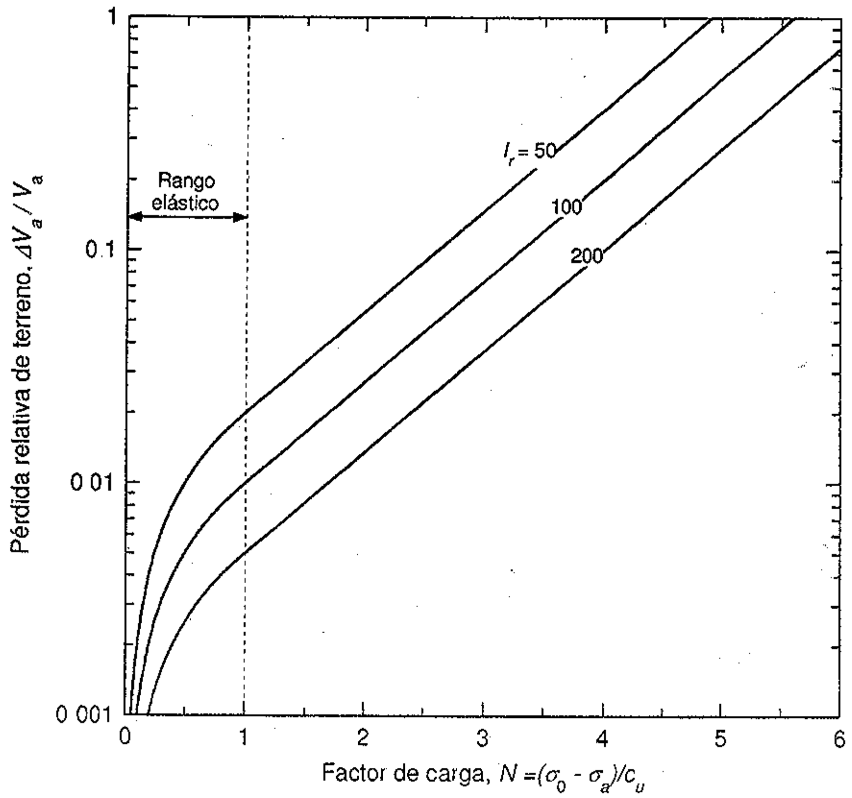

Figura 7. Material elastoplástico (Tresca). Pérdida de terreno, $\Delta V_a/V_a$ (log)

El valor de la constante de integración queda definido por el desplazamiento en la frontera elástica (32). Dado que la ley de desplazamientos en la zona elástica (31) es del tipo ($u = C/r$), dicha ley es válida también en la zona plástica

Obviamente, la ley (31) vale para N>1. Para N<1 (rango elástico), rige la ec (2).

El desplazamiento de la pared de la cavidad viene por tanto dado por las expresiones (2) y (31) para $r=a$ (Figura 6):

$$\varepsilon_a = \frac{u_a}{a} = \begin{cases} = \dfrac{1}{2G}(\sigma_0 - \sigma_a) = \dfrac{1}{2I_r} N & \text{para} \quad N \le 1 \\ = \dfrac{1}{2I_r} e^{N-1} & \text{para} \quad N \ge 1 \end{cases} \tag{36}$$

La pérdida relativa de terreno resulta:

$$\frac{\Delta V_a}{V_a} = 2\frac{u_a}{a} = \begin{cases} = \dfrac{1}{I_r} N & \text{para} \quad N \le 1 \\ = \dfrac{1}{I_r} e^{N-1} & \text{para} \quad N \ge 1 \end{cases} \tag{37}$$

La convergencia relativa y la pérdida relativa de terreno se representan en la Figura 6 y Figura 7, ambas en función del factor de carga N, para valores usuales del índice de rigidez (50-200). La pérdida relativa de terreno se representa en escala logarítmica, que es lo habitual. Puede verse que en el rango elástico (N<1) las deformaciones son pequeñas, inferiores al 1%. Para valores de N de 2 a 3 la pérdida relativa de terreno está entre el 1 y el 10%. Para N superior a 5 o 6, la deformación crece desmesuradamente, llegando a suponer prácticamente el cierre de la sección y la rotura. Es interesante observar que, en el rango elastoplástico (N>1), las leyes son paralelas, es decir, que un aumento de una unidad del factor de carga supone que la pérdida de terreno se multiplica por e (=2,71), sea cual sea la rigidez I_r del terreno.

Es habitual representar las expresiones (36) en un diagrama como el indicado en la Figura 8. La curva que representa la evolución de la convergencia (u_a/a) al disminuir el confinamiento (σ_a/σ_0) se denomina curva característica del terreno. Se ha dibujado para diversos valores de la cohesión respecto a la presión inicial, es decir, del factor de carga bruto, N_0. La escala del eje horizontal viene definida por el valor de la convergencia relativa para excavación total en régimen elástico $(u_a/a = \sigma_0/2G)$. Para factor de carga bruto superior a 5, la convergencia aumenta desmesuradamente, y a efectos prácticos constituye rotura. Esto ya se comentó al analizar la Figura 6 (en realidad ambas figuras son distintas representaciones de una misma expresión).

2.3 Material de Mohr-Coulomb

El material de Tresca es representativo de terrenos arcillosos, en los que la excavación es suficientemente rápida para suponer que es un proceso sin drenaje. Para otros casos, es necesario disponer de la solución para material de Mohr-Coulomb.

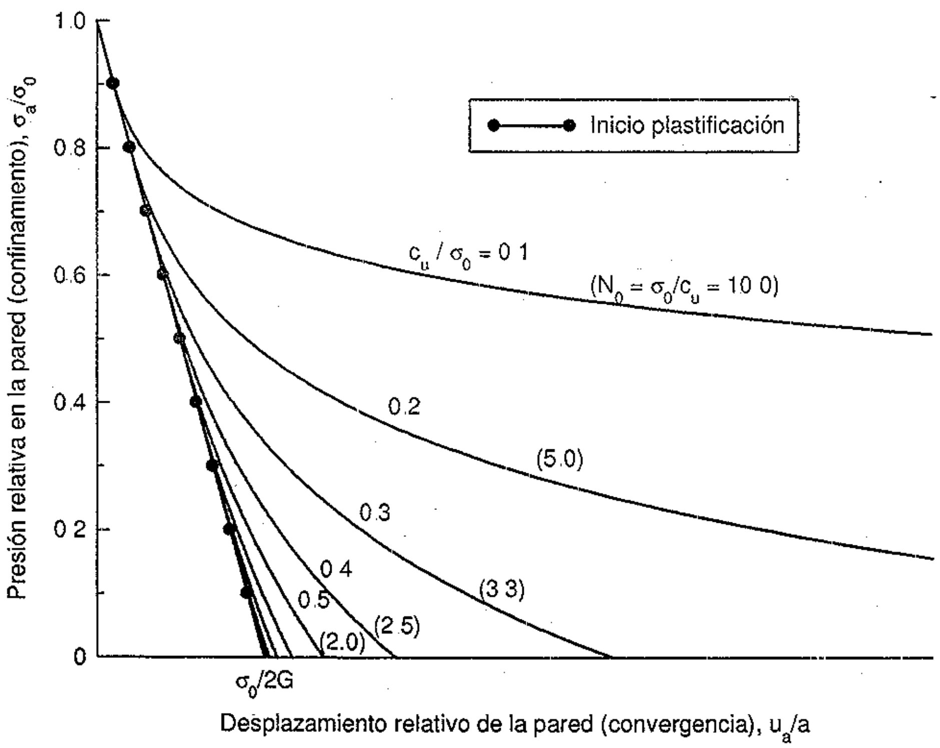

Figura 8. Material de Tresca. Diagrama convergencia-confinamiento

2.3.1 Parámetros

Este material está definido, en su deformabilidad elástica, por los parámetros generales G, ν (sin la particularidad de que ν=1/2).

En cuanto a la resistencia, el criterio de Mohr-Coulomb se expresa:

$$f = (\sigma_1 + c\,\mathrm{cotg}\,\phi) - (\sigma_3 + c\,\mathrm{cotg}\,\phi)\frac{1+\mathrm{sen}\,\phi}{1-\mathrm{sen}\,\phi} = 0 \tag{38}$$

siendo c la cohesión y ϕ el ángulo de rozamiento interno. Además, para las deformaciones plásticas es preciso considerar comportamiento no asociado, con un ángulo de dilatancia, ψ, diferente del de rozamiento (ver Apartado 2.3.5).

En el material de Tresca se definieron unos parámetros adimensionales de uso frecuente: el factor de carga N y el índice de rigidez I_r. En el caso de cohesión y rozamiento no hay una propuesta similar, aunque puede hacerse una generalización mediante la Teoría de la Plasticidad. La ecuación (12) se escribe en el caso general:

$$\sigma_0 = \sigma_a N_q + c N_c \tag{39}$$

N_c y N_q están ligados por el teorema de los estados correspondientes:

$$N_c = (N_q - 1)\,\mathrm{cotg}\,\phi \;\rightarrow\; N_q = 1 + N_c\,\mathrm{tg}\,\phi \tag{40}$$

Eliminando N_q entre estas las ecuaciones (39) y (40) se puede despejar N_c. Alternativamente, se puede eliminar N_c y despejar N_q. Se llega a:

$$N_c = \frac{\sigma_0 - \sigma_a}{c + \sigma_a\,\mathrm{tg}\,\phi} \quad ; \quad N_q = \frac{\sigma_0 + c\,\mathrm{cotg}\,\phi}{\sigma_a + c\,\mathrm{cotg}\,\phi} \tag{41}$$

Al igual que en el caso ϕ=0, se puede utilizar como factor de carga el valor de N_c:

$$N = N_c = \frac{\sigma_0 - \sigma_a}{c + \sigma_a\,\mathrm{tg}\,\phi} \tag{42}$$

que supone una generalización de la expresión (10) añadiendo a la cohesión la resistencia friccional movilizada por la presión de la pared σ_a.

En cuanto al índice de rigidez, también admite una generalización semejante:

$$I_r = \frac{G}{c + \sigma_a\,\mathrm{tg}\,\phi} \tag{43}$$

Ambos factores se reducen a los ya definidos para el material de Tresca en el caso de que el ángulo de rozamiento tienda a cero.

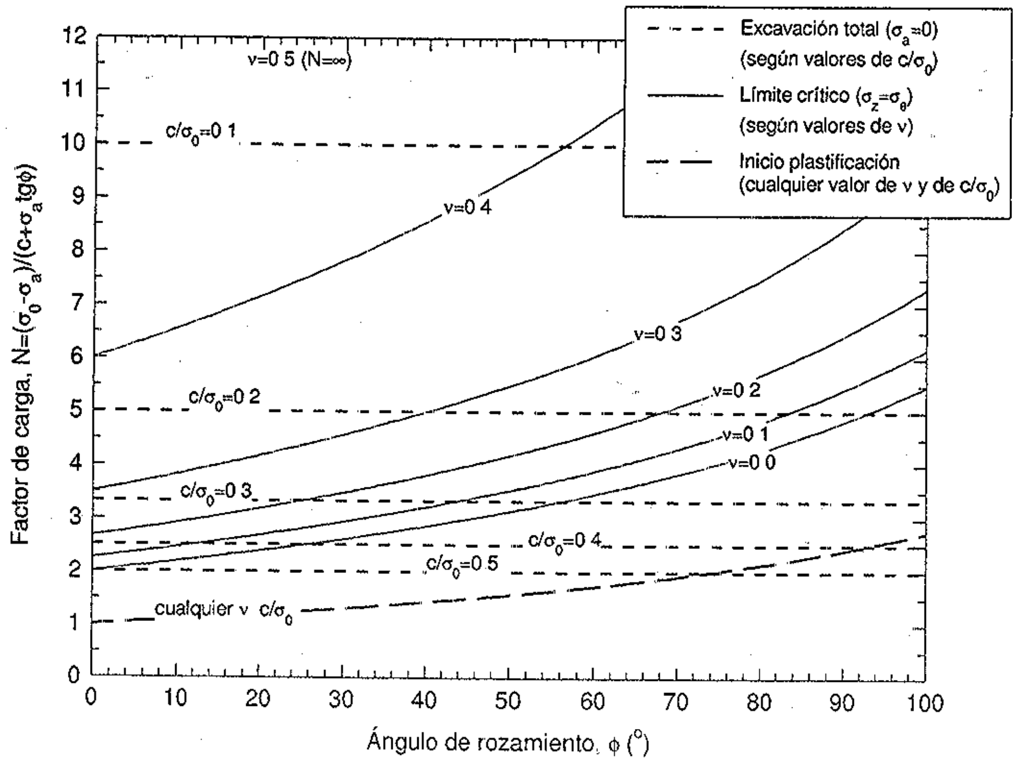

Figura 9. Material de Mohr-Coulomb. Límite de validez de σ_z como tensión principal intermedia. Comparación con inicio de plastificación y con excavación total.

2.3.2 Inicio de la plastificación

Al igual que en el caso anterior, se producirá cuando las tensiones elásticas en la pared alcancen a cumplir estrictamente el criterio de plastificación f=0 (ec. 38) con $(\sigma_1 = \sigma_\theta = 2\sigma_0 - \sigma_a), (\sigma_3 = \sigma_r = \sigma_a)$. Resulta una presión en la pared:

$$\sigma_a = \sigma_0(1 - \operatorname{sen}\phi) - c\cos\phi \tag{44}$$

que se reduce a (17) para ϕ=0. Utilizando el factor de carga generalizado (42), el inicio de la plastificación se expresa como:

$$N = \frac{\cos\phi}{1 - \operatorname{sen}\phi} \tag{45}$$

2.3.3 Solución en tensiones. Límite de validez de $\sigma_\theta \geq \sigma_z \geq \sigma_r$.

El criterio de Mohr-Coulomb, igual que el de Tresca, no depende de la tensión principal intermedia, σ_2. Si continuamos aceptando la hipótesis de que la tensión longitudinal al túnel es la intermedia $(\sigma_1 = \sigma_\theta; \sigma_2 = \sigma_z; \sigma_3 = \sigma_r)$, se puede despejar de (38) la tensión circunferencial en función sólo de la radial:

$$\sigma_\theta = -c\,\mathrm{cotg}\,\phi + (\sigma_r + c\,\mathrm{cotg}\,\phi)\frac{1+\mathrm{sen}\,\phi}{1-\mathrm{sen}\,\phi} \tag{46}$$

Entonces, el sistema (18) formado por la ecuación de equilibrio interno y la de plasticidad sigue conduciendo a una ecuación diferencial en σ_r de variables separadas, cuya integración en la zona plástica da:

$$\sigma_r = -c\,\mathrm{cotg}\,\phi + (\sigma_a + c\,\mathrm{cotg}\,\phi)\left(\frac{r}{a}\right)^{\frac{2\,\mathrm{sen}\,\phi}{1-\mathrm{sen}\,\phi}} \tag{47}$$

La tensión circunferencial se deduce entonces de (46):

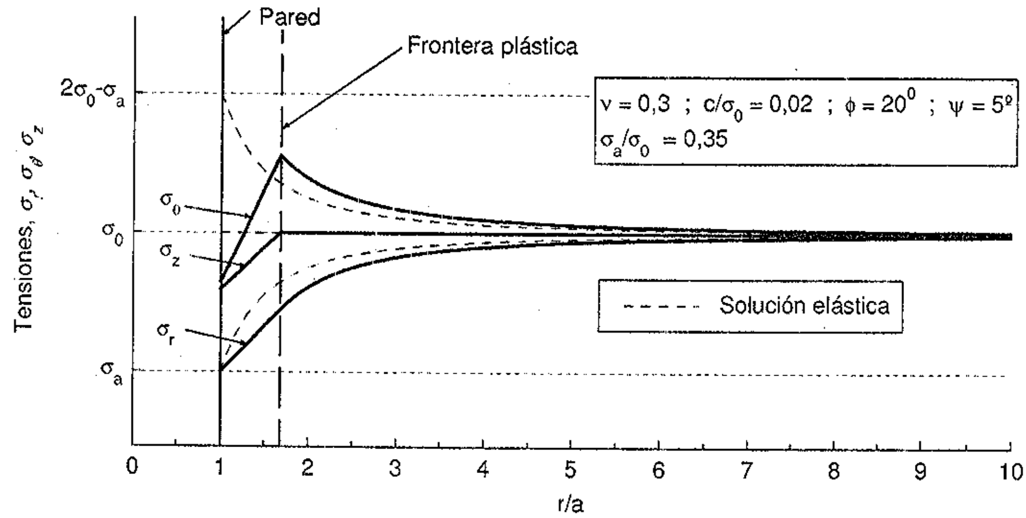

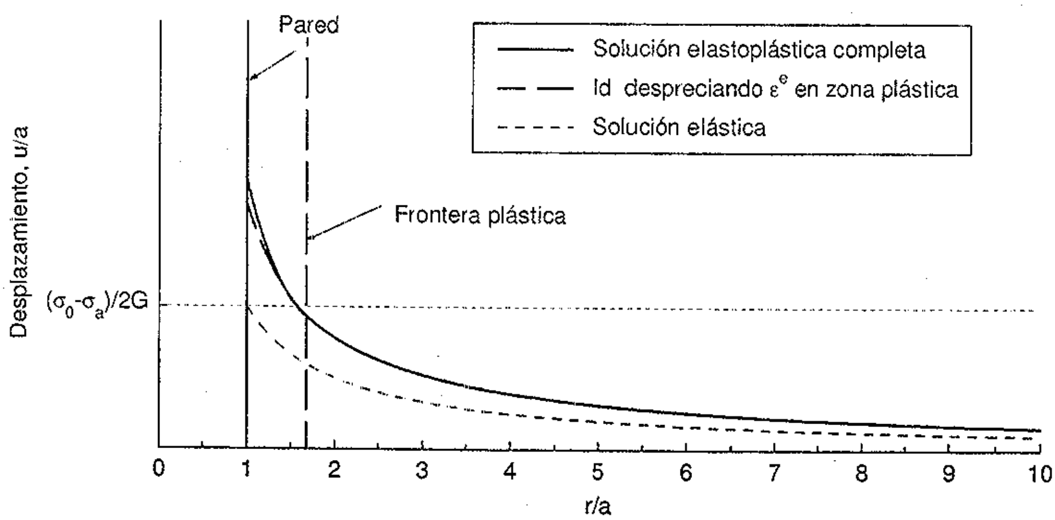

Figura 10. Material de Mohr-Coulomb. Tensiones y desplazamientos en el terreno:

Caso $\sigma_a/\sigma_0 = 0{,}35$: $\sigma_\theta \geq \sigma_z \geq \sigma_r$ en todos los puntos. Solución correcta

$$\sigma_\theta = -c\,\mathrm{cotg}\,\phi + \frac{1+\mathrm{sen}\,\phi}{1-\mathrm{sen}\,\phi}\left(\sigma_a + c\,\mathrm{cotg}\,\phi\right)\left(\frac{r}{a}\right)^{\frac{2\,\mathrm{sen}\,\phi}{1-\mathrm{sen}\,\phi}} \tag{48}$$

Por último, para la tensión longitudinal σ_z se puede seguir el mismo razonamiento que en el caso de material de Tresca. Sin embargo, al ser el coeficiente de Poisson distinto de 1/2, las ecuaciones (25) conducen ahora a:

$$\sigma_z = (1-2\nu)\sigma_0 + \nu(\sigma_r + \sigma_\theta) \tag{49}$$

Esto supone que σ_z no tiene por qué ser siempre intermedia entre las tensiones radial y circunferencial. Se cumple en el caso elástico al ser $(\sigma_r + \sigma_\theta = 2\sigma_0)$, y también

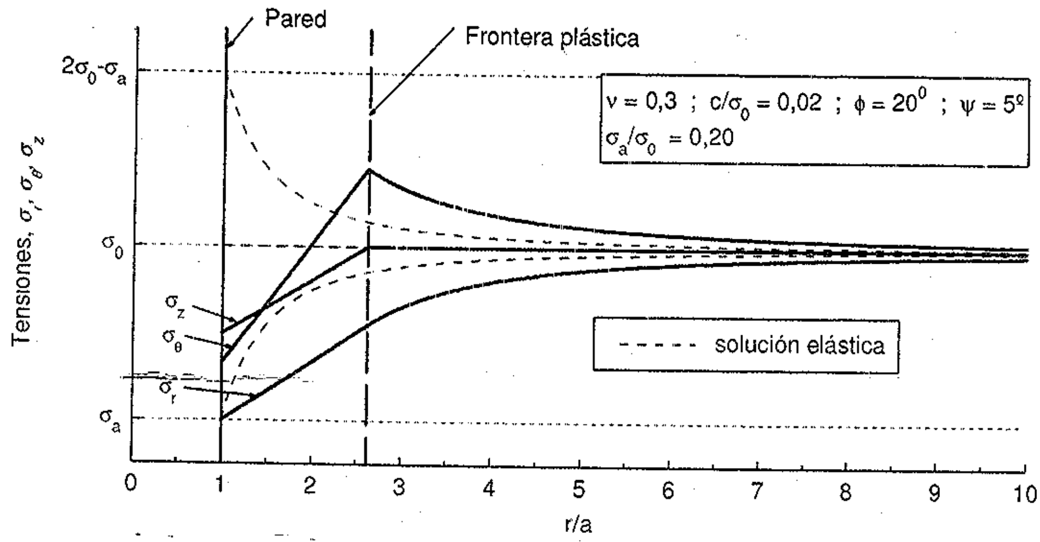

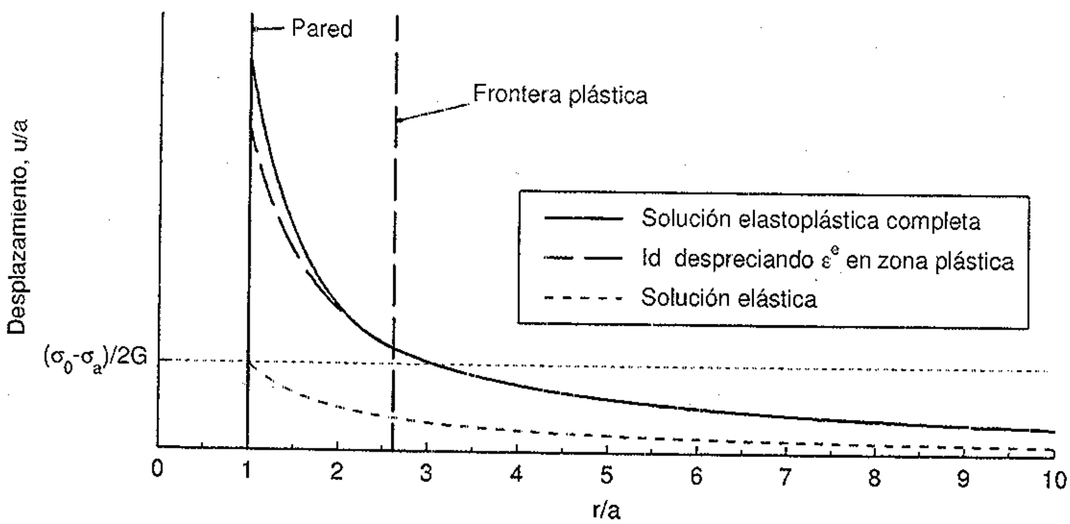

Figura 11. Material de Mohr-Coulomb. Tensiones y desplazamientos en el terreno:

Caso $\sigma_a/\sigma_0 = 0{,}20$: $\sigma_z \geq \sigma_\theta \geq \sigma_r$ en parte de la zona plástica en el de Tresca al ser $(\nu = 1/2)$. Sin embargo, en el caso general de Mohr-Coulomb es preciso comprobarlo.

Si se sustituyen las expresiones (47) y (48) en (49) resulta que σ_z está comprendida entre las otras dos sólo para valores del confinamiento relativamente altos. El valor límite mínimo de la presión de la pared σ_a para el que se cumple dicha condición viene dado por:

$$N_{crit} = \frac{\sigma_0 - \sigma_a}{c + \sigma_a \operatorname{tg}\phi} = \frac{2(1-\nu)\cos\phi}{(1-2\nu)(1-\operatorname{sen}\phi)} \tag{50}$$

Esta expresión se representa en la Figura 9. Para ϕ=0 y ν=1/2 (Material de Tresca), el límite es infinito, y la tensión σ_z es siempre la intermedia. Sin embargo, no es así para otros valores de ϕ o de ν. En la misma figura se han dibujado los valores de N correspondientes a inicio de plastificación (ec. 45) y a excavación total $(\sigma_a = 0)$. En gran parte de los casos, sobre todo para valores pequeños de la cohesión, se llega a $(\sigma_z = \sigma_\theta)$ para una presión de pared intermedia entre ambas.

Pasado este límite de la presión de la pared, la solución se complica extraordinariamente, pues las tensiones extremas σ_1 y σ_3 pasan a ser σ_z y σ_r, respectivamente, con lo que en el sistema de dos ecuaciones (62) aparecen las tres tensiones (σ_z, σ_θ, σ_r), y ya no puede resolverse sin hacer intervenir las deformaciones.

En la Figura 10 se presenta la distribución de tensiones en el terreno en un caso con confinamiento $\sigma_a/\sigma_0 = 0{,}35$ en el que, como puede verse, se mantiene la tensión σ_z como intermedia. En la Figura 11 se representa el mismo caso, pero con un confinamiento menor, $\sigma_a/\sigma_0 = 0{,}20$. En este caso, σ_z es mayor que σ_θ en la parte de la zona plástica más próxima al túnel, por lo que la solución presentada y dibujada en la figura es incorrecta.

La mayor parte de los textos ignoran este problema. Sólo unos pocos hacen referencia a él, citando el límite de validez de la solución (Sagaseta, 1998; Yu y Rowe, 1998). Este criterio es el que se adopta aquí. Se señalan únicamente los límites teóricos de la solución obtenida, pero en ningún caso se intenta obtener la solución general rigurosa, que, por las dificultades citadas, no es posible de forma analítica

2.3.4 *Extensión de la zona plástica. Tensiones en la zona elástica*

La situación de la frontera elástica-plástica se establece, como en el caso de material de Tresca, imponiendo la condición de la distribución elástica de tensiones $(\sigma_r + \sigma_\theta = 2\sigma_0)$ a las tensiones en la zona plástica (47,48). Se llega a:

$$\frac{R}{a} = \left[(1-\operatorname{sen}\phi)\frac{\sigma_0 + c\operatorname{cotg}\phi}{\sigma_a + c\operatorname{cotg}\phi}\right]^{\frac{1-\operatorname{sen}\phi}{2\operatorname{sen}\phi}} = \left[(1-\operatorname{sen}\phi)(1+N\operatorname{tg}\phi)\right]^{\frac{1-\operatorname{sen}\phi}{2\operatorname{sen}\phi}} \tag{51}$$

Esta expresión se representa en la Figura 12 en función del factor de carga generalizado, N (la curva para ϕ=0 coincide con la de la), y en ella se indica su límite de

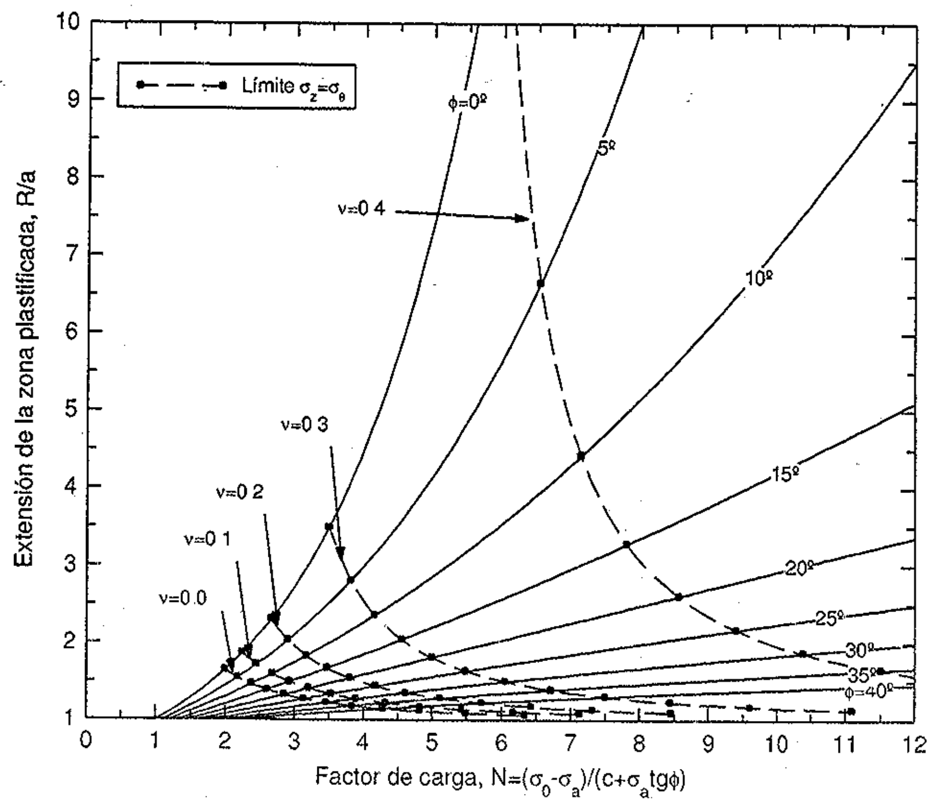

Figura 12 Material de Mohr-Coulomb. Radio de la zona plastificada

validez Con relación al caso de ϕ=0, la zona plástica, para iguales valores del factor de carga, se reduce considerablemente al aumentar el rozamiento

En la zona elástica, las tensiones son las correspondientes a una cavidad ficticia de radio R con una presión en su pared igual a la tensión radial obtenida para la frontera plástica (ec 47 para $r=R$), que es la dada por la ec (44). Las tensiones resultan:

$$
\begin{aligned}
\sigma_r &= \sigma_0 - (\sigma_0 \operatorname{sen}\phi + c\cos\phi)\frac{R^2}{r^2} \\
\sigma_\theta &= \sigma_0 + (\sigma_0 \operatorname{sen}\phi + c\cos\phi)\frac{R^2}{r^2} \\
\sigma_z &= \sigma_0
\end{aligned}
\tag{52}
$$

2.3.5 *Solución en desplazamientos*

Por lo que se refiere a los desplazamientos, en la zona elástica se obtienen de forma similar al caso sin rozamiento, considerando una cavidad ficticia de radio R sometida a una presión de pared igual al valor de σ_r en dicho punto. El desplazamiento en la frontera plástica resulta:

$$
\frac{u_R}{R} = \frac{\sigma_0 + c\operatorname{cotg}\phi}{2G}\operatorname{sen}\phi \tag{53}
$$

Para la zona plástica, la condición de cambio de volumen nulo (33) ya no es aplicable. Debe usarse la ley de comportamiento elastoplástico. Para que la solución sea realista se requiere considerar un ángulo de dilatancia, ψ, distinto del de rozamiento interno (material de tipo "no asociado"), que establece que debe haber una expansión volumétrica plástica igual a la máxima distorsión plástica multiplicada por el seno del ángulo de dilatancia:

$$\varepsilon_{vol}^{p} = -\gamma_{max}^{p} \operatorname{sen}\psi \qquad (54)$$

Puede verse que para ψ=0, esta ley se reduce a la (33).

Las deformaciones plásticas se pueden expresar como la diferencia entre las totales y las elásticas, con lo que la expresión anterior lleva a:

$$(\varepsilon_r + \varepsilon_\theta) - (\varepsilon_r^e + \varepsilon_\theta^e) = -\operatorname{sen}\psi\left[(\varepsilon_\theta - \varepsilon_r) - (\varepsilon_\theta^e - \varepsilon_r^e)\right] \qquad (55)$$

Expresando las deformaciones totales en función de los desplazamientos $(\varepsilon_r = du/dr\,;\varepsilon_\theta = u/r)$, la ecuación anterior se transforma en:

$$\frac{du}{dr} + \frac{1+\operatorname{sen}\psi}{1-\operatorname{sen}\psi}\frac{u}{r} - \varepsilon_r^e - \frac{1+\operatorname{sen}\psi}{1-\operatorname{sen}\psi}\varepsilon_\theta^e = 0 \qquad (56)$$

Esta es una ecuación diferencial lineal, que puede integrarse analíticamente, ya que las deformaciones elásticas que aparecen en ella pueden obtenerse en función de r aplicando la ley de Hooke a las tensiones (47,48). Resulta:

$$\frac{u}{a} = \frac{\sigma_0 + c\operatorname{cotg}\phi}{2G}\left[A\frac{r}{a} + B\left(\frac{r}{a}\right)^{k} + C\left(\frac{r}{a}\right)^{-\alpha}\right] \qquad (57)$$

siendo:

$$A = -(1-2\nu)$$

$$B = (1-\operatorname{sen}\phi)\frac{1-2\nu+\operatorname{sen}\phi\operatorname{sen}\psi}{1-\operatorname{sen}\phi\operatorname{sen}\psi}\left(\frac{R}{a}\right)^{1-k}$$

$$C = \left[1-2\nu+\operatorname{sen}\phi-(1-\operatorname{sen}\phi)\frac{1-2\nu+\operatorname{sen}\phi\operatorname{sen}\psi}{1-\operatorname{sen}\phi\operatorname{sen}\psi}\right]\left(\frac{R}{a}\right)^{\alpha+1}$$

$$\alpha = \frac{1+\operatorname{sen}\psi}{1-\operatorname{sen}\psi} \quad ; \quad k = \frac{1+\operatorname{sen}\phi}{1-\operatorname{sen}\phi}$$

En la pared de la cavidad $(r = a)$:

$$\varepsilon_a = \frac{u_a}{a} = \frac{\sigma_0 + c\operatorname{cotg}\phi}{2G}(A+B+C) \qquad (58)$$

Los distintos libros y publicaciones suelen presentar los resultados anteriores de forma parcial, y no siempre coinciden entre sí. Ello es debido a que se hacen distintas hipótesis, que no siempre se exponen. Las más comunes son suponer en la ecuación (55) que el ángulo de dilatancia, ψ, es igual al de rozamiento, ϕ (comportamiento asociado), o despreciar las componentes elásticas $\left(\varepsilon_r^e, \varepsilon_\theta^e\right)$ en la zona plástica.

Esta última hipótesis es la que más simplifica el cálculo, pues hace que en la ecuación (56) desaparezca el término independiente, con lo que, además de no tener que hacer intervenir las tensiones a través de la ley de Hooke, resulta una ecuación de variables separadas. El resultado es entonces:

$$\frac{u}{a} = \frac{\sigma_0 + c \cot g \phi}{2G} \operatorname{sen} \phi \left(\frac{R}{a}\right)^{\alpha+1} \left(\frac{r}{a}\right)^{-\alpha} \tag{59}$$

y en la pared de la cavidad:

$$\varepsilon_a = \frac{u_a}{a} = \frac{\sigma_0 + c \cot g \phi}{2G} \operatorname{sen} \phi \left(\frac{R}{a}\right)^{\alpha+1} \tag{60}$$

Las leyes de desplazamientos (57) y (59) se han representado en los casos de la Figura 10 y Figura 12 Puede verse que la simplificación de despreciar las deformaciones elásticas en la zona plástica da un error relativamente pequeño, que aumenta al crecer el tamaño de dicha zona.

2.4 Material de Hoek-Brown

En macizos rocosos, es usual el empleo del criterio empírico no lineal de Hoek-Brown (1980), que tiene por expresión:

$$f = (\sigma_1 - \sigma_3) - \sqrt{m \sigma_c \sigma_3 + s \sigma_c^2} = 0 \tag{61}$$

donde σ_c es la resistencia a compresión simple de la roca sana y m y s otros dos parámetros del modelo

Este criterio permite despejar la tensión circunferencial $(\sigma_\theta = \sigma_1)$ en función de la radial $(\sigma_r = \sigma_3)$, con lo que el sistema de ecuaciones para las tensiones tiene la misma forma general:

$$\begin{aligned} &\frac{d\sigma_r}{dr} - \frac{\sigma_\theta - \sigma_r}{r} = 0 \\ &\sigma_\theta = f(\sigma_r) = \sigma_r + \sqrt{m \sigma_c \sigma_r + s \sigma_c^2} \end{aligned} \tag{62}$$

Eliminando σ_θ resulta:

$$\frac{d\sigma_r}{f(\sigma_r) - \sigma_r} = \frac{dr}{r} \tag{63}$$

que sigue siendo una ecuación diferencial de variables separadas, y permite obtener analíticamente la solución para σ_r en la zona plástica. La única constante de integración se obtiene de la condición de contorno de presión σ_a en la pared. Conocido σ_r, la tensión σ_θ se obtiene del criterio de rotura (segunda ecuación 62). Se llega a:

$$
\begin{aligned}
\sigma_r &= \frac{1}{m\sigma_c}\left[\left(\sqrt{m\sigma_c\sigma_a + s\sigma_c^2} + \frac{m\sigma_c}{2}\ln\frac{r}{a}\right)^2 - s\sigma_c^2\right] \\
\sigma_\theta &= \sigma_r + \sqrt{m\sigma_c\sigma_r + s\sigma_c^2}
\end{aligned}
\qquad (64)
$$

Con respecto a la tensión longitudinal, se mantienen las mismas reservas sobre su condición de tensión intermedia que con el modelo de Mohr-Coulomb. Para

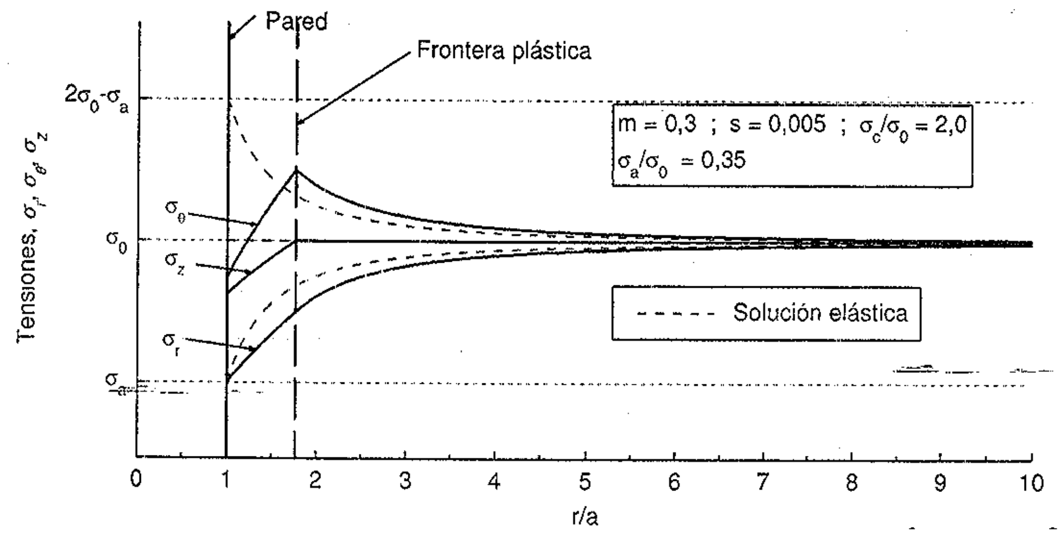

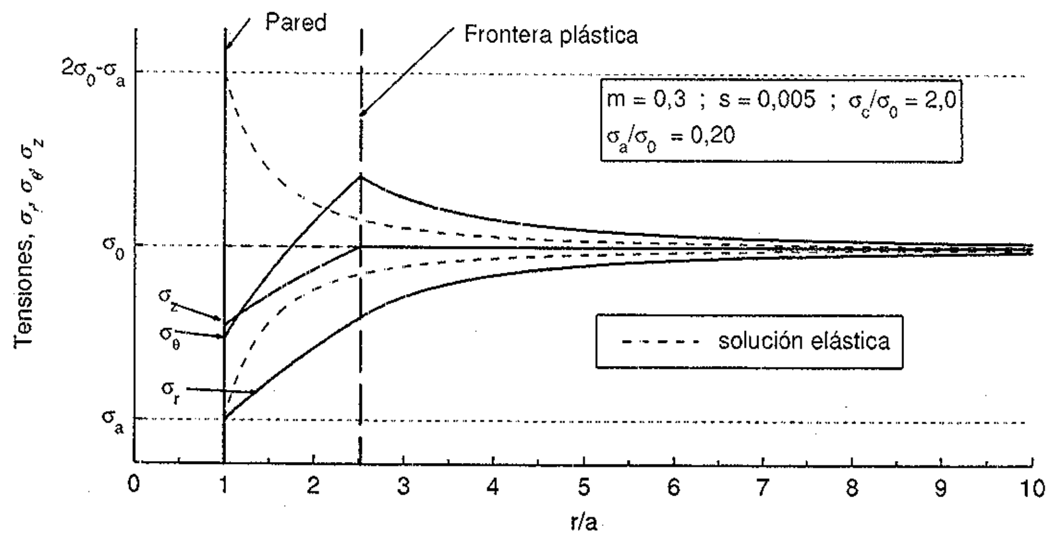

Figura 13. Material de Hoek-Brown. Tensiones y desplazamientos en el terreno. Casos:

a) $\sigma_a/\sigma_0 = 0{,}35$: $\sigma_\theta \geq \sigma_z \geq \sigma_r$ en todos los puntos. Solución correcta

b) $\sigma_a/\sigma_0 = 0{,}20$: $\sigma_z \geq \sigma_\theta \geq \sigma_r$ en parte de la zona plástica confinamientos relativos pequeños, σ_z puede pasar a ser la tensión mayor.

Serrano (1997) presenta una solución elegante y práctica del caso general no lineal, utilizando los parámetros de Lambe (p,q), y los parámetros auxiliares (β,ζ):

$$\beta = \frac{m\sigma_c}{8} \quad ; \quad \zeta = \frac{8s}{m^2}$$
$$p = \frac{\sigma_\theta + \sigma_r}{2} \quad ; \quad q = \frac{\sigma_\theta - \sigma_r}{2} \tag{65}$$

Con ellos, el criterio de Hoek-Brown resulta:

$$p + \beta\zeta = \frac{q^2}{2\beta} + q \tag{66}$$

Las tensiones en la zona plástica:

$$q = q_a + 2\beta \ln\frac{r}{a}$$
$$p = \frac{q^2}{2\beta} + q - \beta\zeta \tag{67}$$

El radio de plastificación:

$$\frac{R}{a} = e^{\frac{q_R - q_a}{2\beta}} \tag{68}$$

En las expresiones anteriores, los valores de q en la pared y el la frontera plástica son, respectivamente:

$$q_a = \sqrt{2\beta(\sigma_a + \beta\zeta)}$$
$$q_R = -\beta + \sqrt{\beta^2 + 2\beta(\sigma_0 + \beta\zeta)} \tag{69}$$

En la Figura 13 se presentan las distribuciones de tensiones en el terreno. Igual que para el material de Mohr-Coulomb, se consideran dos casos con distintos grados de confinamiento, tales que en el primero se mantiene σ_z como la tensión intermedia y en el segundo no.

En cuanto a las soluciones para los desplazamientos, la solución completa y rigurosa es mucho más compleja, pues la no linealidad del criterio implica que los coeficientes de la ecuación diferencial (56) ya no son constantes, por lo que no es posible su integración en forma cerrada y debe hacerse numéricamente. Las soluciones analíticas que aparecen en algunos textos y se utilizan en programas se obtienen haciendo simplificaciones sobre el comportamiento del material, tales como suponer un cierto valor de la deformación volumétrica media en la zona plástica.

3 TENSIONES INICIALES ANISÓTROPAS

En este caso las tensiones iniciales son :

$$\sigma_v = \sigma_0 \quad ; \quad \sigma_h = k_0 \sigma_0 \tag{70}$$

siendo k_0 el coeficiente de empuje lateral. Con esto, se pierde la simetría axial del problema. Sólo existe solución analítica en el rango elástico.

Kirsch (1898) resolvió, tanto en tensión plana como en deformación plana, el caso de un orificio circular en un medio sometido a una tensión uniforme en una dirección, utilizando el método de las funciones de Airy. Superponiendo esta solución (con un giro de 90°) para las tensiones iniciales horizontal y vertical, se obtiene la solución general.

La solución aparece en numerosos textos, pero en muchos de ellos (p.ej., Poulos y Davis, 1974) las expresiones de los desplazamientos no son correctas, pues se supone que las cargas exteriores $(\sigma_0, k_0\sigma_0)$ se aplican <u>después de realizada la excavación</u>. Esta puede ser la situación real cuando se analizan las tensiones en orificios de chapas metálicas al actuar cargas exteriores (que fue el objetivo inicial de la solución de Kirsch), pero no en el caso de túneles. En este caso, interesan los desplazamientos producidos por la excavación, descontando las deformaciones iniciales, gravitatorias, producidas por el peso propio del terreno antes de la excavación del túnel. Pender (1980) hace notar este error y presenta la solución correcta, que es la siguiente:

Tensiones:

$$\begin{aligned}
\sigma_r &= \sigma_0\left[\frac{1+k_0}{2}\left(1-\frac{a^2}{r^2}\right)+\frac{1-k_0}{2}\left(1-4\frac{a^2}{r^2}+3\frac{a^4}{r^4}\right)\cos 2\theta\right]+\sigma_a\frac{a^2}{r^2} \\
\sigma_\theta &= \sigma_0\left[\frac{1+k_0}{2}\left(1+\frac{a^2}{r^2}\right)-\frac{1-k_0}{2}\left(1+3\frac{a^4}{r^4}\right)\cos 2\theta\right]-\sigma_a\frac{a^2}{r^2} \\
\tau_{r\theta} &= -\sigma_0\frac{1-k_0}{2}\left(1+2\frac{a^2}{r^2}-3\frac{a^4}{r^4}\right)\operatorname{sen} 2\theta \\
\sigma_z &= \sigma_0\left[k_0(1-2\nu)+\nu\left(\frac{1+k_0}{2}-\frac{1-k_0}{2}4\frac{a^2}{r^2}\cos 2\theta\right)\right]
\end{aligned} \tag{71}$$

Desplazamientos:

$$\begin{aligned}
\frac{u}{a} &= \frac{1}{2G}\frac{a}{r}\left\{\sigma_0\left[\frac{1+k_0}{2}+\frac{1-k_0}{2}\left(4-4\nu-\frac{a^2}{r^2}\right)\cos 2\theta\right]-\sigma_a\right\} \\
\frac{v}{a} &= -\frac{1}{2G}\frac{a}{r}\sigma_0\left[\frac{1-k_0}{2}\left(2-4\nu+\frac{a^2}{r^2}\right)\operatorname{sen} 2\theta\right]
\end{aligned} \tag{72}$$

Tensiones en la pared $(r = a)$:

$$
\begin{aligned}
&\sigma_{ra} = \sigma_a \\
&\sigma_{\theta a} = 2\sigma_0\left(\frac{1+k_0}{2} - \frac{1-k_0}{2} 2\cos 2\theta\right) - \sigma_a \\
&\tau_{r\theta a} = 0 \\
&\sigma_{za} = \sigma_0\left[k_0(1-2\nu) + \nu\left(\frac{1+k_0}{2} - \frac{1-k_0}{2} 4\cos 2\theta\right)\right]
\end{aligned}
\qquad (73)
$$

Desplazamientos en la pared:

$$
\begin{aligned}
&\frac{u_a}{a} = \frac{1}{2G}\left\{\sigma_0\left[\frac{1+k_0}{2} + \frac{1-k_0}{2}(3-4\nu)\cos 2\theta\right] - \sigma_a\right\} \\
&\frac{v_a}{a} = -\frac{1}{2G}\sigma_0\left[\frac{1-k_0}{2}(3-4\nu)\operatorname{sen} 2\theta\right]
\end{aligned}
\qquad (74)
$$

Las tensiones varían a lo largo de la pared de la cavidad. Además, la tensión media ya no se mantiene igual a la inicial, como ocurría en el caso isótropo. En la Figura 14 se representa un diagrama polar de la variación de la tensión circunferencial σ_θ a lo largo de la pared entre clave (θ=0) y hastial (θ=90°) para k_0<1. La tensión es siempre de compresión, con valores en hastiales muy superiores a las del caso isótropo. Si k_0<1/3, aparecen tracciones en la zona de la clave. Obviamente, la situación se invierte si k_0>1.

En cuanto a los desplazamientos, también varían a lo largo de la pared y no son puramente radiales. Dependen del coeficiente de Poisson. La deformación volumétrica del terreno ya no es nula. En la Figura 15 se representa un caso típico. Cuando se aplica en la pared una presión σ_a uniforme e igual a la presión media, $\sigma_{0m} = \sigma_0(1+k_0)/2$, el túnel se ovaliza sin pérdida de terreno, contrayéndose verticalmente y expandiéndose horizontalmente en la misma cuantía. Al reducir la presión σ_a toda la pared va deformándose hacia el interior, llegando a producirse contracción horizontal.

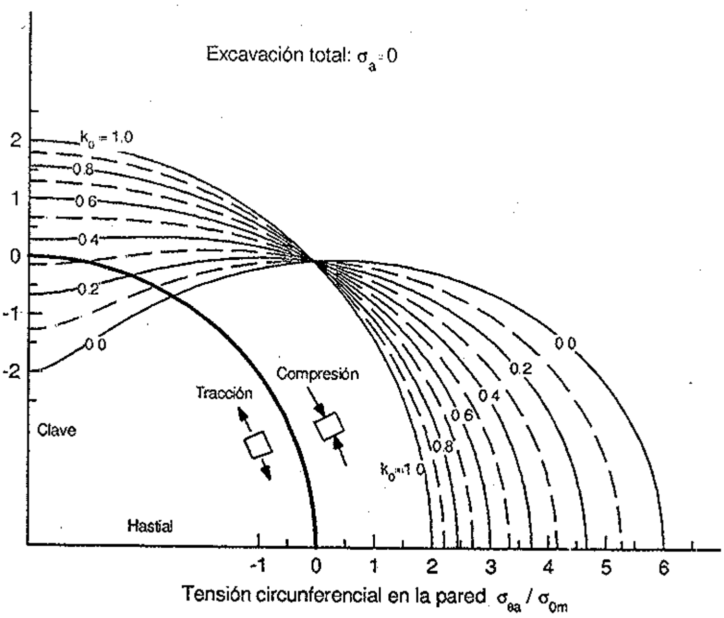

Figura 14. Solución de Kirsch. Tensiones circunferenciales (σ_θ) en la pared

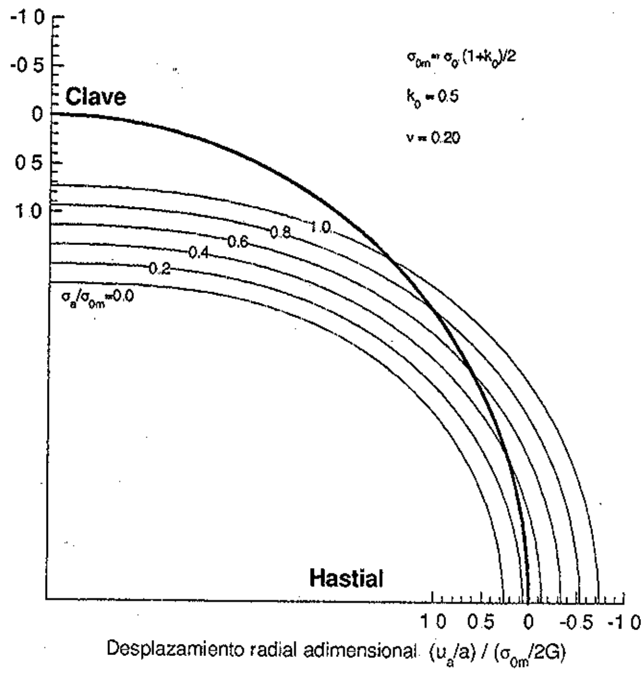

Figura 15. Solución de Kirsch Desplazamientos radiales de la pared

La deformación del túnel puede considerarse compuesta, por una parte, de una convergencia uniforme media u_{am}, y una distorsión. La pérdida de terreno vale:

$$\frac{\Delta V_a}{V_a} = 2\varepsilon_{am} = 2\frac{u_{am}}{a} = \frac{1}{G}\left(\frac{1+k_o}{2}\sigma_0 - \sigma_a\right) \tag{75}$$

Esta pérdida de terreno es igual a la que da la ecuación (7), tomando una presión inicial isótropa igual a la presión media

La distorsión del túnel se puede cuantificar mediante la diferencia entre los desplazamientos en clave y hastial respecto al radio del túnel:

$$\delta = \frac{u_{a(\theta=0)} - u_{a(\theta=\pi/2)}}{a} = \frac{\sigma_0}{2G}\frac{1-k_0}{2}(3-4\nu) \tag{76}$$

Esta ovalización es independiente de la presión interna σ_a (siempre que ésta sea uniforme). Se representa en la Figura 16 para el caso de excavación total (σ_a=0)

4 TÚNEL A PROFUNDIDAD FINITA

Mindlin (1940), utilizando coordenadas curvilíneas bipolares, obtuvo la solución en tensiones en el rango elástico para el caso de existencia de superficie libre a una distancia finita del túnel, considerando incluso gradiente de tensiones iniciales con la

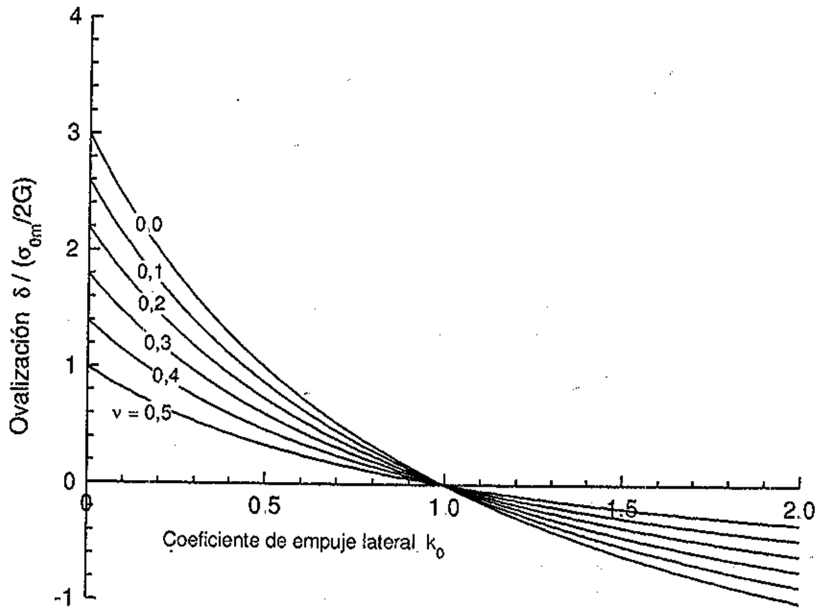

Figura 16. Solución de Kirsch. Ovalización del túnel

profundidad. Sus resultados indican que la influencia de la superficie en la distribución de tensiones no es importante si la profundidad del túnel es mayor de 2 ó 3 diámetros[1]

En cuanto a las deformaciones, es interesante el análisis presentado por Verruijt (1997, 2000) mediante técnicas de variable compleja. Considera la condición de superficie libre a una altura h sobre el eje del túnel, pero manteniendo para las tensiones iniciales su isotropía (k_0=1) y uniformidad (es decir, ignorando su gradiente con la profundidad). Los desplazamientos de la pared del túnel son:

$$\frac{u_a}{a}=\frac{\sigma_o-\sigma_a}{2G}\left[1+2(1-\nu)\frac{\cos\theta}{h/a-\cos\theta}\right]$$
$$\frac{v_a}{a}=\frac{\sigma_o-\sigma_a}{2G}2(1-\nu)\frac{\operatorname{sen}\theta}{h/a-\cos\theta} \qquad (77)$$

Aunque k_0=1, la presencia de la superficie hace que los desplazamientos varíen a lo largo de la pared, y tengan componente tangencial. Se representan en la Figura 17

La pérdida de terreno es:

$$\frac{\Delta V_a}{V_a}=2\varepsilon_{am}=2\frac{u_{am}}{a}=\frac{\sigma_o-\sigma_a}{G}\left[1+2(1-\nu)\frac{2h/a\left(h/a-\sqrt{(h/a)^2-1}\right)-1}{1-h/a\left(h/a-\sqrt{(h/a)^2-1}\right)}\right] \qquad (78)$$

---

[1] La solución original de Mindlin, aunque es relativamente accesible, suele tomarse de otros textos posteriores. Verruijt y Booker (2000) han encontrado que algunos (Poulos y Davis, 1991) contienen errores significativos en los valores numéricos.

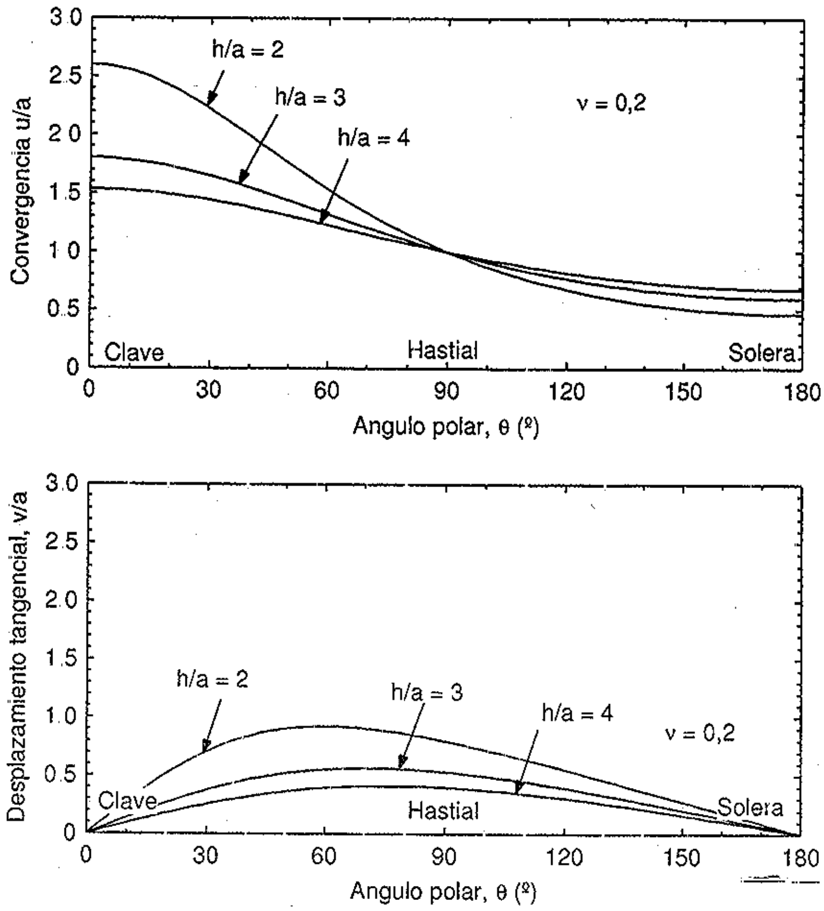

Figura 17. Profundidad finita (Verruijt, 1997). Desplazamientos de la pared

Comparando esta expresión con (7), el factor entre corchetes denota la influencia de la superficie en la pérdida de terreno. Toma valores menores que 1,10 para $h/a>3$, y aumenta abruptamente sólo para recubrimientos menores de un diámetro (Figura 18-a).

En cuanto a la ovalización, resulta (Figura 18-b):

$$\delta = \frac{\sigma_0 - \sigma_a}{2G}(1-\nu)\frac{1}{(h/a)^2 - 1} \tag{79}$$

Para el rango usual de h/a, la ovalización relativa (cociente entre ovalización y convergencia media) es inferior a 0,20.

La presencia de la superficie implica también desplazamientos radiales diferentes en clave (θ=0) y solera (θ=π). El túnel experimenta entonces un movimiento vertical de descenso, que puede calcularse de (77):

$$\frac{s_z}{a} = \frac{u_{(\theta=0)} - u_{(\theta=\pi)}}{a} = \frac{\sigma_0 - \sigma_a}{2G}(1-\nu)\frac{2h/a}{(h/a)^2 - 1} \tag{80}$$

Su valor relativo a la convergencia media varía entre 0,4 y 1,0.

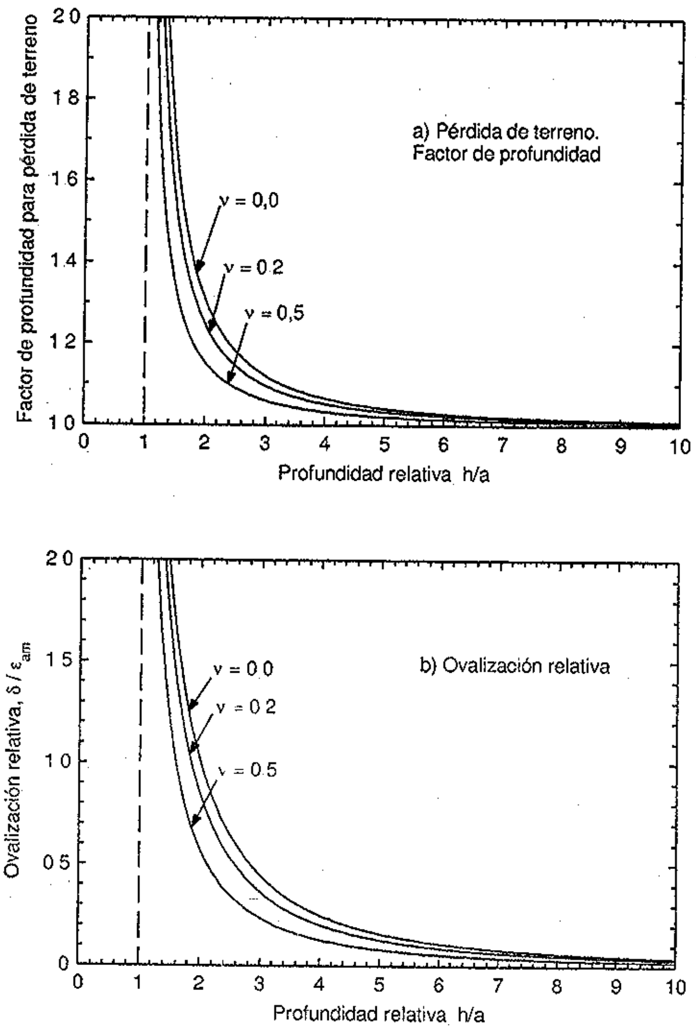

Figura 18. Solución de Verruijt (1997). Parámetros de deformación del túnel

5 INTERACCIÓN TERRENO-REVESTIMIENTO

En los apartados anteriores se ha descrito el estado de tensiones y deformaciones alrededor del túnel la hacer la excavación, manteniendo una presión interior, σ_a. En la realidad, esta presión en la pared la proporciona el revestimiento. Entonces, la presión σ_a no es conocida, sino que es el resultado de la interacción del terreno y el revestimiento. El mecanismo es el siguiente:

a) El terreno se deforma progresivamente, y la pared del túnel se contre, al reducirse la presión en la pared. Si no se coloca revestimiento, se llega al equilibrio final con confinamiento nulo. La ley que relaciona el confinamiento con la convergencia es la que se ha denominado curva característica del terreno, y viene dada por la expresión (5) para terreno elástico, (36) para material de Tresca, (58) para material de Mohr-Coulomb, y expresiones diferentes para otros comportamientos. En la Figura 8 se representó el caso de material de Tresca.
b) En un cierto momento del proceso, se instala un revestimiento, consistente en un anillo de un cierto material (hormigón proyectado o moldeado in situ, cerchas,

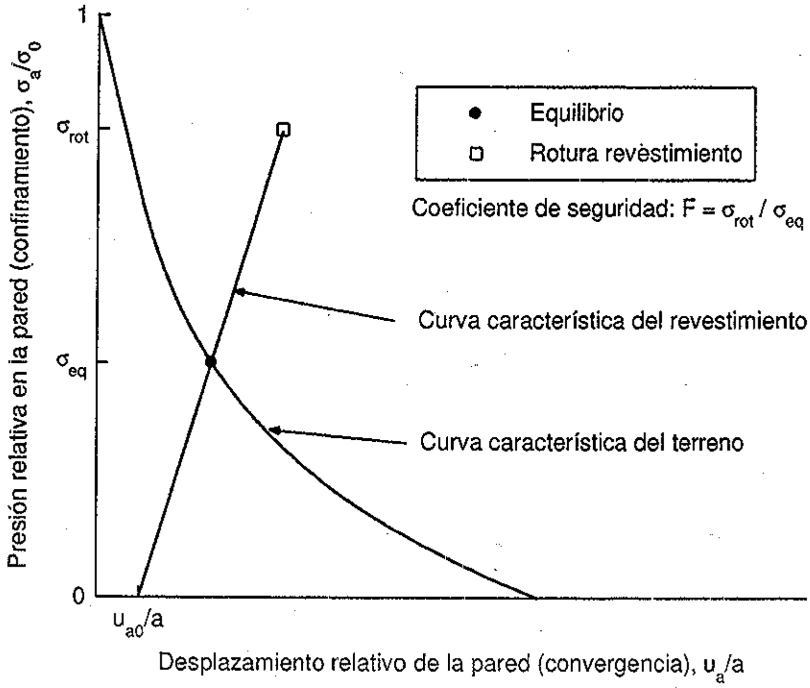

Figura 19. Interacción terreno-revestimiento. Diagrama convergencia-confinamiento

bulones, etc). Este anillo tiene una cierta rigidez frente a la carga exterior ejercida por el terreno. En el caso básico estudiado, esta carga es uniforme y la deformación del anillo es puramente radial, con ~~una~~ convergencia definida por:

$$\frac{u_r}{a} = \frac{u_a - u_{a0}}{a} = \frac{\sigma_a}{k} \tag{81}$$

siendo u_r la contracción radial del revestimiento, u_a la del terreno y u_{a0} la del terreno en el momento de colocar el revestimiento. La rigidez k del revestimiento, si éste es un anillo delgado de espesor e y módulo de elasticidad E_r, vale:

$$k = \frac{E_r e}{a} \tag{82}$$

c) El equilibrio se alcanza cuando la presión entre el terreno y el revestimiento satisface simultáneamente las leyes presión-desplazamiento (curvas características) del terreno (5,36,58) y del revestimiento (81).

En la Figura 19 se ilustra este mecanismo de interacción, y el equilibrio final alcanzado. Eventualmente, la rotura del revestimiento se producirá cuando se alcance la tensión límite del material que lo constituye.

Cuanto menos resistente o más deformable sea el terreno, más arriba estará situada su curva característica (ver Figura 8), con lo que, para un mismo revestimiento, mayor será la presión de equilibrio y la deformación necesaria para alcanzarla.

La Figura 20 ilustra la influencia de la rigidez del revestimiento. Para un mismo terreno, cuanto más flexible sea el revestimiento, menor será la presión de equilibrio, a

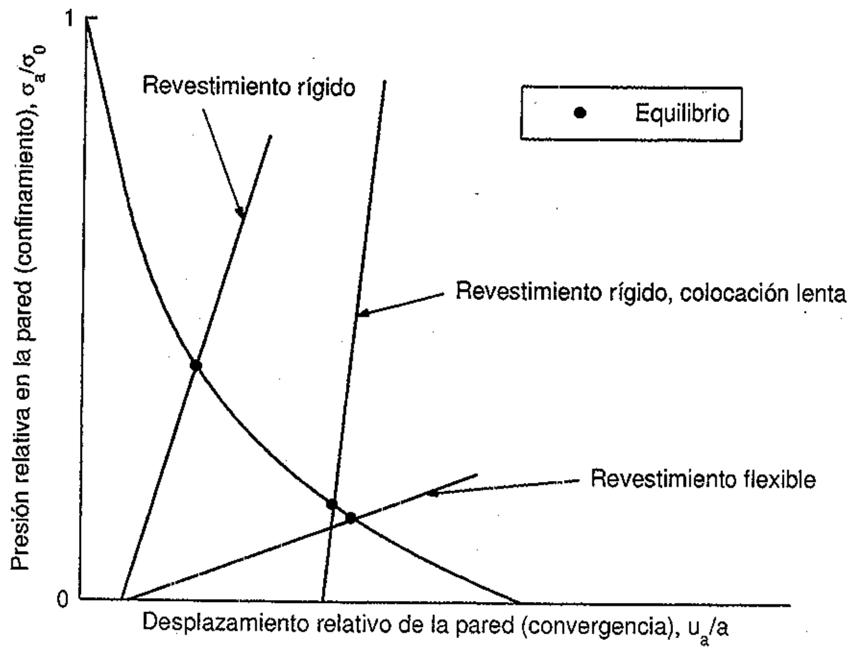

Figura 20. Influencia de la rigidez del revestimiento y velocidad de colocación

costa de una mayor deformación. Sin embargo, la menor rigidez lleva normalmente asociada una menor resistencia, con lo que el coeficiente de seguridad a rotura disminuye. Por último, es importante observar que un revestimiento muy rígido, pero colocado tarde, o que tarda en alcanzar su rigidez (lentitud de fraguado), produce el mismo resultado que un revestimiento flexible pero de actuación más rápida (aunque con mayor seguridad frente a rotura, obviamente)

Los conceptos descritos son el fundamento de la interacción terreno-revestimiento y constituyen la base moderna del dimensionamiento de túneles. Se ha considerado el caso de simetría axial (túnel circular, tensiones iniciales isótropas), que lleva a que el revestimiento trabaja como un anillo sometido a compresión pura (antifunicular de las cargas). En la realidad, esto no es así, y en los apartados 3 y 4 se han considerado casos no simétricos (aunque sólo en régimen elástico). La extensión al campo elastoplástico y la consideración de la interacción terreno-revestimiento, con éste trabajando a axil y flexión, requiere el empleo de métodos numéricos, de elementos finitos. Actualmente estos métodos son de uso habitual en el proyecto de túneles, siguiendo los principios de la interacción descritos.

6 REFERENCIAS

Clough, G.W. y Schmidt, B. 1981. Design and performance of excavations and tunnels in soft clay. Cap. 8 de *'Soft Clay Engineering'* (E.W. Brand y R.P. Brenner, eds.). Elsevier. Amsterdam.

Hoek, E. y Brown, E.T. 1980. Underground Excavations in Rock. Inst. of Mining and Metallurgy. Londres.

Mindlin, R.D. 1940. Stress distribution around a tunnel. Trans. ASCE, 105,1117-1140.

Pender, M.J. 1980. Elastic solutions for a deep circular tunnel. Géotechnique 30,216-222.

Poulos, H.G. y Davis, E.H. 1991. *Elastic Solutions for Soil and Rock Mechanics*. 2ª ed. Centre for Geot. Research. Sydney.

Sagaseta, C. 1998. On the role of analytical solutions for the evaluation of soil deformations around tunnels. Proc. 3rd. Europ. Conf. Num. Meth. Geot. Engg. Udine (NUMGE 98). *Appl of Numerical Methods to Geotechnical Problems* (A. Cividini, ed.). Pp. 3-24. Springer.

Serrano, A.A. 1997. *Elementos de estática de los túneles*. E.T.S. Ing. Caminos. Univ. Polit. Madrid.

Verruijt, A. 1997. A complex variable solution for a deforming circular tunnel in an elastic half-plane. Int. J. Num. Anal. Meth. Geom. **21**,77-89.

Verruijt, A. y Booker, J.R. 2000. Complex variable analysis of Mindlin's tunnel problem. Proc. Booker Memorial Symp. Sydney. *Developments in Theoretical geomechanics* (D.W. Smith y J.P. Carter, eds.). A.A. Balkema. Rotterdam.

Yu, H.S. y Rowe, R.K. 1998. Plasticity solutions for soil behaviour around contracting cavities and tunnels. Res. Rep. 165.06.1998. The University of Newcastle. Australia.

ELSEVIER

Computers and Geotechnics 28 (2001) 445–468

COMPUTERS AND GEOTECHNICS

www elsevier com/locate/compgeo

Patterns of soil deformations around tunnels. Application to the extension of Madrid Metro

C. González *, C. Sagaseta

Universidad de Cantabria, Departamento de Ciencias e Ingeniería del Terreno y de los Materiales, Avda. de Los Castros, s/n, 39005 Santander, Spain

Received 16 June 2000; received in revised form 28 November 2000; accepted 29 January 2001

Abstract

In the period 1995–1999 more than 30 km of new tunnels have been constructed for the Madrid Metro. Most of them are excavated with EPB shield through stiff Tertiary layers The paper presents the application of numerical and analytical solutions to the soil deformations measured during these works. About 60 test-sections have been analysed, some of them including measurement of vertical and horizontal displacements within the ground. The values of the solution parameters (ground loss, tunnel ovalization, soil volumetric deformation) have been obtained by fitting the measured movements The variation of all of the parameters with tunnel geometry and soil type is discussed. © 2001 Elsevier Science Ltd All rights reserved

Keywords: Soft ground tunnels; Soil deformation; Subsidence; Analytical solutions

1. Introduction

The analysis of soil deformations around tunnels has been one of the fields of application of numerical methods in the past. It has usually been argued that factors such as the complex soil stress–strain behaviour and particularly the details of the construction procedure could not be incorporated in the analysis in a suitable form. However, in recent years, some developments have increased the applicability of these methods:

- non-linear models have been implemented in most available codes, and factors such as plastic strains, or stress-path dependence can be considered in a reasonable way;

* Corresponding author. Tel.: +34-942-20-18-13; fax: +34-942-20-18-21.
E-mail addresses: gonzalca@unican.es (C. González), sagasetac@unican.es (C. Sagaseta).

0266-352X/01/$ - see front matter
PII: S0266-352X(01)00007-6

Nomenclature

a	tunnel radius
c, ϕ	effective cohesion and friction
c_u	undrained shear strength
h	depth of tunnel axis
k_{0t}	initial lateral stress coefficient in total stresses
p_0	initial total vertical stress
u,v	radial and tangential displacements of the tunnel wall
u_0	uniform radial displacement
u',v'	distortion component of tunnel wall displacements
u_z	uniform vertical settlement of the tunnel
I_r	rigidity index (G/c_u)
N_0	gross overload factor, for unlined tunnel (p_0/c_u)
N_f	overload factor at the tunnel face ($(p_0-p_f)/c_u$)
N_i	overload factor at the tunnel wall ($(p_0-p_i)/c_u$)
N_c,N_q	overload factors for c,ϕ material
α	exponent for volumetric compressibility
δ	ovalization ($\delta=\max(u')/a$)
ε:	radial contraction (u_0/a)
ε_S	ground loss ($\varepsilon_S=2\varepsilon$)
η	relative vertical settlement of the tunnel ($\eta=(u_z/a)/\varepsilon$)
μ	Poisson's ratio
ν	angle of dilatancy
ρ	relative ovalization ($\rho=\delta/\varepsilon$)

- the three dimensional character of the problem can also be incorporated, and the advance of the tunnelling process can be simulated also with an acceptable degree of accuracy;
- on the other hand, the tunnel construction methods themselves have changed, and the tunnelling operations are increasingly mechanised. This has the side effect of an easier simulation in the analysis. The advance of an earth pressure balance (E.P.B.) shield, with controlled face pressure and tail grout can be modelled much better than a hand-excavated tunnel, highly dependent on the quality of workmanship.

A number of numerical analyses have been presented, either referring to particular tunnelling projects or to generic problem types [11]. In three dimensional models, the actual advance step is reproduced, and the face and tail grout pressures, as well as stiffening of grout with time, are considered.

Plane strain analyses are also used, requiring the introduction of parameters to simulate the actual advance of the tunnel (face stress relief, length of ground supported by fresh grout, etc.). With a careful selection of the appropriate parameters, these models are still highly valuable, even for very refined analyses [2].

In spite of the complex processes taking place around the tunnel, the patterns of soil deformation at some distance are relatively smooth, involving only moderate or small strains. This leads to a general type of approach in which the tunnel construction operations are not reproduced in themselves, but represented by their overall effects in the deformation of the surrounding soil (ground loss, distortion, etc.). Then, the distribution of the movements in the far field can be analysed by different procedures, either empirical, numerical or even analytical.

Empirical methods were developed, assuming simplified functions for the distribution of movements, which are matched with the results of observations in actual tunnels. The use of the Gaussian curve for the surface settlement profile, proposed by Peck [19] is still the most used tool for this purpose. However, it does not give information about other components of deformation. Its extension to cover horizontal displacements or inner soil movements are doubtful, and lacking of a solid basis of observations in actual cases.

Analytical solutions for these distant deformation have been presented in recent years either restricted to linear elastic soil, or based on kinematical conditions [23,31].

The first part of the paper is devoted to the analysis of the deformations in the immediate vicinity of the tunnel, and the definition of representative parameters by means of analytical and numerical methods. Then, the patterns of distant deformations are considered. Finally, the solutions are applied to ~~some~~ illustrative cases, particularly to the extension of the Madrid Metro, in the period 1995–1999.

2. Tunnel deformation

In the general case of a circular tunnel of radius a at finite depth, h, uneven initial stresses ($\sigma_{v0} \neq \sigma_{h0}$) and stress gradient with depth, the displacements of the tunnel wall are non-uniform and with radial and tangential components ($u(\theta)$, $v(\theta)$). This deformation can be considered as the sum of several fundamental modes (Fig. 1):

- a uniform radial displacement, u_0, which can be expressed as a radial contraction ($\varepsilon = u_0/a$) or as a unit ground loss ($\varepsilon = \Delta S/S_0 = 2\pi a u_0/\pi a^2 = 2\varepsilon$);
- an ovalization or distortion of the tunnel without change of section (no ground loss). The radial displacements (u') are predominant over the circumferencial ones (v'). The distortion is usually taken positive as depicted, i.e. with vertical shortening. It is defined by $\delta = \max(u')/a$. Sometimes, the relative ovalization parameter, ρ is used ($\rho = \delta/\varepsilon$);
- a downward uniform movement, u_z, with no distortion. It can also be represented by the non-dimensional ratio $\eta = (u_z/a)/\varepsilon$.

The main available solutions for the determination of these magnitudes are listed below. A more detailed review has been presented by Sagaseta [25].

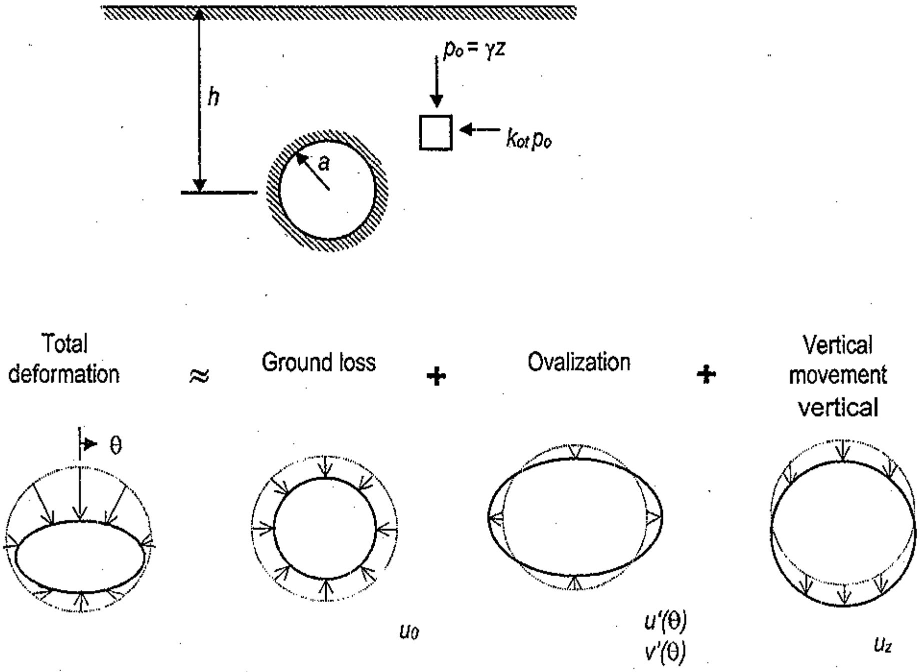

Fig. 1. Components of deformation of the tunnel.

2.1. Ground loss. Axial symmetry

The simplest case is a circular tunnel of radius a, infinite length, excavated at infinite depth in a soil initially subjected to uniform isotropic compression, p_0, ($\sigma_{v0} = \sigma_{h0} = p_0$). A uniform pressure, p_i ($p_i \leqslant p_0$), is left acting at the tunnel wall.

The problem is one-dimensional, and a closed form solution is possible, even in the elastoplastic range. The stress changes are maximum at the tunnel wall, so the plastic zone is a concentric annulus of radius R around the tunnel. Of the above modes of deformation, only the pure ground loss exists.

2.1.1. *Purely cohesive case* (G, $\mu = 1/2$, c_u, $\phi = 0$)

The solution for this case is very simple and well known. It is usually written in terms of a stability factor, $N = (p_0 - p_i)/c_u$. This parameter was originally introduced by Peck [19] and called 'overload factor', to analyse the stability conditions at the tunnel face. For tunnels in clay, it is often used as a reference, but sometimes it is not clear which pressure is subtracted from the overburden pressure p_0. The following notation is proposed here:

- gross overload factor: $N_0 = p_0/c_u$, the one that would develop if the tunnel was excavated and left unlined. It can reach values of up to 8 or 10 in very soft soils (c_u is related to p'_0);
- face overload factor: $N_f = (p_0 - p_f)/c_u$, where p_f is the pressure at the tunnel face, which is only non-zero in closed face tunnelling (air pressure, EPB or slurry shield);

- wall overload factor: $N_i = (p_0 - p_i)/c_u$, where p_i is the pressure at the tunnel wall, i.e. at the soil-lining interface.

The radial contraction is:

$$\varepsilon = \frac{1}{2}\varepsilon_s = \begin{cases} \frac{p_0 - p_i}{2G} = \frac{1}{2I_r}N_i = \frac{1}{2I_r}(1 - \frac{p_i}{p_0})N_0 & \text{if } N_i \leqslant 1 \text{(elastic)} \\ \frac{1}{2I_r}e^{N_i - 1} = \frac{1}{2I_r}e^{(1-\frac{p_i}{p_0})N_0 - 1} & \text{if } N_i \geqslant 1 \quad \text{(elastic–plastic)} \end{cases} \tag{1}$$

where I_r is the rigidity index (ratio of shear stiffness to strength, $I_r = G/c_u$).

2.1.2. General case (G, μ, *c*, ϕ, ν)

The solution for the general case with cohesion c, friction angle ϕ, and dilatancy angle ν, is more complex and of less direct applicability. The incompressibility condition in the case $\phi = 0$ has several implications that simplify the solution, and that are lost in the general frictional case. On the other hand, the volumetric strains in the soil imply that the ground loss at the tunnel and the volume of settlements at the surface no longer coincide. In real cases, only the latter of these two parameters is measured, and this decreases the practical interest of evaluation of the ground loss at the tunnel.

Besides these reasons (or perhaps due to them), there is no universal agreement about the use of non-dimensional parameters similar to the overload factor or rigidity index defined above for the undrained case. As a consequence, the expressions for stresses and displacements given in the literature use different parameters and notation. Their results are not always coincident, sometimes due to printing errata, and in other cases to the consideration of different simplifying assumptions, not always stated explicitly.

From the application of the Theory of Plasticity, the following two factors can be defined:

$$\begin{aligned} N_q &= \frac{p_0 + c\cot\phi}{p_i + c\cot\phi} \\ N_c &= (N_q - 1)\cot\phi = \frac{p_0 - p_i}{c + p_i\tan\phi} \end{aligned} \tag{2}$$

It follows from this that any of the factors N_c or N_q above can be used as load parameters. N_q gives generally simpler expressions, but the factor N_c has the advantage of reducing to the overload factor N_i when $\phi \to 0$. So, both N_c and N_q can be used, having in mind that they are linked by (2). The rigidity index, I_r, can be generalised accordingly as:

$$I_r = G/(c + p_i\tan\phi).$$

At the onset of plasticity at the tunnel wall, the following critical load factors result:[1]

$$N_{qe} = \frac{1}{1-\sin\phi}; \quad N_{ce} = \frac{\cos\phi}{1-\sin\phi} \tag{3}$$

The general expression for the elastoplastic radial contraction (for $N_q \geqslant N_{qe}$) is:

$$\begin{aligned} \varepsilon = \frac{1}{2}\varepsilon_s = \frac{p_0 + c\cot\phi}{2G}[1-2\mu]\left[\left(1+\frac{\sin\phi}{1-2\mu}\right)\left(\frac{R}{a}\right)^{1+m} - 1\right] \\ -\frac{p_i + c\cot\phi}{2G}\frac{1-2\mu+\sin\phi\sin\nu}{1-\sin\phi\sin\nu}\left[\left(\frac{R}{a}\right)^{k+m} - 1\right] \end{aligned} \tag{4}$$

where R is the radius of the plastic zone, and:

$$k = \frac{1+\sin\phi}{1-\sin\phi}; \quad m = \frac{1+\sin\nu}{1-\sin\nu} \text{ and } \frac{R}{a} = \left(\frac{N_q}{N_{qe}}\right)^{\frac{1-\sin\phi}{2\sin\phi}} \tag{5}$$

It is usual to find simplified versions of Eq. (4). The most common assumption is to neglect the elastic component of strains in the plastic region. The resulting expression is:

$$\varepsilon = \frac{1}{2}\varepsilon_s = \begin{cases} \frac{1}{2I_r}N_c & \text{if } N_q < N_{qe} \quad \text{(elastic)} \\ \frac{1}{2I_r}N_{ce}\left(\frac{N_q}{N_{qe}}\right)^{\frac{1-\sin\phi\sin\nu}{\sin\phi(1-\sin\nu)}} & \text{if } N_q > N_{qe} \quad \text{(elastic–plastic)} \end{cases} \tag{6}$$

Eqs. (6) and (4) give very similar results. Sometimes, further simplifications are made, the most frequent being: zero plastic volume change ($\nu = 0$), associative behaviour ($\nu = \phi$), or some uniform volumetric strain along the plastic zone.

2.2. Non-symmetric deformation. ovalization, vertical translation

In the cases of finite depth, uneven initial stresses or stress gradient with depth, the problem is two-dimensional, and the analytical solution is restricted to the elastic regime.

[1] It has been assumed implicitly that the intermediate principal stress acts along the tunnel axis, i.e. in the direction of plane strain: $\sigma_\theta \geqslant \sigma_z \geqslant \sigma_r$. It can be easily proved that this always happens for incompressible soil ($\phi = 0$, $\mu = 1/2$). However, in the general case, it only holds for moderate values of the load factor [24,32].

2.2.1. *Elastic solutions*

The problem with total initial stresses being different in vertical (p_0) and horizontal directions ($k_{0t}\, p_0$) ($k_{0t} \neq 1$), keeping the assumption of infinite depth, was solved by Kirsch [10] and can be found in any textbook of elasticity. However, in its original presentation, the solution was given for the case of stresses acting on a medium with a pre-existing hole. For application to tunnelling, the interest is focused on the excavation of the cavity in a pre-stressed medium. The stresses are the same in both cases, but the displacements are different (in the pre-existing hole case, they do not vanish with the distance to the tunnel) [20,29].

The radial contraction is:

$$\varepsilon = \frac{u_0}{a} = \frac{p_0}{2G}\left(\frac{1+k_{0t}}{2} - \frac{p_i}{p_0}\right) \tag{7}$$

and the tunnel ovalization results:

$$\delta = \frac{\max(u')}{a} = \frac{p_0}{2G}\frac{1-k_{0t}}{2}(3-4\mu) \tag{8}$$

For the case of a near surface tunnel, Mindlin [16] obtained the elastic solution for the stresses, considering also initial stress gradient with depth. His results indicate that the influence of the surface on the stress distribution is not significant for depth-to-diameter ratios over ~~2 or 3~~. Regarding the deformations, there is a recent solution by Verruijt [30], using complex variable techniques. The boundary condition of the stress-free surface is considered, but keeping the assumptions of isotropic ($k_{0t} = 1$), and uniform initial stresses (no gradient with depth). The tunnel wall displacements are:

$$\begin{aligned} \frac{u}{a} &= \frac{p_0 - p_i}{2G}\left[1 + 2(1-\mu)\frac{\cos\theta}{\frac{h}{a} - \cos\theta}\right] \\ \frac{v}{a} &= \frac{p_0 - p_i}{2G}2(1-\mu)\frac{\sin\theta}{\frac{h}{a} - \cos\theta} \end{aligned} \tag{9}$$

This means a radial contraction, ε, and ovalization, δ:

$$\varepsilon = \frac{p_0 - p_i}{2G}\left[1 + 2(1-\mu)\frac{2\frac{h}{a}\left(\frac{h}{a} - \sqrt{\left(\frac{h}{a}\right)^2 - 1}\right) - 1}{1 - \frac{h}{a}\left(\frac{h}{a} - \sqrt{\left(\frac{h}{a}\right)^2 - 1}\right)}\right] \tag{10}$$

$$\delta = \frac{p_0 - p_\mathrm{i}}{2G}(1-\mu)\frac{1}{\left(\dfrac{h}{a}\right)^2 - 1} \tag{11}$$

The factor in brackets in Eq. (10) denotes the influence of the free surface on the radial contraction. It is only significant (greater than 1.10) for $h/a<3$. On the other hand, the presence of the free surface implies that the radial displacements are different at the crown ($\theta=0$) and invert ($\theta=\pi$). So, a third component of the tunnel deformation emerges: a uniform downward movement, u_z, shown in Fig. 1. It can be calculated from (9) as:

$$\frac{u_z}{a} = \frac{p_0 - p_\mathrm{i}}{2G}(1-\mu)\frac{2\dfrac{h}{a}}{\left(\dfrac{h}{a}\right)^2 - 1} \tag{12}$$

The value of this component relative to the average radial contraction, $\eta = (u_z/a)/\varepsilon$, ranges from 0.2 to 0.6 for the usual cases. It must be noticed that this component is only responsible for the settlement of the crown being larger than the invert heave, as usually observed in real tunnels. For a relative ovalization $\rho=0.2$ and a relative settlement $\eta=0.4$, the crown settlement results in being twice as large as the invert heave.

2.2.2 *Influence of plastic strains*

All the above analytical solutions of non-symmetric cases are restricted to linear elastic ground. Their extension to elastic–plastic material requires numerical analysis.

It has been shown that in the elastic range, the relative ovalization, $\rho=\delta/\varepsilon$, due to changes in the pressure at the tunnel wall, is of the order of 0.1–0.2. As a general rule, shear strains in the plastic range can increase indefinitely with no further increase of the applied stresses, whilst volumetric strains are always bounded and related to changes in the mean confining pressure. Hence, it can be expected that the relative ovalization increases when significant plastic zones develop around the tunnel. This presumable trend is investigated by numerical analysis in the following paragraphs.

The goal is to isolate the influence of plastic strains on the degree of ovalization of a circular shallow tunnel. In order to eliminate other factors, such as k_0 effects, gradient of p_0 with depth or non-symmetric tunnelling operations, the medium is considered as prestressed with a uniform pressure, p_0, and the tunnelling operations are reduced to even variations of the inner wall pressure, p_i.

The soil is considered as purely cohesive elastic-perfect plastic material (G, c_u, $\mu=0.5$, $\phi=0$, $\nu=0$). The influence of the shear strength is considered by the gross overload factor, N_0, in the range 1–6, and a constant rigidity index $I_\mathrm{r}=200$. Two values of the tunnel relative depth are considered, $h/a=3$ and 5. Two alternative construction processes are examined.

- Sequence A: Excavation by reducing the wall pressure, p_i, from p_0 to zero (full excavation or failure). This is representative of open face tunnelling.
- Sequence B: Increase of the pressure p_i beyond p_0. This intends to reproduce ideal pressurised face tunnelling, with grouting at the shield tail.

The analysis is carried out in plane strain, with 8-noded quadrilateral elements for the soil, using CRISP program [3].

The results, in terms of radial contraction, ε and ovalization, δ, are shown in Fig. 2. In all cases, deformations for sequences A and B (excavation and grouting pressure) are opposite (there is no reason to expect differences in loading and unloading of the tunnel wall in the absence of gravity and k_0 effects).

For the deep case ($h/a=5$), the radial contraction ε follows closely the theoretical solution for infinite depth [Eq. (1)], but some degree of ovalization is observed. In the elastic range, δ is positive for excavation and negative for grouting (i.e. the tunnel shortens or expands more vertically than horizontally). However, plastic deformations reverse the trend, and the values of δ and ε have opposite sign. This means that lateral displacements are greater than vertical ones, and the tunnel deforms into a vertical ellipse for excavation and into a horizontal ellipse for tail grouting.

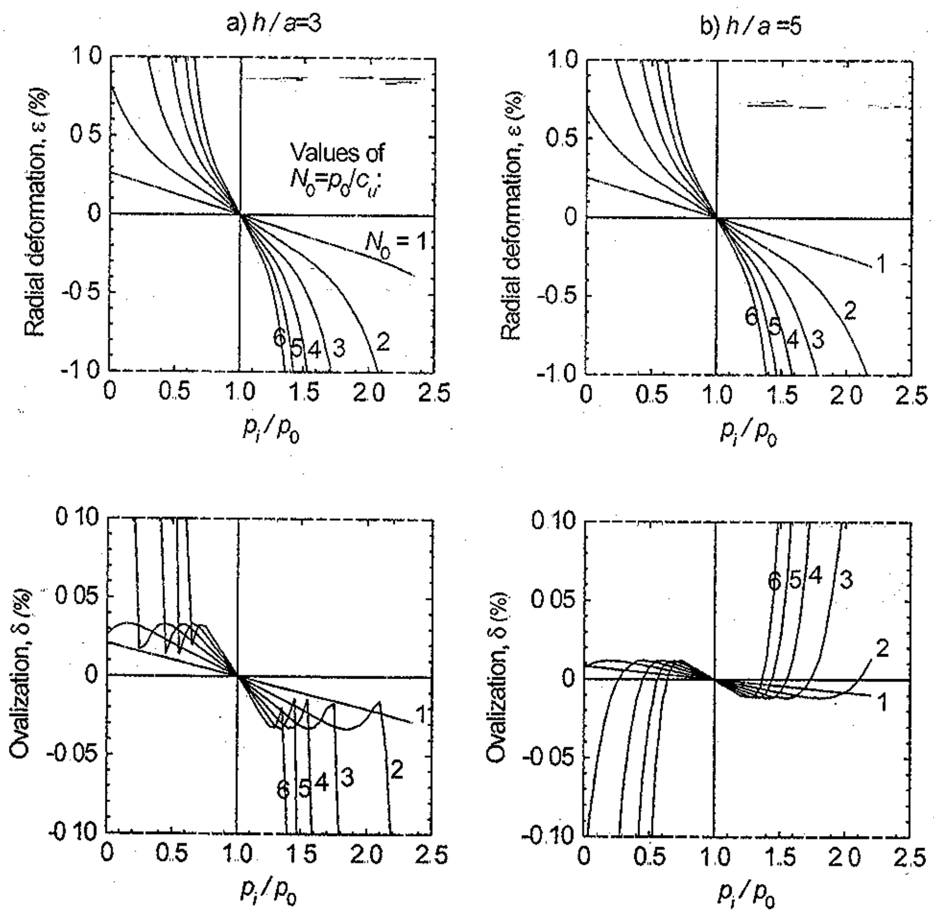

Fig. 2. Numerical analysis of a shallow tunnel. Radial deformation and ovalization.

For the shallow case ($h/a=3$), the deformation trends are similar in the elastic range and for moderate plastic strains. However, for a value of N_i of about 1.6–2.2, a sudden reverse of the ovalization takes place, followed by a roof failure of the tunnel. In this case, the vertical deformation of the tunnel is always greater than the lateral one.

As a result, the relative ovalization of the tunnel can take any value within a very wide range. In general, relative ovalization increases as soil strength decreases. Horizontal deformations are dominant in deep tunnels, but in shallow cases, there can be a reversal of the pattern, and roof deformation can be the major one. These trends can be significantly altered by the conjugate effects of k_0 and gravity (weight of the shield, etc.).

2.3. Application

Fig. 3 shows the results of centrifuge tests of a circular tunnel in clay [12], in which the inner pressure p_i is decreased progressively until collapse. Two tests are presented, with h/a ratios of 4.34 and 7.22. The numerical results presented in the preceding section for h/a of 3 and 5 have been superimposed in the figure, as well as the case of infinite depth, for a rigidity index of 200, indicated by the authors as representative for the case. In the initial part of the curves, near the elastic range, both tests give similar values of the ground loss. This indicates a relatively small effect of

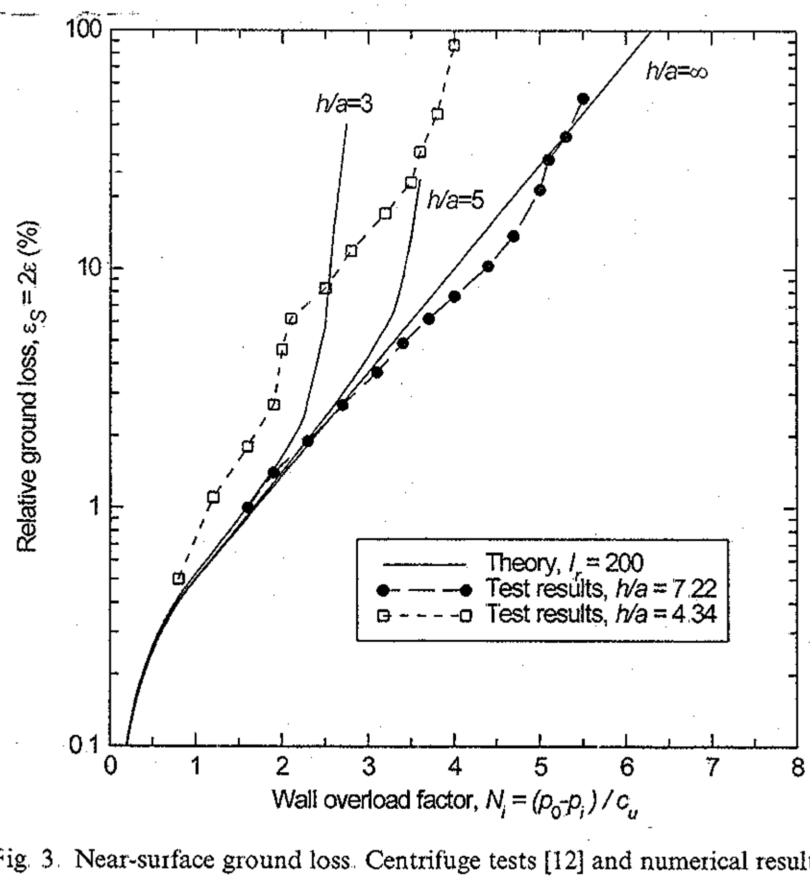

Fig. 3. Near-surface ground loss. Centrifuge tests [12] and numerical results.

the free surface. For the plastic range, the deeper case follows closely the theoretical curve. However, in the shallower case the measured ground loss is higher, in agreement with the results of the numerical analysis.

There are many reported measurements of ground loss in actual tunnels in clay. However, in most cases the overload factor at the face, N_f, is used as reference. As commented above, in order to compare with analytical predictions, the relevant parameter is N_i at the tunnel wall. The pressure p_i is not known. So, it must be taken as variable, expressing the solution in terms of the gross overload factor, N_0, and the unknown value of the pressure ratio p_i/p_0, as in (1).

This is plotted in Fig. 4 for an average rigidity index ($I_r = 100$), together with the results of actual observations. It is clearly seen that closed face tunnels give lower ground losses, at relatively higher lining pressures. For conventional excavation, without shield, there are only cases with N_0 up to 2. The range for open face shields extends to $N_0 = 4$, and beyond this limit there are only cases with pressurised face. There are some remarkable exceptions: four points of conventional (no shield) tunnelling, with $N_0 > 7$, corresponding to Chicago Metro, excavated under air pressure in 1940 [19]; there is also a noticeable case of open shield tunnelling in a soil with $N_0 = 9$ with moderate ground loss (4.3%), in a section of San Francisco BART [19].

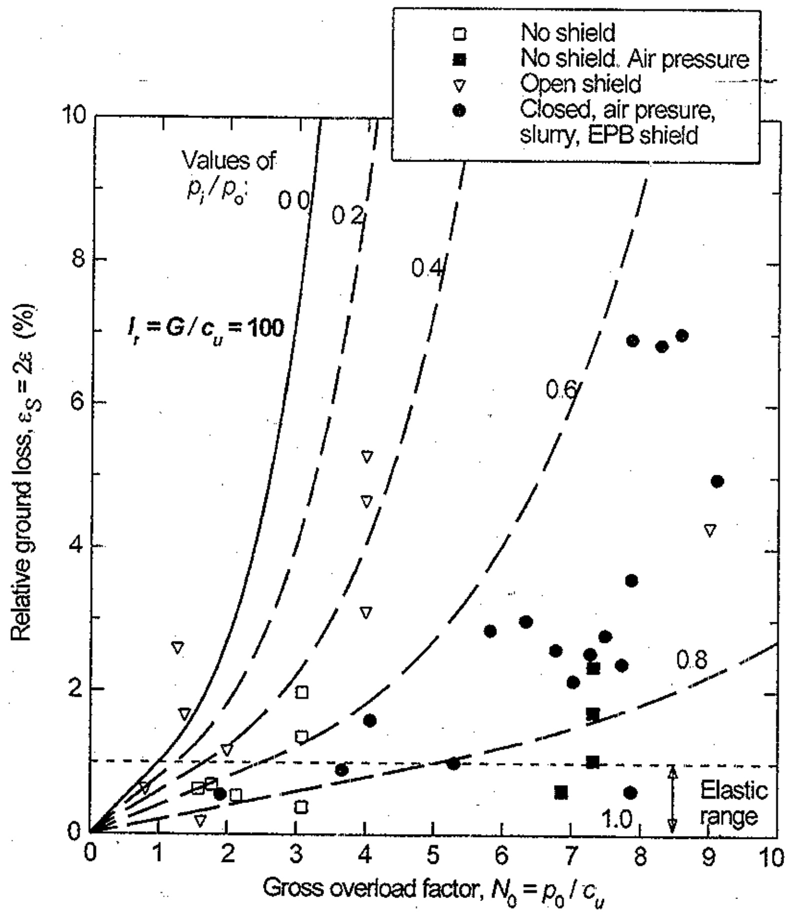

Fig. 4. Measured ground loss in tunnels in clay.

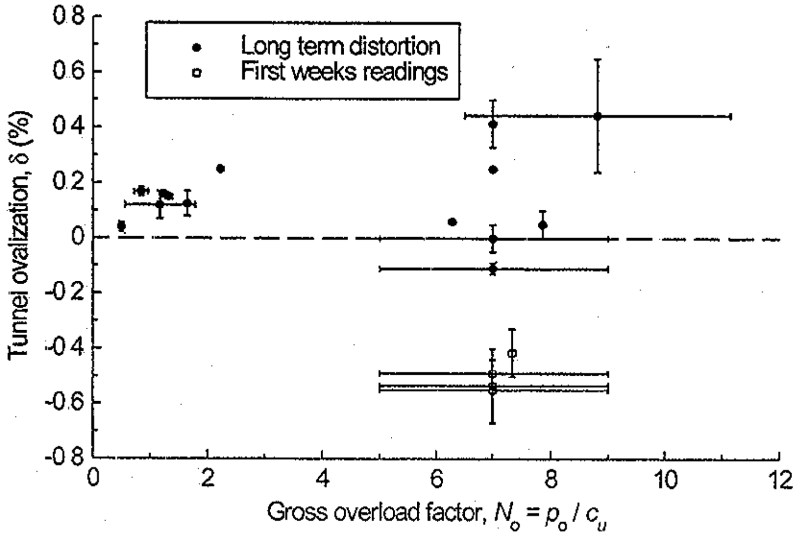

Fig. 5. Measured ovalization in tunnels in clay (data from Peck [19])

There are fewer data on measurements of tunnel ovalization. Fig. 5 shows cases compiled by Peck [19] for open face tunnels in clay. The absolute value of the distortion tends to increase with N_0. For large N_0 values, the distortions tend to be negative in the first weeks, and then the deformation is reversed to positive ovalization. Comparing with Fig. 4, the order of magnitude of the distortion is about one tenth of the ground loss. However, this analysis is only qualitative, because the distortion is measured in ~~the~~ lining, so all the movements before the lining erection are ignored. In contrast, the ground loss is measured as the surface settlement volume, so it includes all the deformation.

3. Distant deformation

For the distribution of far field movements, the influence of construction details and tunnel precise geometry is not so important, due to attenuation with distance. As a result, soil deformation follows relatively simple patterns. On the other hand, the influence of the soil surface becomes of primary importance, and must be considered in any realistic analysis. This explain the success of empirical methods to fit the patterns of soil deformation. The use of the error curve, proposed by Peck [19] and Schmidt [27], has become the most efficient tool to fit the final transverse profiles of surface settlements. The success of this approach is based on its capability for reproducing the actual patterns of settlement profiles, but there is no theoretical basis for it. Some further extensions of the error curve have been introduced for horizontal displacements, and movements near to face, but based on a limited evidence.

A theoretical approach to this problem was proposed by Sagaseta [23], based on solutions for incompressible irrotational fluid flow (Fig. 6). This solution has been applied to tunnelling and also to a number of problems related to ground loss or injection (pile driving, pipe jacking, compensation grouting). It is outlined in the following paragraphs.

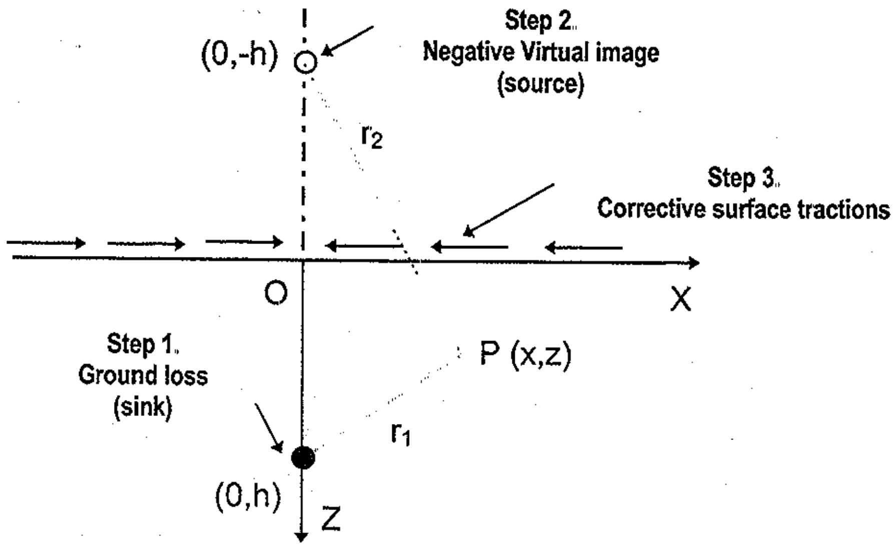

Fig. 6. Near-surface ground loss. Virtual image technique [23]

3.1. Ground loss at finite depth

First, the undrained ground loss in an infinite space is considered, reducing the tunnel to a point sink (Step 1), with the conditions of incompressibility and spherical symmetry determining a radial field of displacements, decreasing with the distance to the sink. The surface is considered by using a virtual image technique (Step 2), combined with corrective surface tractions (Step 3), for which elastic solutions for the half space are used. It is easily proved that the displacements at the surface are twice those that would occur if the sink was in an infinite space.

The final displacement field due to a ground loss ε_S (radial deformation ε) is given by:

$$
\begin{aligned}
s_x &= -\varepsilon a\frac{a}{h}\left[x'\left(\frac{1}{r_1'^2}+\frac{1}{r_2'^2}\right)-4x'z'z_2'\frac{1}{r_2'^4}\right]\\
s_z &= -\varepsilon a\frac{a}{h}\left[\frac{z_1'}{r_1'^2}-\frac{z_2'}{r_2'^2}+\frac{2z'\left(x'^2-z_2'^2\right)}{r_2'^4}\right]
\end{aligned}
\tag{13}
$$

where $z_1=(z-h)$, $z_2=(z+h)$, and r_1 and r_2 are the distances to the sink and its image, respectively (Fig. 6). The prime (′) denotes that the magnitudes are scaled by the tunnel depth, h.

At the soil surface ($z=0$):

$$
\begin{aligned}
s_{x(z=0)} &= 2\varepsilon a\frac{a}{h}\frac{x'}{1+x'^2}\\
s_{z(z=0)} &= 2\varepsilon a\frac{a}{h}\frac{1}{1+x'^2}
\end{aligned}
\tag{14}
$$

These expressions imply that the displacement vector at the surface is addressed towards the tunnel centre. The complex variable solution by Verruijt [30] has confirmed that only for extremely shallow tunnels ($h/a<2$), there is a significant departure from this.

3.2. Tunnel ovalization

Referring to the deformation components at the tunnel wall, step 1 in the analysis (Fig. 6) implies a pure radial ground loss, and steps 2 and 3 give a significant downward movement, but only a very small ovalization. Recently, Verruijt and Booker [31] have presented an extension of the above analysis including the effect of the ovalization. For the sink in the infinite space, Kirsch's solution is used, neglecting the third order terms, $(a/r)^3$. The displacements are written in terms of the radial tunnel deformation ε, and the ovalization δ, instead of p_0, p_i and k_{0t}. In this way, δ is taken as a basic input parameter, as the ground loss, regardless its origin (uneven stresses, different support conditions at the crown and at the sides, or plastic deformations that imply maximum movements at the crown).

For $\mu=1/2$, the displacement field due to the tunnel ovalization, δ, is:

$$
\begin{aligned}
s_x &= \delta a \frac{a}{h}\left[x'\left(\frac{x'^2-z_1'^2}{r_1'^4}+\frac{x'^2-z_2'^2}{r_2'^4}\right)-4x'z'\frac{x'^2-3z_2'^2}{r_2'^6}\right] \\
s_z &= \delta a \frac{a}{h}\left[z_1'\left(\frac{x'^2-z_1'^2}{r_1'^4}+\frac{x'^2-z_2'^2}{r_2'^4}\right)-4z'z_2'\frac{3x'^2-z_2'^2}{r_2'^6}\right]
\end{aligned}
\tag{15}
$$

These displacements must be added to (13) to give the total displacement field

The transversal settlement troughs given by (14) are wider than usually measured in actual cases [24,28]. The ovalization tends to reduce this lateral spreading, thus giving a better reproduction of actual measurements.

3.3. Soil compressibility. Plastic strains

The volumetric strains in the plastic range (soil positive or negative dilatancy) can also contribute to give settlement profiles more concentrated than in the undrained, constant volume case. In order to include these effects, the use of an exponent in the denominator of the settlement profile Eq. (14) was proposed [17,24]. This was based on the fact that in non-elastic medium, the displacements in the plastic zone attenuate with a power of the distance, $O(1/r^\alpha)$, $\alpha>1$. For purely plastic deformation, α coincides with the dilatancy coefficient m defined in (4), which is in the range 1–3. However, in real cases, the value for α must be an average between this upper limit in the plastic zone around the tunnel and $\alpha=1$ in the elastic region.

3.4. Combined effect. General solution

The simultaneous consideration of the ground loss, ovalization and volumetric compressibility leads to the following general expressions [8], where higher order terms have been neglected:

$$\frac{s_x}{2\varepsilon a\left(\frac{a}{h}\right)^{2\alpha-1}} = -\frac{x'}{2r_1'^2\alpha}\left(1-\rho\frac{x'^2-z_1'^2}{r_1'^2}\right) - \frac{x'}{2r_2'^2\alpha}\left(1-\rho\frac{x'^2-z_2'^2}{r_2'^2}\right) + \frac{4x'z'}{2r_2'^2\alpha}\left(\frac{z_2'}{r_2'^2}-\rho\frac{x'^2-3z_2'^2}{r_2'^4}\right)$$

$$\frac{s_z}{2\varepsilon a\left(\frac{a}{h}\right)^{2\alpha-1}} = -\frac{z_1'}{2r_1'^2\alpha}\left(1-\rho\frac{x'^2-z_1'^2}{r_1'^2}\right) + \frac{z_2'}{2r_2'^2\alpha}\left(1+\rho\frac{x'^2-z_2'^2}{r_2'^2}\right) - \frac{1}{2r_2'^2\alpha}\left(2(z'+\rho)\frac{x'^2-z_2'^2}{r_2'^2}+4\rho z'z_2'\frac{3x'^2-z_2'^2}{r_2'^4}\right)$$

and at the surface ($z=0$):

$$\begin{aligned} s_x &= -2\varepsilon a\left(\frac{a}{h}\right)^{2\alpha-1}\frac{x'}{(1+x'^2)^\alpha}\left(1+\rho\frac{1-x'^2}{1+x'^2}\right) \\ s_z &= 2\varepsilon a\left(\frac{a}{h}\right)^{2\alpha-1}\frac{1}{(1+x'^2)^\alpha}\left(1+\rho\frac{1-x'^2}{1+x'^2}\right) \end{aligned} \quad (17)$$

4. Application

4.1. General aspects

The solution (16) is defined by three parameters: ε, δ and α. Their values in a given case can be obtained if the displacements are known in at least three points. In practice more values are needed, and the following trends are usually observed.

- Particular values of the displacement have a wide scatter. Better fitting is obtained if some smoothing, averaging or integration of the measurements is performed. The volume of surface settlements, the maximum settlement, and the equivalent abscissa of the inflection point (at which the settlement is 0.61 s_{max}), easily obtained from the measurements, are convenient parameters for this purpose.
- If only surface settlements are measured, it is not possible to separate the effects of α and $\rho(=\delta/\varepsilon)$. There is always a family of values (α,ρ), giving practically identical settlement profiles. To obtain individual values of α and ρ,

it is necessary to know soil displacements inside the soil (inclinometers or extensometers).

- In some cases, the tunnel construction can be divided into elementary operations (staged excavation, twin tunnels, face and tail deformations in shield tunnelling). Then, the above solution can be applied to each individual operation and their effects superimposed. The expressions are linear for ε and δ, but not for α. Hence, the values of ε and δ can be added only if α is kept constant for all the process.
- The value of α must be 1.0 in clays (at least for short term deformations). In granular materials, $\alpha > 1$, but not very high, specially for deep tunnels. A reasonable upper bound can be $\alpha = 2$ in any case and keep $\alpha \cong 1$ for $h/a > 8$
- With shield tunnelling in very soft soils, the ratio of vertical to horizontal displacements at the tunnel face and at the tail can be very different. As shown in the numerical analyses presented above, tail grouting in soft soils can produce greater lateral displacements. The resulting relative ovalization can take almost any value (positive or negative), depending on the face and grout pressures distributions.

4.2. Some illustrative cases

The solution has been applied to some illustrative examples taken from the literature, with available measurements of vertical and horizontal displacements, at the surface and inside the soil. Table 1 shows for each case the relevant tunnel data, the main parameters of the soil deformation (relative volume of settlements, V_s and maximum settlement, s_{max}), and the parameters of the solution (ε, δ, ρ, α) giving the best fit to the measurements.

The first five cases are for open face tunnelling, either with shield or hand excavation. The ground loss is usually over 2% ($\varepsilon > 1\%$), with moderate ovalizations ($\rho \leqslant 1$). The last five cases, with pressurised face shield (air pressure, slurry or E.P.B) give less ground loss, with ε below 1%, reaching almost zero or even negative values. For the cases in clay, the value of $\alpha = 1$ has been forced, whilst in granular soils it has been left free, in the range 1–2.

It is also remarkable the high ovalization resulting in the N-2 (San Francisco) and Mexico sewers. In both cases, the ground is extremely soft, and hence the tail grout can induce a widening of the horizontal diameter, as it was shown above.

4.3. Madrid Metro extension

The new extension plan of the Madrid Metro for the period 1995–1999 has included the construction of more than 30 km of new tunnels and 35 stations. Sixty-four per cent of the tunnel length was excavated with EPB (earth pressure balanced) shields, 21% with hand mining (Belgian method) and 21% in cut and cover.

Most of the urban area of Madrid is settled on Tertiary (Pliocene) deposits, covered by Quaternary sediments associated with the Manzanares river and its tributaries, and also by frequent man-made fills. All the Tertiary materials are very stiff, heavily

Table 1
Results of application of the analytical solution to some documented cases

Case	Ground	Tunnel data			Surface settlements		Parameters of the solution				Reference
		h (m)	a (m)	Method	V_s (%)	s_{max} (mm)	ε (%)	δ (%)	ρ	α	
Green Park, London	Stiff clay	29.4	2.07	Open shield	1.6	6.5	1.2	0.84	0.7	1.0	Attewell and Farmer [1]
Thunder Bay	Soft clay	10.7	1.24	Open shield	8.3	50	7.5	7.5	1.0	1.0	Palmer and Belshaw [18]
Heathrow express	Stiff clay	19	4.25	Open face	1.5	40	1.0	0.8	0.8	1.0	Deane and Bassett [5]
Sewer Bangkok	Clay	18.5	1.33	Open face	3.8	12	3.4	3.4	1.0	1.0	Phienwej [21]
Baixa Station Lisbon	Sand	25	5.6	Open face	0.8	30	2.4	2.4	1.0	1.5	Sagaseta et al. [26]
Sewer Cairo	Clay	14	2.6	Air pres. shield	1.2	15	0.75	0.6	0.8	1.0	El Nahas et al. [6]
N-2 San Francisco	Soft clay	10	1.8	EPB shield	3.1	30	0.95	3.34	3.5	1.0	Clough et al. [4]
Sewer Mexico City	Soft clay	12.75	2.0	EPB shield	3.6	30	0.4	1.8	4.5	1.0	Romo [22]
Lyon Metro P1-S1	Silt, sand	16	3.13	Slurry shield			0.162	0.355	2.2	1.7	Kastner et al. [9]
				(†)[a]			−0.121	0.000	0.0		
							0.041	0.355	8.7		
Lyon Metro P2-S	Silt, sand	13	3.13	Slurry shield			0.015	0.076	5.1	1.7	Kastner et al. [9]
				(†)			−0.191	0.020	−0.1		
							−0.176	0.096	−0.6		

[a] (†): The first row of values is for the passage of the tunnel face, the second one for the incremental movements due to the tail grout and third one the final (accumulated) displacements.

overconsolidated. From top to bottom, the following layers are found: (i) "*arena de miga*", a clayey sand, with the clay forming bonds between the sand particles; (ii) "*tosco*", a stiff sandy clay; (iii) "*peñuela*", a stiff marly clay; and (iv) gypseous marl, with some layers of gypsum rock.

The unconfined compressive strength increases with the fines content, from 200 to 400 kPa in the sandy materials up to 1500–2000 kPa in the *tosco* and *peñuela*. The vertical deformation moduli obtained from plate loading tests are in the range 30–150 MPa, also increasing with fines content, and approximately 2–3 times greater in the horizontal direction. The values from self-boring pressure meter tests are significantly higher, in the range 400–1300 Mpa.

The presence of occasional layers with expansive properties within the *peñuela* has caused some major problems in building foundations in the South of Madrid, but there is no record of any significant incidence in tunnelling works.

Past experience indicates that for open face tunnelling, the relative volume of settlements is below 1%, except in the presence of local weak zones, such as clean water-bearing sand lenses, quaternary sediments, man-made fills, etc. [7]. For EPB tunnelling, the relative volume of settlements is generally below 0.5%, showing a good correlation with the cover in Tertiary materials [14].

The design criteria were to accept maximum surface settlements of 5 mm under buildings and 17 mm in open areas. A large monitoring plan was implemented, with a total of 9000 instruments installed: points for surface settlements and horizontal displacements, control of building movements, inclinometers and extensometers (multiple rod type and sliding micrometers), as well as earth pressures, forces and stresses in tunnel lining, etc. A central control unit was created, where all the readings of the instruments were collected, together with the data furnished by the tunnelling machines. A detailed description can be found in Melis et al. [15].

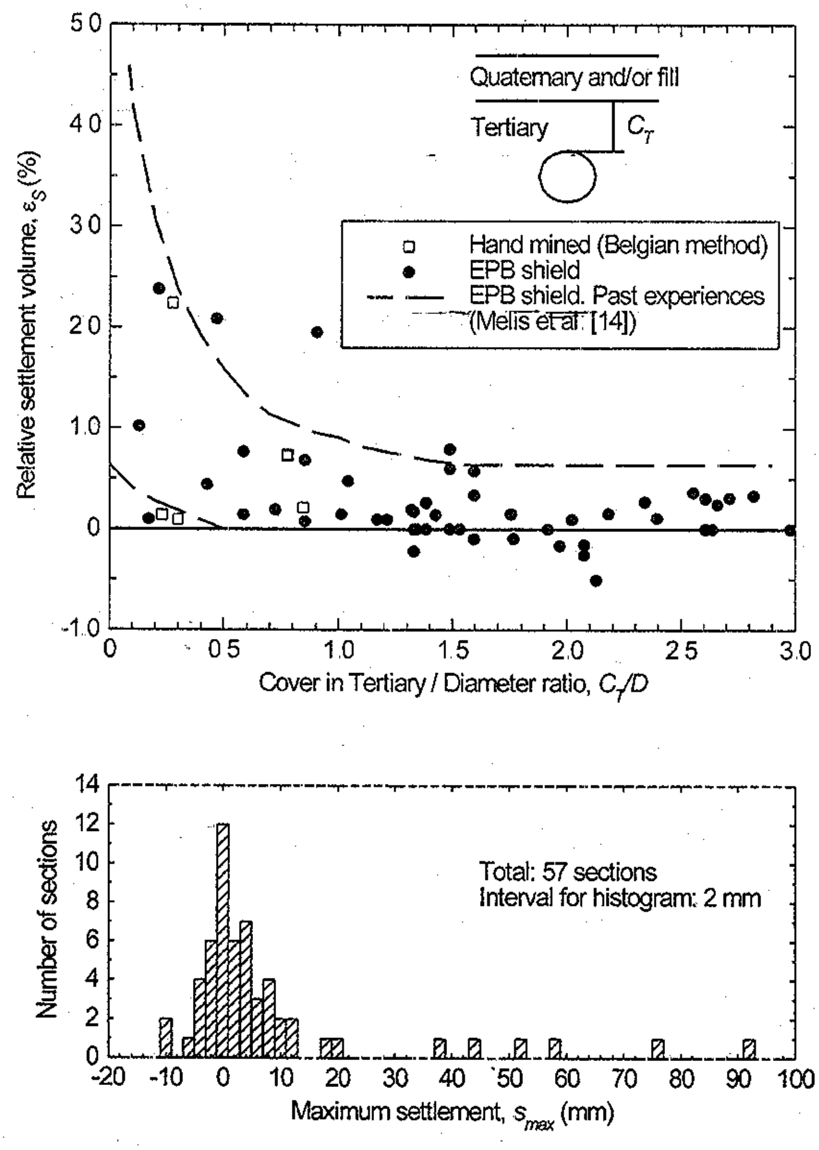

Fig. 7. Madrid Metro, summary of maximum settlements and volume of settlements.

Different studies have been conducted to interpret all these data, from empirical or semi-empirical analysis to 3-D numerical models for the tunnelling process [13]. In the present paper, the solution (16) has been applied. Fifty-seven test sections have been analysed, 6 of them excavated by open face hand tunnelling (Belgian method) and 51 with EPB shield. Fig. 7 shows a summary of the maximum surface settlements and volume of settlements.

From the EPB shield sections, there are 13 with surface heave, and 12 sections with movements smaller than 1 mm (i.e. within the range of accuracy of the

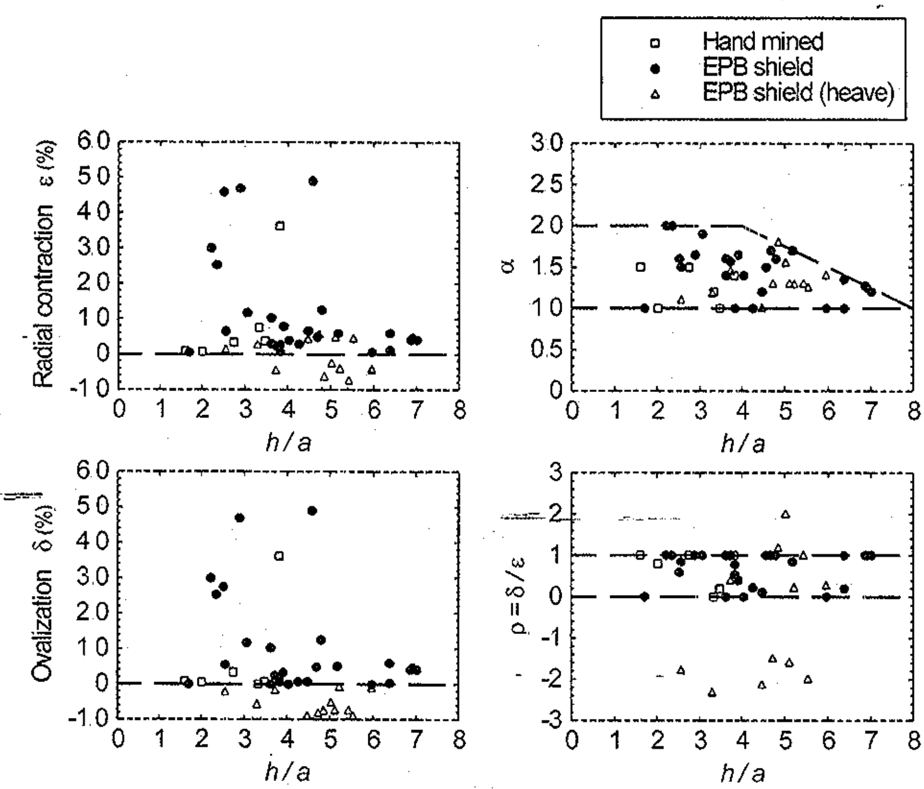

Fig. 8. Madrid Metro, summary of fitted solution parameters

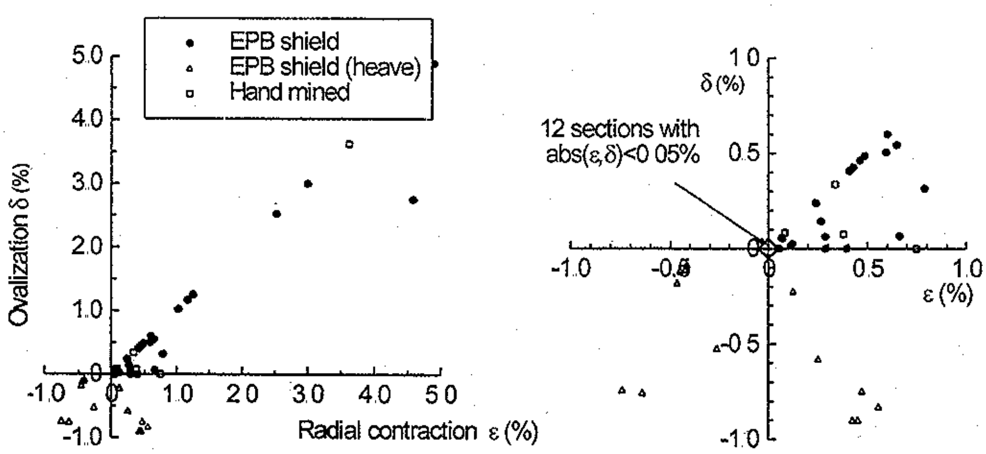

Fig. 9 Madrid Metro, ovalization and radial contraction.

measurements). In the remaining 26 sections, the settlements are generally of a few millimetres, with the exception of 5 cases, with larger movements (> 40 mm). For hand mined tunnelling, 5 sections have settlement of some millimeters, and one 57 mm.

In each section, the values of ε, δ and α have been obtained by fitting the measured movements, subjected to the restrictions above commented. The resulting parameters are summarised in Fig. 8, plotted against the relative depth, h/a. None of the parameters shows a tendency to vary with the depth. This is reasonable, because the depth has already been considered as an independent variable in the formulation. The parameters can vary with the soil type and tunnelling process, but not with the tunnel geometry.

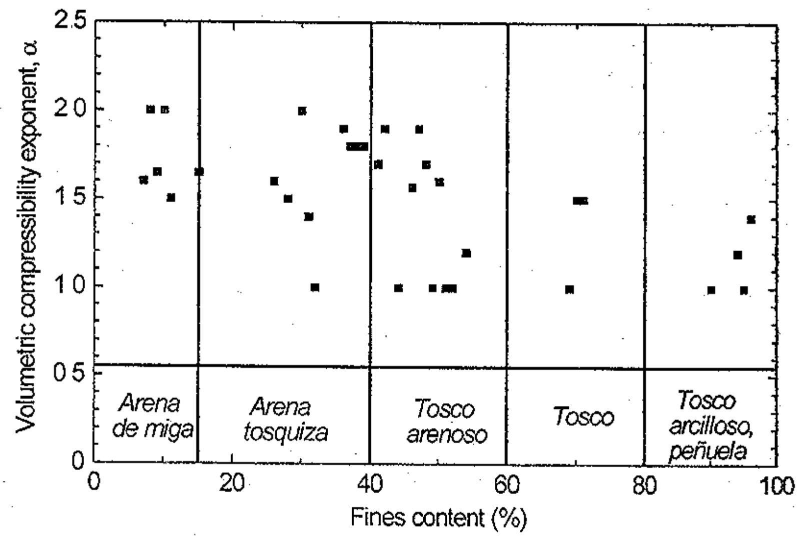

Fig. 10. Madrid Metro, volumetric compressibility exponent, α.

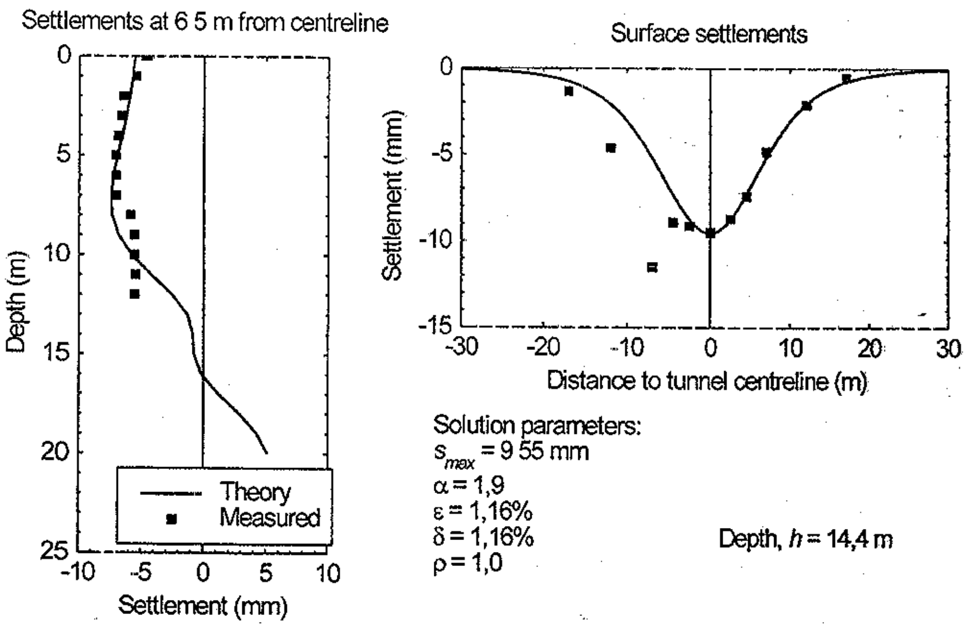

Fig. 11. Madrid Metro, EPB shield, section with settlements (line 9, section 9).

The ground loss at the tunnel is roughly constant. The radial contraction ε is generally below 0.5%, with the exception of the six sections with large movements, associated with small cover in Tertiary material, in which ε is between 2 and 5%. The ovalization is shown in Fig. 9 against the radial deformation. There are still few data, but it seems that the relative ovalization tends to increase ($\rho \to 1$) when the

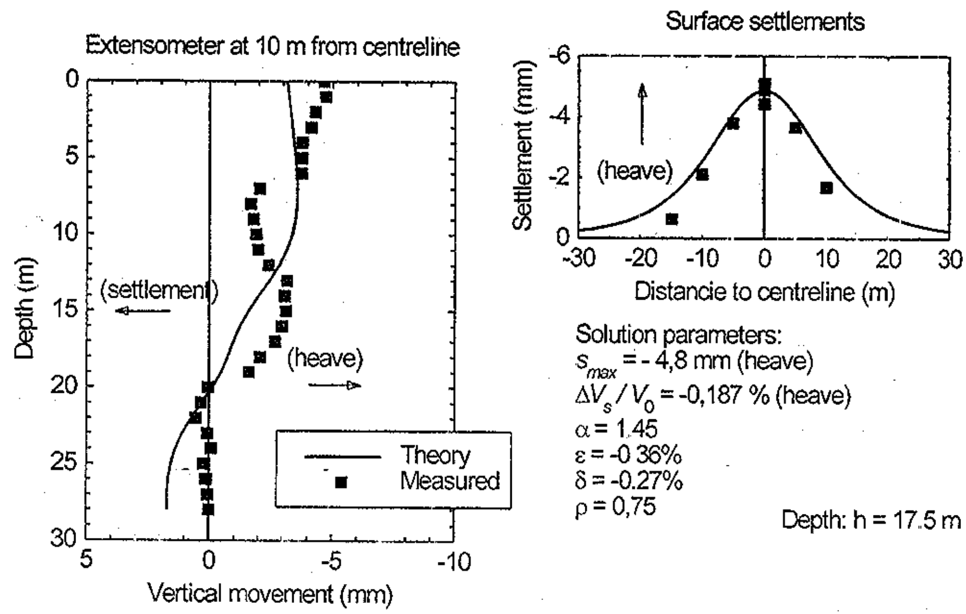

Fig. 12. Madrid Metro, EPB shield, section with surface heave (lines 7–4, section 24).

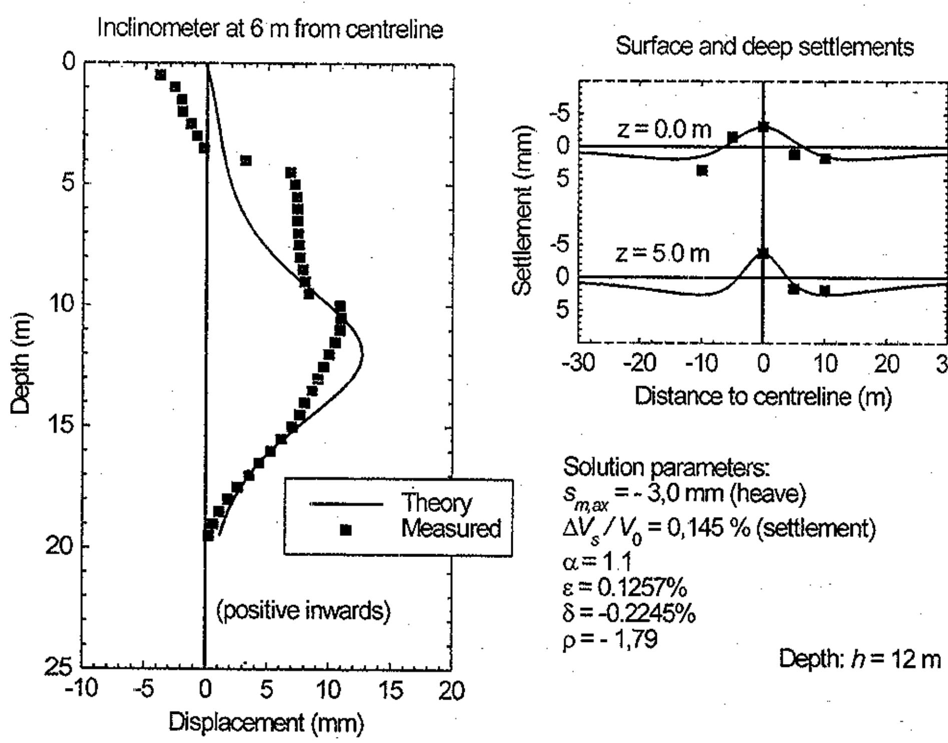

Fig. 13. Madrid Metro, EPB shield, section with heave and settlements (line 4-1 section 6).

magnitude of the deformation increases. This could reflect the fact that when large movements develop, it is mainly due to crown instability, with a smaller increase in the lateral displacements. With respect to the volumetric strain exponent, α, Fig. 10 shows the obtained values as a function of the dominant soil type in each section. There is some tendency to decrease with the increase in fines content, approaching $\alpha=1$ for clay materials.

The next figures show some examples of the displacement patterns observed in the analysed sections. Fig. 11 is a typical case with general settlements of a few millimetres, in sandy soil. The solution parameters have bee fitted using the surface settlements and extensometer readings at 6 m from the tunnel axis. Radial contraction and ovalization are both positive (1.16%). Fig. 12 corresponds to a case of general surface heave due to excessive face and tail grout pressures, which are reproduced by negative radial contraction (−0.36%) and negative ovalization (−0.27%). Finally, Fig. 13 is for an intermediate case, with surface heave near the axis, but settlement at some lateral distance. Here the fitting parameters are negative ovalization (−0.22%), but positive radial contraction (0.13%)

5. Conclusions

The results of measurements of ground deformation during the construction of the Madrid Metro extension plan have been interpreted using a general analytical solution. The soil ~~displacements are~~ written in terms of the tunnel deformation components: radial contraction and ovalization, and a parameter to cover soil volumetric compressibility.

The results show that the solution can reproduce with reasonable accuracy the pattern of soil deformation in a wide range of cases, from limited deformations of a few millimetres to larger displacements associated with small cover in competent ground. Settlements and heave associated to large values of face and tail grout pressures can also be reproduced

Acknowledgements

The work has been supported by the Comunidad de Madrid through a contract with Fundación Torres Quevedo of the Universidad de Cantabria. The authors wish to thank Dr. M. Melis and Mr. I. Matías for their help and permission to publish the data, and also the members of the Central Control Unit for the Instrumentation, Mr. P. Romo and Mr. L. Blanco.

References

[1] Attewell PB, Farmer IW. Ground deformations resulting from shield tunnelling in London clay. Can Geot J 1974;11(3):380–95.

[2] Bernat S, Cambou B, Dubois P. Assessing a soft soil tunnelling numerical model using field data. Géotechnique 1999;49(4):427–52.
[3] Britto AM, Gunn MJ. Critical state soil mechanics via finite elements. Chichester: E. Horwood, 1990.
[4] Clough GW, Sweeny BP, Finno RJ. Measured soil response to EPB shield tunnelling. Journal of Geot Engg ASCE 1983;109(2):131–49.
[5] Deane AP, Bassett RH. The Heathrow express trial tunnel. Geotechnical Engineering. Proc Inst Civ Engrs 1995;113:144–56.
[6] El-Nahhas FM, Ahmed AA, Esmail KA. Prediction of ground subsidence above tunnels in Cairo. Proc 14th Int Conf Soil Mech Found Eng Hamburg 1997;3:1453–6.
[7] Escario V, García JM, Moya JF, Oteo C, Sagaseta C. Geotechnical problems during the construction of the Madrid subway extension. In 'Case History Volume'. Japanese Soc Soil Mech Found Engng Tokyo, Japan. 1981.
[8] González C. Deformaciones alrededor de túneles en suelos. Doctor thesis (under prep). University of Cantabria, Spain, 2000.
[9] Kastner R, Ollier C, Guibert G. In situ monitoring of the Lyon Metro D line extension. In: Mair RJ, Taylor RN editors. Geot Aspects of underground construction in soft ground. London, 1996 p. 701–6.
[10] Kirsch G. Die Theorie der Elastizität und der Bedurfnisse der Festigkeitslehre. VDJ 1898;42(29): 799.
[11] Lee KM, Rowe RK. Finite element modeling of the three-dimensional ground deformations due to tunneling in soft cohesive soils: part I — method of analysis; part II — results. Computers and Geotechnics 1990;10:87–138.
[12] Mair RJ, Gunn MJ, O'Reilly MP. Ground movements around shallow tunnels in soft clay. Proc 10th Int Conf Soil Mech Found Eng Stockholm 1981;1:323–8.
[13] Medina L. Estudio de los movimientos originados por la excavación de túneles con escudos de presión de tierras en los suelos tosquizos de Madrid. Doctor thesis. Univ de La Coruña, Spain, 1999.
[14] Melis MM, Arnáiz M, Oteo C, Mendaña F. Ground displacements in Madrid soils due to tunnel excavation with earth pressure TBM. Proc 14th Int Conf Soil Mech Found Eng Hamburg 1997;3:1433–6.
[15] Melis MM, Agueda F, Mendaña F, Ruiz J, Oteo C, Rodríguez JM et al. Las obras de ampliación del Metro de Madrid (special issue). Revista de Obras Públicas 1997; 3369:3–185 (In Spanish).
[16] Mindlin RD. Stress distribution around a tunnel. Trans ASCE 1940;105:1117–40.
[17] Oteo CS, Sagaseta C. Some Spanish experiences on measurement and evaluation of ground displacements around urban tunnels. In: Mair RJ, Taylor RN editors. Geothermic Aspects of Underground Construction in Soft Ground, London, 1996 p. 731–6.
[18] Palmer JH, Belshaw DJ. Deformations and pore pressures in the vicinity of a precast, segmented concrete-lined tunnel in clay. Can Geot J 1978;17:174–84.
[19] Peck RB. Deep excavations and tunnelling in soft ground. In: Proc 7th Int Conf Soil Mech Found Eng Mexico, 1969. State-of-the-Art Volume, p. 225–90.
[20] Pender MJ. Elastic solutions for a deep circular tunnel. Géotechnique 1980;30:216–22.
[21] Phienwej N. Ground movements in shield tunnelling in Bangkok soils. In: Proc 14th Int Conf Soil Mech Found Eng Hamburg 1997. Vol. 3, p. 1469–72.
[22] Romo MP. Soil movements induced by slurry shield tunneling. In: Proc 14th Int Conf Soil Mech Found Eng Hamburg 1997. Vol. 3, p. 1473–84.
[23] Sagaseta C. Analysis of undrained soil deformation due to ground loss. Géotechnique 1987; 37(3):301_320.
[24] Sagaseta C. Author's reply. Géotechnique 1988;38(4):647–649.
[25] Sagaseta C. On the role of analytical solutions for the evaluation of soil deformations around tunnels. In: A. Cividini, editor. Application of numerical methods to geotechnical problems. Invited Lecture. CISM Courses and Lectures No. 397, 1998. p. 3–24.
[26] Sagaseta C, Sánchez-Alciturri JM, González C, López A, Gómez P, Pina R. Soil deformations due to the excavation of two parallel underground caverns. In: Proc 12th Eur Conf Soil Mech Found Eng Amsterdam, 1999. Vol. 3, p. 2125–31.

[27] Schmidt B. Settlements and ground movements associated with tunnelling in soil. PhD thesis. University of Illinois 1969.
[28] Schmidt B. Discussion. Géotechnique 1988;38(4):647.
[29] Uriel AO, Sagaseta C. Selection of parameters for underground construction. In: Proc 12th Int Conf Soil Mech Found Eng R Janeiro, Brasil, 1989. Vol. 4, p. 2521–51.
[30] Verruijt A. Complex variable solutions of elastic tunnelling problems. Geotechnical Laboratory, Delft University of Technology 1996.
[31] Verruijt A, Booker JR. Surface settlements due to deformation of a tunnel in an elastic half plane. Géotechnique 1996;46(4):753–7.
[32] Yu HS, Rowe RK. Plasticity solutions for soil behaviour around contracting cavities and tunnels. Res. Rep. 165 06 98. The University of Newcastle, Australia, 1998.

AFTES

RECOMMENDATIONS ON

THE CONVERGENCE-CONFINEMENT METHOD

AFTES welcomes comments on this paper

Version 1 - Approved by Technical Committee on 14/11/2001

Text submitted by
Marc PANET (EEG SIMECSOL) - Chairman, WG1

assisted by
Anne BOUVARD (COYNE & BELLIER) - **Bruno DARDARD** (SNCF INGENIERIE) -
Pascal DUBOIS (CETU) - **Olivier GIVET** (EEG SIMECSOL) - **Alain GUILLOUX** (TERRASOL) -
Jean LAUNAY (DUMEZ GTM) - **Nguyen MINH DUC** (LMS) - **Jean PIRAUD** (ANTEA) -
Hubert TOURNERY (SCETAUROUTE DTTS) - **Henry WONG** (ENTPE) Vice Chairman

Notation

Geometry

- R radius of circular tunnel section
- d unsupported tunnel length from working face
- x distance from working face to any given tunnel cross section

Time

- t time after working face has passed any given tunnel cross section
- T_A characteristic time of rate of advance of working face
- T_M time characterising the rate of time-dependent deformation of the ground
- T_S time characterising creep behaviour of support

Displacement, Convergence

- u, u_R, radial displacement of a point on tunnel wall
- u_0 value of u at working face
- u_d value of u at distance d from working face
- u_∞ value of u at very long distance from working face
- u_{ns} value of u for unsupported tunnel
- $C(x)$ convergence at section at distance x from working face

Speed

- V_A rate of advance of working face

Stresses

- σ, σ_R radial stress on tunnel wall massif
- σ_0 natural stress tensor, natural stress value with hydrostatic tensor

Ground properties

- E Young's modulus of ground
- n Poisson's ratio of ground
- G shear modulus of ground
- σ_c uniaxial compressive strength

Support properties

- E_S Young's modulus of support
- v_S Poisson's ratio of support
- K_S stiffness of support
- K_{SN} normal stiffness of support
- K_{SF} bending stiffness of support
- p_S support pressure

Decompression

- λ confinement loss
- λ_0 confinement loss at working face
- λ_d confinement loss at distance d from working face
- λ_e confinement loss at boundary of elastic zone

SOMMAIRE

1 - INTRODUCTION

Designing tunnel support was for many years considered too complex for strict engineering analysis and remained an empirical art repeating techniques that had proven satisfactory under similar geological conditions in the past This similarity approach was based on qualitative factors that were neither well-defined nor interpreted in any consistent way

The analytical methods which are a basic tool for construction engineers were found to be unsuitable for tunnel support design This left the way open for dogmatic claims about the universal suitability of certain methods and techniques, claims failing to stand up to quantitative analysis

The difficulty of designing tunnel support arises mainly from

• inadequate knowledge of ground behaviour under conditions associated with tunnel driving,

• insufficient data on the natural state of stress in the ground, and

• the fact that it is a three-dimensional problem

The last point is due to the fact that the engineer needs to analyse the interaction between the ground and the support near the working face

Additionally, time-dependent response dictated by the rheological properties of the ground may also have to be considered

The convergence-confinement method is a simplified method of analysing this interaction between the ground and the support In its basic form using extreme axisymmetry assumptions, it becomes a two- or one-dimensional problem, providing a simple understanding of the ground/support interaction processes occurring near the working face

These Recommendations describe the general principles of the convergence-confinement method, including the rules for selecting the confinement loss value, which is the keystone of the method. They also describe the field of application of the method and its relationship to other existing methods

Contrary to what is mistakenly assumed in the usual design methods, the ground/support interaction is not generally amenable to dealing separately with actions applied to the structure and the structure's stresses and deformations Addressing these two factors separately is the main reason for the inadequacy of the methods previously proposed

In fact, tunnel support design methods can be classified into four types:

• Purely empirical methods indicating the most appropriate type of support for a situation defined from various geotechnical classification systems

• Methods for determining the loads acting on the support, regardless of support type and deformation

• Support design methods which consider loads exerted by the ground as input data but allow for support stiffness and deformation and the reactions of the surrounding ground

• More recent methods taking full account of the ground/support interaction

These methods, which are the subject of earlier AFTES Recommendations [1], are briefly reviewed in the following.

1.1 - Empirical methods based on geotechnical classification systems

Various rock classification systems have been proposed The most widely used are Bieniawski's RMR [7] and N Barton's Q system [3] They attribute a lumped score to the rock based on several quantified parameters The overall score determines support type

This approach must not be confused with a different use of the RMR and Q index for determining the geomechanical properties of rock (Hoek & Brown) [14]

AFTES has proposed a method entitled "Tunnel Support Type Selection" described in interim Recommendations in the September 1976 special issue of *Tunnels et Ouvrages Souterrains* The parameters used for support selection are rock strength as measured on laboratory specimens, fragmentation (RQD index) and weathering, hydrogeology, tunnel cover and cross section, and tunnel environment. Another important feature is that the rock strength classification is to some degree dependent on tunnel driving method (presplitting or mechanical excavation) A matrix identifies, for a given situation, unsuitable support methods, feasible methods and appropriate methods Unlike the RMR and Q classifications, there is no information on unsupported length, steel rib inertia and spacing, rock bolt density and bolt length, or shotcrete thickness

These methods had the merit of introducing the need for a quantitative description of the ground But since they are based on case histories whose relevance has not been addressed, they tend to repeat past mistakes They are in standard use, mainly abroad, and can be useful aids at the project planning stage.

1 2 - Methods giving loads exerted by the ground on the support

These methods determine the extent of the failure zone Purely static considerations then determine the reaction that needs to be exerted by the support to keep the failure zone stable

These methods implicitly assume that severe convergence has occurred for failure mechanisms to occur; the corresponding displacements are not necessarily acceptable for the support structure

Methods differ in the way they define the failure zone

In the methods recommended by Terzaghi (fig. 1) and Protodiakonof, the shape of the failure zone is given Its extent depends on the mechanical strength of the ground and tunnel cover.

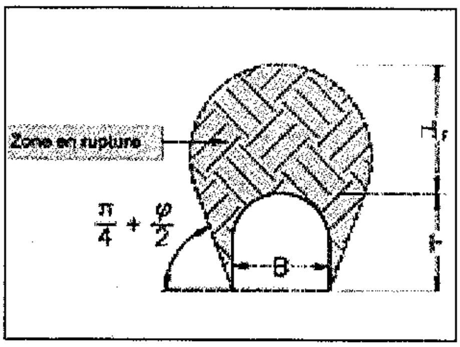

Figure 1 - Definition of failure zone above tunnel crown according to K Terzaghi

Caquot [8] defines the failure zone by analysing the extent of the plastic zone around a circular tunnel

These methods are justified when the failure mechanism considered is independent of the support method

This may be the case with a shallow tunnel where there is a possibility of a sinkhole appearing at ground level.

It also concerns the case of rock tunnels where the stresses around the opening are well below the uniaxial compressive strength of the rock and the deformations caused by the tunnelling are very slight The only significant displacements that can occur are due to pre-existing discontinuities opening or causing blocks to slide. Three-dimensional structural analysis will reveal joint sets of constant direction, and allows the engineer to determine the maximum dimensions of blocks liable to be unstable for the actual size and direction of the tunnel excavation Here, the support merely serves to prevent potentially unstable blocks from falling or sliding Methods based on structural analysis are appropriate in such situations (fig 2).

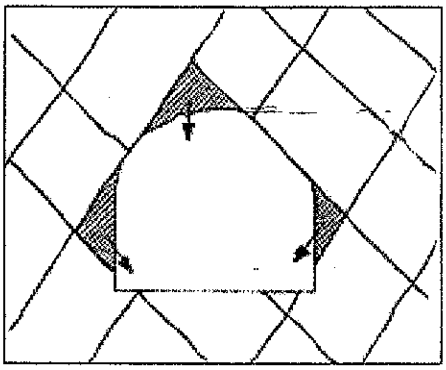

Figure 2 - Unstable rock blocks intersected by the tunnel

1 3 - Methods of analysing support exposed to predetermined loads

These methods deriving from conventional structural design based on strength of materials theory are the normal complement to the methods described above, and the same remarks apply

However, what is known as the "hyperstatic reactions" method deserves special mention The support is modelled as bars and the ground reaction, as springs (fig 3). It is an attempt to address the interaction between the ground and support The load on the support comes from the actions needed to maintain the failure zone in equilibrium and the reaction of the ground to yielding of the support

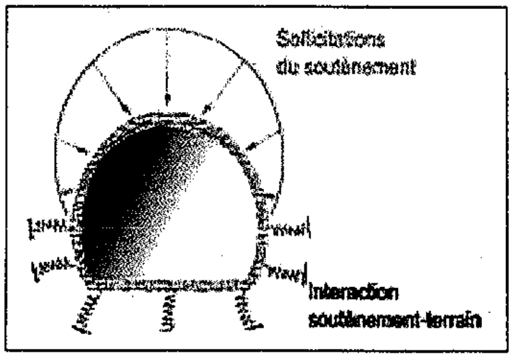

Figure 3 - Principle of hyperstatic reactions method

This method has frequently been used, despite the structural engineer's perplexity as to the distinction between the zone exposed to ground actions and the zones exposed to ground reactions to support displacements Setting spring stiffness is critical. Results may even become very surprising when heading and benching. The method is still frequently used and may be useful, especially for shallow tunnels, because the model is simple to use.

1 4 - Methods addressing ground/support interactions

Strict engineering analysis of the ground/support interaction is feasible by three-dimensional computer modelling by various methods, lumped together under the name "composite solid methods " They use a finite element or finite difference approach, or separate elements This type of modelling may include for

- support structure and geometry with constitutive equations for this structure,
- the geometry of the various geomechanical units identified around the tunnel with their constitutive equations, and
- unnel excavation phases and support installation.

The advantages of this type of three-dimensional modelling are incontrovertible and they will probably become commonplace in future with the inexorable progress in computer methods with in which young engineers are increasingly familiar. At present, their use and interpretation is still considered slow and complex and involves difficulties in running sensitivity analyses on parameters whose determination involves much uncertainty, especially geotechnical parameters

Somewhat paradoxically, these models are mainly used for very complex underground openings where it is difficult to assess the true influence of the simplifications needed to make them more like more routine design problems. The LCH1 cavern currently being built for CERN is a good example of three-dimensional modelling of a highly complex underground ensemble of large, intersecting chambers and shafts (fig 4).

The convergence-confinement method does away with the need for a complex three-dimensional model. It is based on the two-dimensional analysis of the interaction between the support and the ground. It is therefore much simpler This type of analysis has been proposed by several authors, the first probably being Fenner [11] in 1938 The same approach was adopted by Pacher [20] in 1964 Their main shortcoming was that they failed to consider ground deformations that occur before the support is installed. With his characteristic "core" line, Lombardi introduced the concept of convergence at the working face [17] Panet & Guellec [21, 1974] advocated including for deformations occurring prior to support installation via the confinement loss factor This is the origin of the convergence-confinement method which was given its name at a1978 AFTES meeting in Paris

The principal advantage of the method is that it allies ease of use with an objective approach to the more important processes involved in the ground/support interaction It allows easy analysis of the sensitivity of parameters which can only be quantified approximately

The first AFTES Recommendations on the convergence-confinement method were issued in 1984 [1]. Abundant research findings since that time, along with much observational data, have made it necessary to re-write the older Recommendations

2 - TUNNEL CONVERGENCE

The loss of confinement caused by tunnel driving causes stress redistribution around the excavation and deformations. Convergence of the tunnel along line *a* is the relative displacement of a diametrically-opposed pair of points on the tunnel wall on this line as the working face advances

Convergence depends on the distance *x* between the instrumented section and the working face, on elapsed time *t* after the working face has passed the instrumented section, on the unsupported distance *d* behind the working face, and on the stiffness of the support; this can be written in general terms:

$$C = C\,[x(t)t,d,K_s]$$

Convergence measurements are usually plotted versus distance to working face and time (fig 5)

Detailed analysis of the curves yields very instructive information about the influence distance of the working face, and therefore, about the extent of the decompressed zone and whether or not time-dependent deformations will occur It also enables a judgement to be made as to the validity of the analytical models

Standard tunnel instrumentation methods give the convergence behind the working face but no data on the convergence which occurs ahead of it (now called 'preconvergence') New design and construction approaches for tunnels in difficult ground provide a more refined analysis of the behaviour of the ground ahead of the working face (cf ADECO-RS method developed by P Lunardi [18, 19]). Since it is not possible to measure preconvergence directly, he proposes measuring extrusion of the ground ahead of the face, i e the displacement of points on the tunnel centre-line ahead of the face as the working face advances. Much can be learned from the amplitude of, and changes in extrusion with reference to the working face, especially for installing temporary support or preconfinement.

Schematically, there are three situations:

- The working face may be stable with little extrusion at the face
- The working face may be stable but exhibits significant extrusion, due to deformations ahead of the face
- The working face may be unstable and collapses

The first two situations are those for which the convergence-confinement method is ideally suited

Its extension to the third case requires prior analysis of the methods of shoring up the working face and of the deformations ahead of the stabilised face Such analysis is beyond the scope of these Recommendations

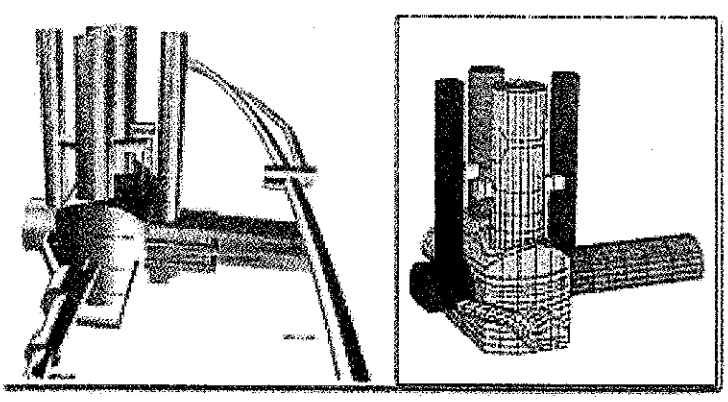

Figure 4 - Model of CERN LCH1 cavern

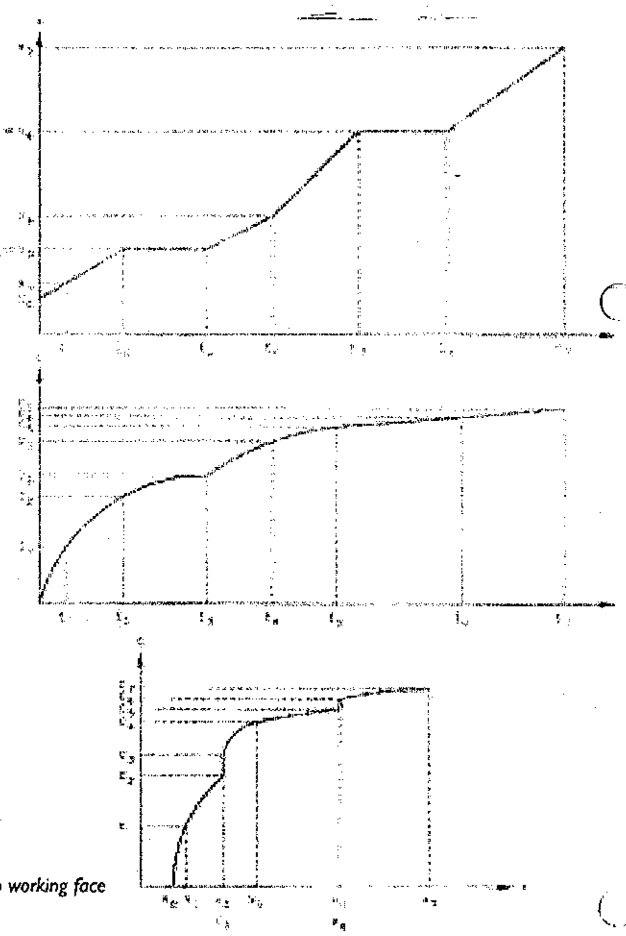

Figure 5 - Tunnel convergence vs time and distance to working face

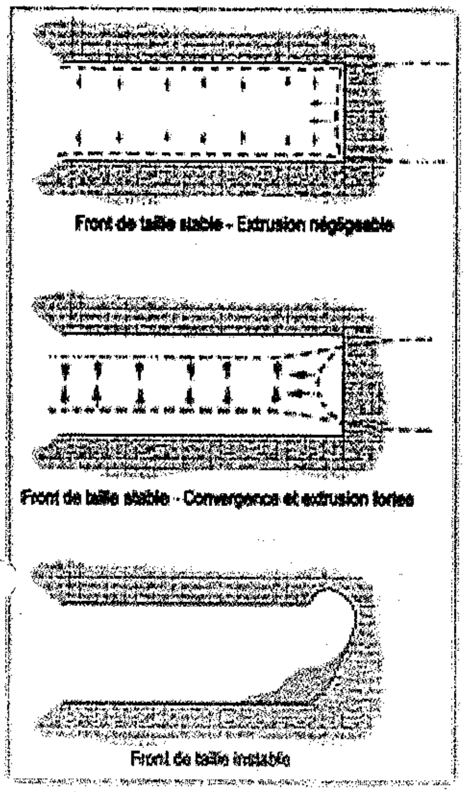

Figure 6 - Extrusion and instability of working face (aftes P Lunardi)

3 - MECHANICAL BEHAVIOUR OF SUPPORT

Support systems oppose convergence of the tunnel walls by exerting a pressure, commonly called the support pressure Support pressure P_S increases with support system stiffness and is limited by the strength of the support material

With a circular tunnel of radius R, we define the normal stiffness modulus of the support K_{SN} as :

$$p_s = K_{SN} \frac{u_R}{R}$$

Only the linear portion of the support strain curve is considered.

With an axisymmetric tunnel, this modulus alone determines support stiffness, but under non-axisymmetric conditions, we also need the stiffness modulus in bending K_{SF}

Typical stiffness moduli for different types of support are given below for an axisymmetric model

3.1 - Circular ring of constant thickness e (e<<R)

$$K_{SN} = \frac{E_s}{1-\nu_s^2} \frac{e}{R}$$

$$K_{SF} = \frac{E_s}{1-\nu_s^2} \frac{I}{R^3}$$

in which

$$I = \frac{e^3}{12}$$

3 2 - Circular ring of n segments of thickness e

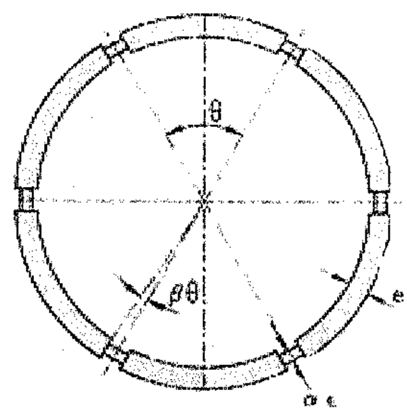

Figure 7 - Model of segmental lining ring

The above expressions are used, with

$$E_s = \frac{\alpha}{\alpha(1-\beta)+\beta} E_s$$

$$I = I_j + \left(\frac{4}{n}\right)^2 \frac{e^3}{12}$$

in which (fig 7)

ae is the equivalent thickness at joints

θ is the angle subtended at centre by a lining segment

$\beta\theta$ is the angle subtended at centre by a joint

Ij is the inertia of the section at a joint

$$I_j = \frac{\alpha^3 e^3}{12}$$

3.3 - Circular steel ribs at spacing s in intimate contact with ground

$$K_{SN} = \frac{E_a A}{sR} \quad ; \quad K_{SF} = \frac{E_a I}{sR^3}$$

in which

A is the area of the rib cross section

E_a is the Young's modulus of steel

I is the moment of inertia of the rolled steel section

These expressions assume the ribs are in near-continuous contact with the ground

3.4 - Rock bolts

The following brief discussion of rock bolt support concerns only the stiffness of this type of support. The subject is dealt with much more fully in the AFTES Recommendations on rock bolting.

- Mechanically anchored rock bolts, longitudinal spacing s_l, transverse spacing s_t

$$\frac{1}{K_{SN}} = \frac{s_t s_l}{R}\left[\frac{4L}{\pi\Phi^2 E_b} + Q\right]$$

$$K_{SF} = 0$$

in which

L is bolt length

Φ is bolt diameter

E_b is the Young's modulus of the bar material

Q is a factor for deformation at the bolt head and anchorage, determined from pull-out tests

- Rock bolts anchored over their whole length

Rock bolts anchored over their whole length and Swellex or Split Set type dowels are considered as rock reinforcing members and their effect is modelled by assuming improved geomechanical properties of the bolted zone

In this way thick shell theory can be applied to the bolted zone, although shell thickness must be taken as less than bolt length "Homogenisation theory' [11] can be used to determine the mechanical properties of this ring It is considered as an equivalent isotropic material with enhanced cohesion

Two dimensionless parameters characterise the role of rock bolts One describes bolt contribution to the stiffness of the homogenised zone:

$$\frac{D_b S_b E_b}{E_s}$$

The other parameter describes bolt contribution to the improved strength of the homogenised zone:

$$\frac{D_b S_b \sigma_{yb}}{\sigma_c}$$

in which D_b, S_b, E_b, s_{yb} are respectively bolt pattern density, bolt cross section, and Young's modulus and yield point of the bolt material

It is usually found that rock bolts contribute little support if only linear strain is considered But in fact, bolting plays a particularly important role under high convergence conditions This can only be understood if rock mass dilatancy is considered, especially in terms of brittle or strain softening behaviour beyond peak strength Analytical methods which do not consider such behaviour underestimate the effect of rock bolting

3 5 - Shotcrete

Shotcrete is widely used for tunnel support. The stiffness to be introduced in analysing ground/support interaction must be based on (i) shotcrete age and (ii) whether or not the shotcrete forms a continuous shell The developing stiffness of green shotcrete allows it to adapt to convergence (cf AFTES Recommendations on shotcrete)

3 6 - Stiffness of some standard support types

The following table presents typical order-of-magnitude stiffness and strain moduli for a few types of support routinely used, in a tunnel of 5m radius

3 7 - Combinations of several types of support

In most cases, a combination of support systems is used If all the types are installed at the same time at the same distance behind the working face, they are assumed to be exposed to the same displacement field, and stiffness moduli are the sum of the stiffness moduli of the constituent systems

If they are not all installed at the same time, support stiffness varies with the distance to the face and this must be allowed for in the convergence-confinement analysis (fig 8)

4 - PRINCIPLE OF CONVERGENCE-CONFINEMENT METHOD

Instead of the three-dimensional problem, the convergence-confinement method [23] addresses a two-dimensional plane strain problem of the ground/support interaction

It consists of applying to the walls of the opening a stress

$$\sigma = (1-\lambda)\sigma_0 \qquad (1)$$

σ_0 is the natural stress in the ground; λ is a parameter simulating the excavation as it increases from 0 to 1 It is called the *confinement loss* (fig 9)

As this parameter decreases in value, the ground loses its confinement, and this loss of confinement causes a displacement u of the walls of the opening such that

$$f_m(\sigma, u) = 0 \qquad (2)$$

This is the *convergence equation for the ground*.

The equation for support behaviour relates the stresses exerted at the wall to the corresponding displacement:

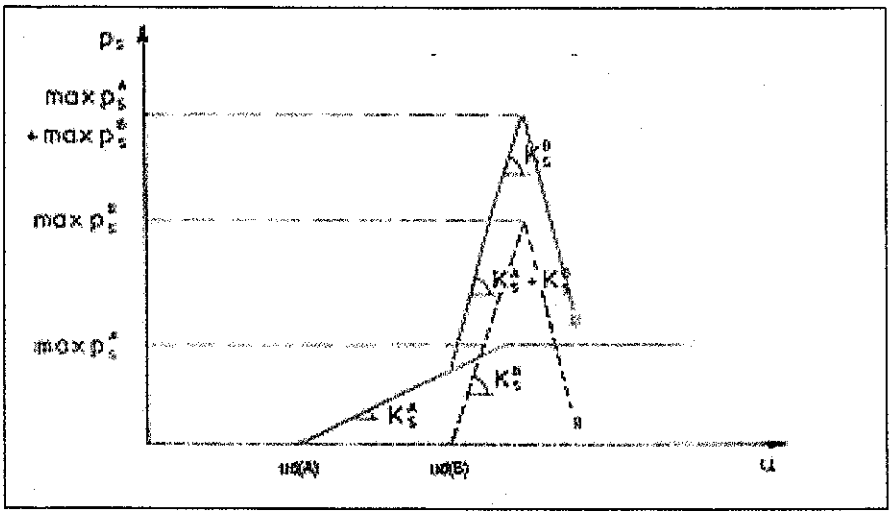

Figure 8 - Confinement curve for combination support system

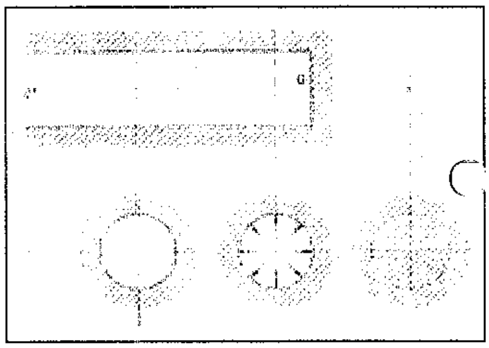

Figure 9 - Change in confinement loss on tunnel centreline

Support	40cm thick *in situ* concrete ring	ring of six 30 cm thick concrete segments	Continuous shell of 10 cm thick shotcrete	Circular HEB 140 steel ribs on 1m centres	Mechanically anchored bolts 18mm dia ... $s_T s_L$ = 1 m
K_{SN} (MPa)	850	750	210	150	60
K_{SF} (MPa)	0,45	0,13	5.10^{-3}	7.10^{-3}	0
Max u_R/R	$2{,}5.10^{-3}$	$1{,}5.10^{-3}$	$3{,}3\ 10^{-3}$	$1\ 10^{-3}$	

$$f_s(\sigma, u) = 0 \quad (3)$$

This is the *convergence equation for the support*

The support is usually installed some distance d behind the working face, called the *unsupported distance*. Displacements u_d will have occurred ahead of the face and in the unsupported zone behind it.

Displacement u_d has a corresponding confinement loss λ_d.

Therefore the preceding equation can be written

$$f[\sigma, (u - u_d)] = 0 \quad (4)$$

The equilibrium which eventually results from the interaction between the ground and the support is found by solving the system of equations (2) and (4).

The confinement loss concept is the key to the method and determining its value λ_d at the time the support is installed is the main challenge.

It should be mentioned that other methods have been proposed to take account of the proximity of the working face limiting convergence at the time of support installation. Svoboda suggests simulating this effect by progressive softening of the ground waiting to be excavated. But these methods have been found to be less practical than the confinement loss method. He did not offer any clear rules for finding the amount of softening from unsupported distance and ground behaviour. Setting it at 90% for deep tunnels and 30% for shallow tunnels appears completely arbitrary.

In the simplest case where there is complete axisymmetry about the centreline and there is no time-dependent deformation of the ground, the convergence-confinement method is amenable to very simple graphic plotting (fig 10).

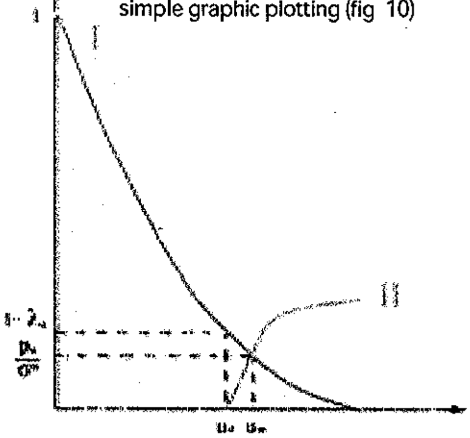

Figure 10 - CAxisymmetric case. Graphic representation of convergence-confinement method

4.1 - Axisymmetric case: linear elastic ground and support

In the simplest case, displacements and stresses are radial, equations (2) and (4) are linear and are written

$$\sigma_R + \frac{E}{1+\nu}\,\frac{u_R}{R} - \sigma_0 = 0$$

$$\sigma_R - K_{SN}\frac{u_R - u_d}{R} = 0$$

K_{SN} is the stiffness modulus of the support.

Solving this system determines the support pressure ps and radial displacement at equilibrium u_R:

$$p_S = \frac{K_{SN}}{2G + K_{SN}}(1 - \lambda_d)\sigma_0$$

$$\frac{u_R}{R} = \frac{2G + \lambda_d K_{SN}}{2G + K_{SN}}\,\frac{\sigma_0}{2G}$$

in which

$$2G = \frac{E}{1+\nu}$$

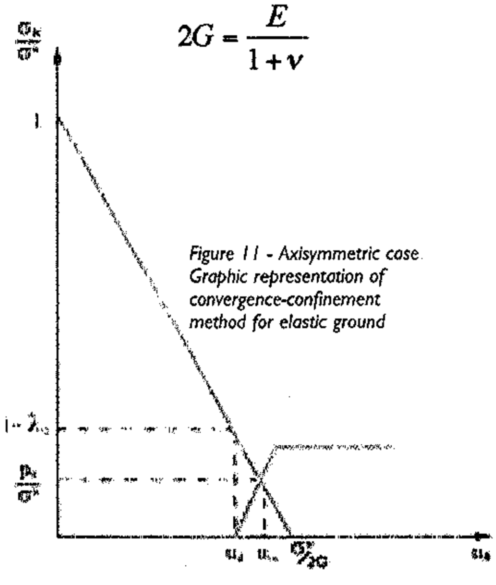

Figure 11 - Axisymmetric case. Graphic representation of convergence-confinement method for elastic ground

4.2 - Axisymmetric case: elastic-plastic ground

When confinement loss approaches unity, the boundary of the elastic response zone is reached at the tunnel wall with a confinement loss value λ_e.

If the plasticity criterion is given by an intrinsic curve whose equation is

$$F(\sigma_1, \sigma_3) = 0$$

then the value of λ_e is given by

$$F[(1+\lambda_e)\sigma_0, (1-\lambda_e)\sigma_0] = 0$$

With $\lambda > \lambda_e$, there appears a plastic zone of radius R_p and the convergence curve of the ground ceases to be a straight line because of the plastic strains.

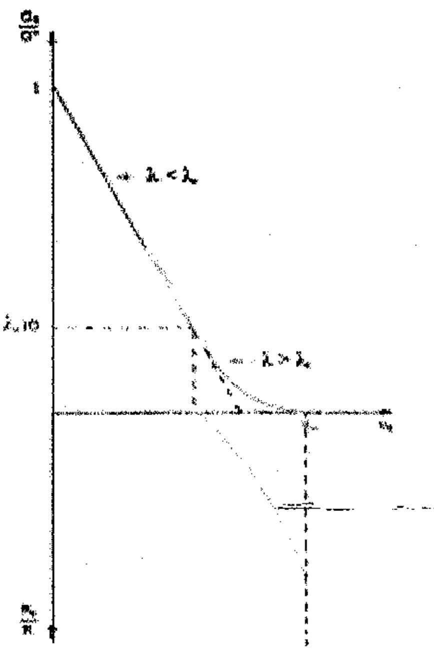

Figure 12 - Axisymmetric case. Convergence curve of ground and change in plastic radius for elastic-plastic ground

The equations for the convergence curves under axisymmetric conditions have been established by various authors for various types of elastic-plastic behaviour laws [23].

5 - DETERMINATION OF CONFINEMENT LOSS

Selecting the confinement loss λ_d corresponding to the convergence occurring before the support starts interacting with the ground is the most critical point in the convergence-confinement method.

λ_d is determined from the convergence equation:

$$f[(1 - \lambda_d)\sigma_0, u_d] = 0$$

The value of λ_d is therefore chosen by determining the radial displacement u_d at the unsupported distance d behind the working face

High u_d displacement values correspond to higher confinement loss values as λ_d approaches unity. This parameter is governed mainly by the length of the unsupported distance behind the face d but it is also dependent on the constitutive equation for the ground and to a lesser extent, on the stiffness of the support.

Accuracy in calculating the support pressure is closely linked to the accuracy of determining λ_d. It is dependent on the slope of the convergence curve near its intersection with the confinement curve. The impact of uncertainty as to the precise value of λ_d on the value of the support pressure should be assessed in all cases

The radial displacement u_d can generally be written

$$u_d = u_0 + a_d\,(u_\infty - u_0)$$

in which

a_d is given approximately by

$$a_d = 1 - \left[\frac{mR}{mR + \xi d}\right]^2$$

m and ξ are coefficients dependent on the constitutive equation for the ground

Therefore u_0, u_∞, m and ξ have to be determined

Common errors are to assign u_0 and u_∞ values for an unsupported tunnel; but then, u_∞ is not the equilibrium radial displacement for a supported tunnel and u_0 is overestimated

What are called implicit methods using values for a supported tunnel have been developed more recently

5.1 - Methods based on convergence in an unsupported tunnel

5.1.1 - Elastic ground behaviour

$$u_\infty = \frac{\sigma_0 R}{2G}$$

$$u_0 = \alpha_0 u_\infty$$

$$\alpha_0 = 0{,}25 \quad ; \quad m = 0{,}75 \quad ; \quad \xi = 1$$

Therefore

$$\lambda_d = 1 - 0{,}75\left[\frac{0{,}75R}{0{,}75R + d}\right]^2$$

It will be seen that this equation yields a confinement loss at the face ($d = 0$) of 0.25, but in fact, the true value depends on the Poisson's ratio. With $0.2<\nu<0.5$, it ranges more or less linearly from 0.20 to 0.3. But with $d/R > 0.25$, confinement loss is almost entirely independent of the Poisson's ratio.

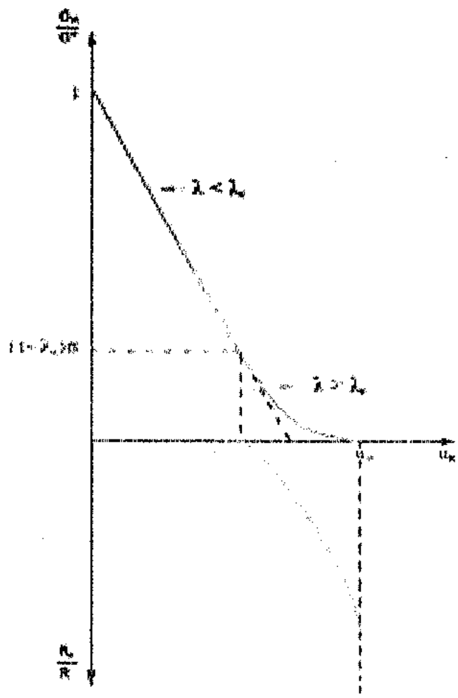

Figure 13 - Axisymmetric case. Radial displacement vs x for different Poisson's ratios

5.1.2 - Elastic-plastic ground behaviour

The value of u_d is determined by assuming similarity with elastic ground conditions, as proposed by Bernaud, Corbetta & Nguyen Minh [5]. This approach consists of obtaining the $U_r = f(x)$ curve for elastic-plastic conditions as a homothetic transform of the corresponding elasticity curve of centre o and ratio $1/\xi$ (fig. 14)

The final radial displacement of the unsupported tunnel is written as

$$u_\infty = \frac{1}{\xi}\,\frac{\sigma_0 R}{2G}$$

Then

$$a_d = 1 - \left[\frac{0{,}75R}{0{,}75R + \xi d}\right]^2$$

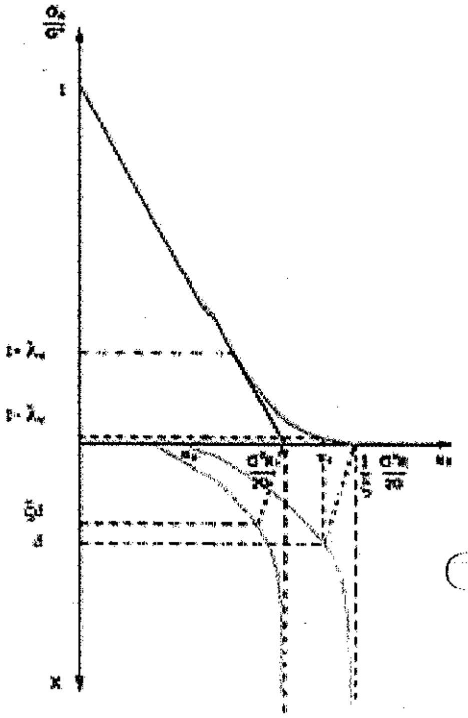

Figure 14 - Application of similarity principle (after Bernaud, Corbetta & Nguyen Minh)

From this:

$$u_d = u_\infty\left[1 - 0{,}75\left(\frac{0{,}75R}{0{,}75R + \xi d}\right)^2\right]$$

5.2 - Methods based on convergence of supported tunnel

These methods allow for the fact that the stiffness of the support limits convergence ahead of and behind the face, so that coefficient λ_d has a lower value than in the methods described above. The effect is obviously more marked when the support is stiff and installed close behind the face

What are called 'implicit' methods have been developed by Bernaud & Rousset [6] and by Nguyen Minh & Guo [14]. These methods give similar results

Nguyen Minh & Guo define two parameters:

$$A = 1 - \frac{u_\infty}{u_{ns\infty}}$$

and

$$B = 1 - \frac{u_d}{u_{nsd}}$$

in which $u_{ns\infty}$ and u_{nsd} are respectively values of u_∞ and u_{nsd} for an unsupported tunnel

They thus arrive at the general equation

$$B = A\left[0{,}45 + 0{,}42A^2\right]$$

This formula and the equations for the convergence and confinement curves make it possible to determine u_∞ and u_0

The following table shows correction factors to be applied to the λ_d value for an unsupported tunnel in elastic ground for different values of *d/R* and normal stiffness modulus of the support, referred to the shear modulus of an elastic ground:

$$k_{sn} = \frac{K_{sn}}{2G}$$

k_{SN} \ *d/R*	0,25	0,50	0,75	1	2
0,25	0,97	0,97	0,98	0,99	0,99
0,50	0,93	0,96	0,96	0,98	0,99
1	0,88	0,92	0,95	0,97	0,98
2	0,83	0,89	0,93	0,96	0,97
5	0,76	0,85	0,89	0,94	0,97
10	0,71	0,82	0,86	0,93	0,96
∞	0,69	0,81	0,85	0,92	0,96

In non-linear ground, iterative methods must be used too determine λ_d. The starting point is the value obtained for an unsupported tunnel, then proceeding to iterate for A and B until the problem converges with little change between successive steps

5 3 - Using convergence-confinement method with two-dimensional computer models

The most common way of using the convergence-confinement method is to investigate a two-dimensional cross section of the tunnel in a finite element model reproducing the exact tunnel geometry and construction phases, with one or more confinement loss values, as discussed above

Values for λ_d are usually found from axisymmetric models, i e for circular tunnels, with hydrostatic natural stresses and uniform ground. Any significant departure from these basic assumptions - tunnel cross section inscribed within a highly eccentric ellipse, highly anisotropic natural stresses, highly heterogeneous ground near the tunnel, shallow ground cover - requires that λ_d should be determined with simplified models. This approach is all the more necessary when support stiffness is high compared to ground deformation characteristics and support is installed close to the working face

For example, when designing a large underground railway station opening, $\lambda_d$was selected on the basis of the convergence data from a three-dimensional model of the unsupported excavation and a two-dimensional model simulating the phases of excavation and support installation

These adaptations of the method require engineering judgement and cannot be readily codified in guidelines

6 - EXTENSION OF CONVERGENCE-CONFINEMENT METHOD TO SUPPORT AHEAD OF THE FACE

The growth of tunnelling in soil and similar difficult ground has produced techniques for shoring up the working face and controlling displacement ahead of it

Slurry and earth pressure balance shields are being rivalled by forepoling and consolidation by bolting and drainage. These techniques are used alone or in combination

They control extrusion of the ground and convergence behind the working face Extending the convergence-confinement method to forepoling situations has been studied by many researchers A method for determining confinement loss behind the face has been proposed for elastic conditions [13], but there is as yet no method for elastic-plastic conditions Nevertheless, in many cases where displacements caused by tunnel driving need to be very tightly controlled, the elasticity approach may be sufficient if plastic deformation is insignificant This may be the case with shallow tunnels

P Aristaghes & P Autuori [2] have made an in-depth analysis of convergence behind the working face of tunnels driven with pressurised shields and have shown the difficulty of using the convergence-confinement method in its strictest form with a single confinement loss value They introduce three efficiency coefficients, for the working face support pressure, the radial pressure around the shield tail, and the grouting pressure behind the segmental concrete lining The object is to predict displacements more accurately, especially surface settlement above shallow tunnels driven with a closed-face shield machine

7 - TIME-DEPENDENT DEFORMATION

Convergence of a tunnel section is found to be due to the working face receding but often also, to deformations which continue to occur when the distance to the working face is much greater than the distance of influence of the face

The processes causing these time-dependent deformations are

- the rheological behaviour of the ground, and
- creep in the support system

When considering the rheological behaviour of the ground, one must, as far as possible, distinguish between the rheological behaviour of the soil skeleton and the development of steady-state pore water flow around the tunnel. It is frequently difficult to make this distinction through lack of data on the hydraulic properties of the ground (permeability coefficient, storage coefficient) and on how the water table is fed

Support creep is an important factor, especially with concrete support systems

Including for these time-dependent deformations when analysing ground/support interactions raises many difficulties which have not yet all been resolved

In the very great majority of practical cases, simplifying assumptions have to be made [22]

The validity of these assumptions must be checked by assessing the characteristic times of the various time-dependent processes:

- Characteristic time of excavation rate:

$$T_A = \frac{d}{V_A}$$

- Relaxation time characterising the time-dependent deformation rate of the ground T_M
- Relaxation time characterising the creep behaviour of the support T_S

Order-of-magnitude values for these characteristic times may be very different and justify the simplifying assumptions introduced

The most common practice is to take a convergence equation with short-term characteristics for the driving and support installation stages, and another convergence equation with long-term characteristics to determine final equilibrium ($T_A << T_M$)

When the permanent lining is installed a long time after the temporary support, intermediate characteristics between the short- and long-term characteristics may be used

However, theoretical developments for viscoplastic axisymmetric conditions [4] show that this is not always justified It is only acceptable with support whose relative stiffness modulus meets the following condition:

$$k_{SN} < \frac{1}{1-2\nu}$$

This condition cannot be satisfied in soil

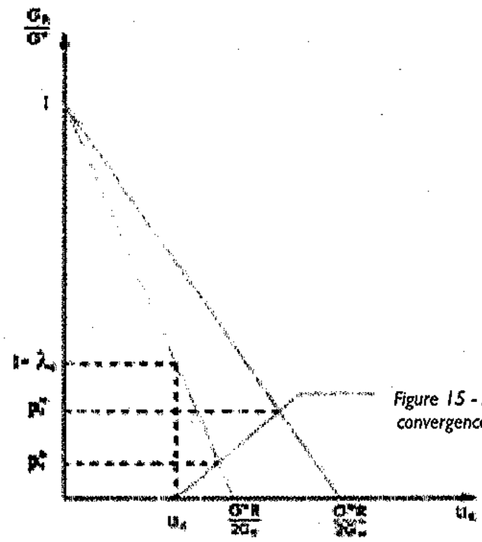

Figure 15 - Axisymmetric case. Graphic representation of convergence-confinement method for viscoelastic ground

BIBLIOGRAPHIE

This list is not exhaustive It only includes literature referred to in the Recommendations

1 AFTES – Recommandations des Groupes de Travail

2 Aristaghes P. & Autuori P. – Cacul des tunnels au tunnelier. Revue Française de Géotechnique (à paraître)

3 Barton N R , Lien R & Lunde J – Engineering classification of rock masses for the design of tunnel support, Rock Mechanics, 6, 1974

4. Berest P. & Nguyen Minh Duc – Modèle viscoplastique pour le comportement d'un tunnel revêtu Revue Française de Géotechnique, 23, 1983

5. Bernaud D., Corbetta F & Nguyen Minh Duc – Contribution à la méthode convergence-confinement par le principe de similitude, Revue Française de Géotechnique,n°54, janvier 1991

6. Bernaud D & Rousset G – La "Nouvelle Méthode implicite" pour l'étude du dimensionnement des tunnels, Revue Française de Géotechnique, n°60, juillet 1992.

7. Bieniawski Z T – Rock Mechanics Design in Mining and Tunnelling, Balkema, Rotterdam,1983

8 Caquot A. & Kerisel J. – Traité de mécanique des sols, 4ème éd , Gauthier-Villars, Paris, 1966

9. Carranza-Torres C & Fairhurst C. – Application of the convergence-confinement method of tunnel design to rock masses that satisfy the Hoek-Brown failure criterion, Tunnelling and Underground Space Technology, 15, n°2, 2000

10 Corbetta F; Bernaud D. & Nguyen Minh D – Contribution à la méthode convergence-confinement par le principe de similitude

11 Fenner R – Untersuchungen zur Erkenntis des Gebirgsdruckes, Glükauf, 74, 1938

12 Greuell E. – Etude du soutènement par boulons passifs dans les sols et les roches tendres par une méthode d'homogénéisation. Thèse, Ecole Polytechnique, Paris, 1993

13 Guilloux A , Bretelle S & Bienvenue F. – Prise en compte des pré-soutènements dans le dimensionnement des tunnels, Revue Française de Géotechnique, n°76, 1996

14 Hoek E & Brown T – Underground Excavations in Rock, Institution of Mining and Metallurgy, London, 1980

15. Nguyen Minh Duc & Guo C – Sur un principe d'interaction massif-soutènement des tunnels en avancement stationnaire Eurock 93, Balkema, Rotterdam, 1993

16 Labiouse V. – Etude par "convergence-confinement" du boulonnage à ancrage ponctuel comme soutènement de tunnels profonds creusés dans la roche Revue Française de Géotechnique, n°65, 1994

17 Lombardi G. – Dimensionning of tunnel linings with regard to constructional procedure. Tunnels and Tunneling, july 1973

18 Lunardi P. – Conception et exécution des tunnels d'après l'analyse des déformations controlées dans les sols et les roches : présoutènement et préconfinement. Revue Française de Géotechnique, n°80, 1997

19. Lunardi P. – The design and construction of tunnels using the approach based on the analysis of controlled deformation in rocks and soils, Tunnels & Tunnelling International, May 2000.

BIBLIOGRAPHIE (suite)

20 Pacher F – Deformations messungen in Versuchsstollen als Mittel zur Erfoschung des Gebirgs verhaltens und zur Bemessung des Ausbaues, Felsmechanik und Ingenieursgeologie, Supplementum IV, 1964

21. Panet M & Guellec P. – Contribution à l'étude du soutènement derrière le front de taille Proc. 3rd Cong Int. Soc Rock Mechanics, vol 2, part B, Denver, 1974

22 Panet M & Guenot A – Analysis of convergence behind the face of a tunnel, International Symposium "Tunneling 82", Brighton, 1982

23. Panet M – Le calcul des tunnels par la méthode convergence-confinement, Presses de l'ENPC, Paris, 1995.

24. Panet M. – Les déformations différées dans les ouvrages souterrains Proc. 4th Int. Congr. ISRM, Montreux, vol 3, Balkema, Rotterdam, 1979

25 Rousset G – Les sollicitations à long terme des revêtements des tunnels. Revue Française de Géotechnique, 32, 1990

26 Wong H, Trompille V. & Dias D. – Déplacements du front du tunnel renforcé par boulonnage prenant en compte le glissement boulon-terrain approches analytique, numérique et données in situ Revue Française de Géotechnique, n°89, 199